공학박사 학위논문

Nanoparticle-mediated Cell Behavior Modulation for the Treatment of Myocardial Infarction

나노입자 기반, 세포 거동조절을 통한 심근경색 치료

2017 년 8 월

서울대학교 대학원

화학생물공학부

한 진

Nanoparticle-mediated Cell Behavior Modulation for the Treatment of Myocardial Infarction

나노입자 기반, 세포 거동조절을 통한 심근경색 치료

지도교수 김 병 수
이 논문을 공학박사 학위논문으로 제출함

2017 년 8 월

서울대학교 대학원
화학생물공학부
한 진

한진의 공학박사 학위논문을 인준함
2017 년 8 월

위 원 장	한 지 숙	(인)
부위원장	김 병 수	(인)
위 원	현 택 환	(인)
위 원	서 상 우	(인)
위 원	이 수 홍	(인)

Abstract

Nanoparticle-mediated Cell Behavior Modulation for the Treatment of Myocardial Infarction

Jin Han

School of Chemical and Biological Engineering

The Graduate School

Seoul National University

Myocardial infarction (MI) is one of the leading causes of death worldwide, and accounts for majority of cardiac-associated disorders. MI originates from reduced blood supply to the heart and subsequent cardiac necrosis, hence, tissue engineering approaches are required for successful cardiac repair. Recently, various types of cells and nanoparticles drew significant attention as efficient therapeutics for cardiac repair, and combinatorial treatments between cells and nanoparticles have been introduced. Even so, majority of nanomaterials have been mostly utilized as delivery carriers, and studies regarding how nanoparticles actively modulate cell behaviors and potentiate the therapeutic efficacy of these cells remain unexplored.

Current dissertation presents the integration of stem or immune cells with most widely used nanoparticles, such as iron oxide nanoparticles or graphene oxide, for the treatment of MI. More specifically, biological role of these nanoparticles

and how innate chemical properties of nanoparticles mediate cell behaviors is elucidated. Major goals of dissertation are summarized as follows; 1) Elucidation of metal ion-delivering capability of iron oxide nanoparticles, and investigation on the modulation of cell signaling transduction and development of intercellular gap junction crosstalk 2) Elucidation of sp^2 chemistry-based intracellular antioxidant chemistry of graphene oxide, and its immune modulatory function for therapeutic polarization of macrophages in MI treatment.

First, we showed that iron oxide nanoparticles can modulate intracellular signaling transduction in cardiac cells, and improve intercellular gap junction formation in stem cell co-culture. Co-culture of stem cells with cardiac cells has windowed a platform for cardiac priming of MSCs prior to *in vivo* transplantation, and active gap junctional crosstalk between stem cells and cardiac cells are crucial in stem cell modification. In this study, we report that iron oxide nanoparticles can augment the expression of gap junction protein connexin 43 in cardiac cells to better form gap junction channels with stem cells. Stem cells co-cultured with nanoparticle-harboring cardiac cells exhibited active biomolecule transfer and showed increased level of electrophysiological cardiac biomarkers and cardiac repair-favorable paracrine secretion. Implanted in rat MI models, cardiac-primed stem cells significantly reduced cardiac fibrosis, promoted cardiac tissue regeneration and function.

Secondly, we exhibited that graphene oxide with carbon-based sp^2 chemistry can function as reactive oxygen species scavenger within the cells and prevent inflammatory activation of macrophages. Furthermore, we functionalized graphene oxide nanoparticles with plasmid DNA to better polarize inflammatory cells at cardiac infarction area into tissue regenerative macrophages. After the onset of MI, excessive amount of inflammatory macrophages propagates at the peri-infarct to exacerbate tissue necrosis, suggesting that uncontrolled differentiation and activation of inflammatory macrophages greatly hamper proper tissue regeneration. In this study, we demonstrated that graphene oxides can act as an

antioxidant to prevent inflammatory activation of macrophages, and further DNA functionalization significantly improved therapeutic polarization of these macrophages. Furthermore, injection of DNA-functionalized graphene oxides in mouse MI models notably reduced immune cell infiltration and mitigated cardiac fibrosis for cardiac performance improvement.

Keywords: iron oxide nanoparticle, graphene oxide, cell behavior, myocardial infarction, tissue engineering

Student Number : 2011-30990

Table of Contents

List of figures

List of tables

Abbreviations

5AZA	5-azacytidine
Ang-1	Angiopoietin 1
bFGF	Basic fibroblast growth factor
BMDM	Bone marrow-derived macrophage
Ca_v	Calcium channel, voltage-dependent
CCK	Cell counting kit
CMC	Cardiomyocyte
cMSC	IONP(+) H9C2 co-cultured MSCs
CSC	Cardiac stem cell
Cx43	Connexin 43
DAPI	4',6-diamidino-2-phenylindole
DLS	Dynamic light scattering
DW	Deionized water
EDV	End-diastolic-volume
EF	Ejection fraction
ELS	Electrophoretic light scattering
ESC	Embryonic stem cell
ESV	End-systolic volume
FA	Folic acid
FACS	Fluorescence activated cell sorting
FITC	Fluorescein isothiocyanate
FS	Fractional shortening
FT-IR	Fourier transform infrared spectroscopy
GO	Graphene oxide
HCN	Potassium/sodium hyperpolarization-activated cyclic nucleotide-gated ion channel

HGF	Hepatocyte growth factor
HNA	Human nuclear antigen
H&E	Hematoxylin and eosin
ICP-MS	Inductively coupled plasma mass spectrometry
IL-10	Interleukin 10
IL-4	Interleukin 4
IL-6	Interleukin 6
iNOS	Nitric oxide synthase
IONP	Iron oxide nanoparticle
iPSC	Induced pluripotent stem cell
JNK	c-Jun N-terminal kinases
LAD	Left anterior descending artery
LPS	Lipopolysaccharide
LVIDd	Left ventricular internal diameters at end-diastole
LVIDs	Left ventricular internal diameters at end-systole
MCP-1	Monocyte chemoattractant protein-1
MEF2C	Myocyte-specific enhancer factor 2C
MGC	Macrophage-targeting/polarizing complex
MHC	Myosin heavy chain
MI	Myocardial infarction
MLC	Myosin light chain
MMC	Mitomycin-C
MNC	Mononuclear cell
MSC	Mesenchymal stem cell
p-c-Jun	Phosphorylated c-Jun
p-JNK	Phosphorylated JNK
PAI-1	Plasminogen activator inhibitor-1
PBS	Phosphate buffer saline
pDNA	Plasmid DNA

PEDF	Pigment epithelium-derived factor
PEG	Polyethylene glycol
PEI	Polyethyleneimine
PlGF	placental growth factor
qRT-PCR	Quantitative reverse transcriptase polymerase chain reaction
rGO	Reduced graphene oxide
RITC	Rhodamine isothiocyanate
ROS	Reactive oxygen species
SMA-α	Smooth muscle actin alpha
TEM	Transmission electron microscopy
TGA	Thermogravimetric analysis
TGF-β	Transforming growth factor beta
TNF-α	Tumor necrosis factor alpha
TTC	Triphenyl tetrazolium chloride
TUNEL	Terminal deoxyribonucleotidyl transferase-mediated biotin-16-dUTP nick-end labeling
uPA	Urokinase-type plasminogen activator
UV-Vis	Ultraviolet-visible spectrometer
VEGF	Vascular endothelial growth factor
vWF	von Willebrand Factor

Chapter 1.

Research backgrounds and objectives

1.1. Myocardial infarction (MI) and current therapeutics

Cardiac disease is one of the leading causes of death worldwide,[1,2] and more than 80 million people have cardiovascular diseases in the U.S. only. Medical costs for all cardiac diseases are expected to be over $800 billion in 2030,[3] and the most common pathway for various forms of heart diseases results in chronic heart failure with a mortality of ~50 % at 5 years.[3] For many of these cardiac disorders, myocardial infarction (MI) contributes to majority of cardiac-associated diseases.[1,4,5] MI occurs from coronary artery occlusion, resulting in low blood supply and oxygen deprivation at the downstream myocardium.[6] Lack of nutrient supply at the myocardium induces necrosis and apoptosis of resident cardiomyocytes, infiltration of inflammatory peripheral macrophages, initiation of inflammation and cardiac tissue remodeling for left ventricular malfunction.[5] Left untreated, these remodeling events further induce cardiac hypertrophy, fibrosis, and electrophysiological challenge in the myocardium for heart failure.[3] Various types of treatments have been introduced for MI, including artery bypass, thrombolytic treatments, and organ transplantation; however, current pharmaceutical approaches cannot provide regenerative tissue engineering therapies for MI.[7-9] Because MI originates from low blood supply and resident cell death, successful therapeutics for MI need to accompany blood vessel formation and cardiac tissue regeneration.[5,9] Additionally, uncontrolled adjustment of inflammation at the damaged myocardium can further exacerbate tissue reconstruction and cause cytotoxic inflammatory damage in the myocardium. In other words, regenerative tissue engineering approaches along with inflammation-modulatory therapeutics are required for effective MI treatment.

Recently, significant advances have been made in MI treatment using cells or biomaterials.[10,11] Cells that can promote tissue regeneration or modulate inflammation, and biomaterials that can encourage such salutary effects of the cells

have gathered much attention for the treatment of MI.[12-16] A number of different cell types, including mesenchymal stem cells (MSCs),[17-20] embryonic stem cells (ESCs),[21-23] induced pluripotent stem cells (iPSCs),[24-26] cardiac stem cells (CSCs)[27,28] and smooth muscle cells[29-32] have all showed salutary effects for MI treatment. Stem cells with cardiac differentiation plasticity, and smooth muscle cells with cardiomyocyte-like muscle phenotype increased wall tension and elasticity. However, crucial therapeutic mechanism involved in cardiac repair has recently been realized to be the paracrine action of the transplanted cells along with their direct differentiation,[33] hence, stem cells that are known as cytokine reservoir have been proposed as the optimal cell source for the treatment of MI.[1,34-36] Stem cells have regenerative potentials to replace the dead cardiomyocytes by differentiation, salvage dying cells, and improve angiogenesis with paracrine action at the infarcted region.[9] Previously, a number of clinical trials using stem cells have shown promising results.[17-20] Among various types of stem cells, MSCs have shown safe and encouraging results in long-term clinical trials.[18,20,37] Transplanted in the infarcted heart, a fraction of MSCs can differentiate into cardiomyocytes and replace infarcted tissues for tissue regeneration and cardiac function improvement.[38-40] However, recent studies demonstrated that the lack of cardiac phenotype in naïve MSCs can pose electrophysiological challenge to worsen MI,[41-44] and cardiac phenotype development in MSCs are required for successful cardiac repair.[45] More recently, the beneficial effects of MSC-derived cytokines have been reported in a number of studies [1,46-48].

In addition to the stem cell therapy, biomaterials-based therapeutics have drawn significant attention as new therapeutic approaches for cardiac tissue engineering.[13,49] Treatments with biomaterials, including nanoparticles, nanofibrous scaffolds, self-assembling peptides, and cardiac patches have all addressed significant improvements in myocardial repair.[13] Biomaterials have mostly been used to deliver therapeutic molecules, including cells, proteins, drugs, and genes.[50-54] Recently, biomaterials that were utilized as cell carriers have demonstrated that

biomaterials can not only deliver cells to the injury site, but also improve the therapeutic potentials of the cells.[45,55-57] These studies showed that biomaterials can significantly improve the therapeutic potentials of the cells by improving their cellular crosstalk or enhance cytokine secretion.[45,55] Additionally, other studies showed the cells implanted at the infarction site with biomaterials exhibited improved cell survival and engraftment for cardiac function improvement.[56,57] These studies show that biomaterials can modulate cell functions to improve therapeutic potentials of the cells, and such perspective provided a new approach of biomaterials-incorporated therapeutics for MI. Biomaterials with topographical, electrical, or chemical properties have been mostly studied to be synergistic with cell therapy, and the combination of cells and biomaterials proposed promising therapeutic options for MI.[45,55,58-70]

1.2. Cell therapy for MI

Stem cells have served as the major source for the treatment of MI for their differentiation plasticity and paracrine activity.[12-28] They propose two widely known therapeutic mechanisms necessary for MI treatment, namely the cardiac differentiation and paracrine activity. Various types of stem cells with their own therapeutic potentials have shown beneficial effects in cardiac tissue regeneration previously,[12-28] however, MSCs with their easy accessibility and safety have emerged as the optimal cell source for MI. More recently, active roles of resident macrophages in inflammation modulation and tissue regeneration have been introduced, and macrophages have demonstrated unique polarization for inflammation initiation and resolution.[6,71-75] To better elucidate their polarization, therapeutic approaches modulating these immune cells at the infarction site have demonstrated successful cardiac repair.[6,71-73,76-81]

1.2.1. MSC-mediated therapy for MI

MSCs have been extensively utilized in cardiac regeneration as the prime cell source, despite the cardiac differentiation plasticity of MSCs is comparatively limited compared to ESCs, iPSCs, or CSCs. MSCs can easily be isolated from the patients, expanded *ex vivo*, and treated in an autologous manner.[9] More recently, the generation and secretion of therapeutic paracrine molecules from MSCs have introduced a paracrine-mediated tissue repair of the injured myocardium.[1,33,82-85] Attributable to these therapeutic properties of MSCs, the POSEIDON trial have demonstrated autologous or allogenic human MSCs can improve cardiac function in patients.[86] Also, the APOLLO trial showed significant enhancement in cardiac function, perfusion and vasculogenesis after the treatment of adipose-derived stem cells.[87] Along with these clinical trials utilizing MSCs, a number of other trials, including the ANGEL, ATHENA, and MyStromal Cell, are currently undergoing for the treatment of chronic MI.[88]

Direct cardiac differentiation of the implanted MSCs has originally been proposed as the major mechanism of stem cell therapy for MI.[9] Hence, differentiating MSCs before *in vivo* implantation has been extensively investigated to improve their therapeutic efficacy. 5-azacytidine (5AZA) has widely been utilized as the primary chemical to differentiate MSCs into cardiomyocytes.[89,90] Besides 5AZA, small molecules such as phorbol myristate acetate have improved cardiomyogenic differentiation of MSCs, which further stimulated electromechanical integration of MSCs at the infarcted myocardium for better cardiac tissue regeneration.[91] Bartunek *et al*. has also demonstrated that pretreatment of MSCs with cardiomyogenic growth factors prior to implantation could also induce cardiac differentiation of MSCs, and enhance cardiac repair when implanted *in vivo*.[92] Other than the utilization of chemical molecules, the co-culture of MSCs with the cardiac cells has also promoted cardiomyogenesis and cardiac priming of MSCs,[45,93-96] which was further promoted through pretreatment of biomaterials[45] or alignment of the cells.[97] Upon implantation into the damaged myocardium, MSCs pre-differentiated into cardiomyocytes have reduced fibrosis, improved angiogenesis and enhanced cardiac functions compared with undifferentiated MSCs.[45,91,92]

Even though the cardiac function improvements after MSC implantation were partially attributable to the differentiation of the MSCs, some studies addressed the population of newly differentiated cardiomyocytes could be too small to explain the significant effects of the MSC therapy.[35] After the onset of MI, millions of resident cardiomyocytes undergo apoptosis and necrosis, hence, the small fraction of MSCs-differentiated cardiomyocytes may not be able to fully explain the meaningful benefits of the implanted MSCs. In such respect, growing evidences suggest that the cytokines secreted from the MSCs could play a major role in promoting cardiac repair.[82,85] MSCs generate and secrete a variety of soluble cytokines that exert paracrine-mediated protective effects on damaged cells and tissues.[33,83,84] These paracrine molecules are responsible for damaged cardiac tissue

reconstruction, neovascularization, blood perfusion, and even immune modulation for cardiac repair.[98] Previous studies demonstrated that the administration of adipose-derived stem cell conditioned medium could recapitulate the beneficial effects of stem cell implantation, suggesting that the therapeutic effects of stem cells could eb attributable to the paracrine activity.[35,47] Gnecchi *et al.* showed that the cell culture media from MSC cultures exhibited cytoprotective effects on primary cardiomyocytes *in vitro* and significantly reduced cardiac fibrosis *in vivo*.[47] Furthermore, secretion of soluble factors by the implanted MSCs protected adjacent cardiomyocytes from necrosis, attenuated cardiac remodeling, and induced angiogenesis.[48] To better elucidate the therapeutic potentials of MSC-derived paracrine molecules, previous studies introduced hypoxic MSC culture conditions or MSC spheroids generating mild hypoxia on MSCs.[45,99-102] Under hypoxic cell culture condition, MSCs secreted broader spectrum of cytokines compared with normoxic cell culture condition. Furthermore, it has also been demonstrated that preconditioning of MSCs in hypoxic cell culture condition could not only stimulate the soluble factor secretion but also result in better cell survival at the infarcted myocardium.[46] Collectively, previous studies showed the improvements in cardiac function was accompanied with both cardiac differentiation and paracrine action of the implanted MSCs. These observations have prompted numerous studies with the development of new therapeutic strategies that can potentiate the therapeutic efficacy of MSCs. In such respect, biomaterials that can greatly improve the cardiac phenotype development in MSCs and harness the paracrine action of MSCs have gained much attention.

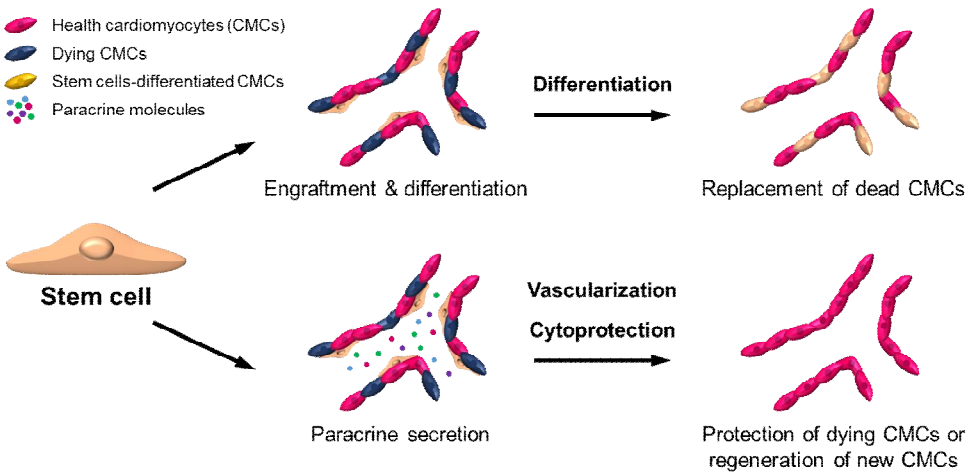

Figure 1.1. Mechanisms involved in stem cell therapy for MI

1.2.2. Macrophage-therapy for MI

Other than the MSC therapy, or biomaterial-based approaches for the synergistic effects with MSCs, researches targeting resident immune cells abundant at the damaged myocardium has attracted much interests to treat MI. Macrophages are the primary and integral responders of the body immune system after MI.[6,71,73,74] Macrophages reside in the healthy heart, and even though their total population may not be as many as that of other immune cells, such as neutrophils or monocytes, their numbers can dramatically vary according to the disease progression.[103] Peripheral monocytes that are derived from spleen or bone marrow can differentiate into macrophage after the onset of MI, and macrophages become the primary cell source that propagate at the damaged myocardium until cardiac fibrosis.[103] During day 1 to 4 after MI, inflammatory peripheral Ly-6C^{high} monocytes are recruited to the myocardium *via* chemotaxis. These inflammatory monocytes further differentiate into classically activated M1 macrophages to initiate inflammation (phase 1).[71,104,105] These M1 macrophages participate in removing dead cells and debris to further initiate granulation and scar formation. Starting at day 4 after the onset of MI, a new type of Ly-6C^{low} monocytes are recruited to the myocardium, and the rebuilding phase begins with their differentiation into alternatively activated M2 macrophages. During this inflammation resolution stage (phase 2), cardiac tissue-dominant populations become reparative M2 macrophages that propagate cardiac repair and angiogenesis.[71,104,105] Unlike M1 macrophages, M2 macrophages contain low contents of inflammatory molecules, instead they release soluble cytokines such as vascular endothelial growth factor (VEGF) and transforming growth factor-β (TGF-β) to support angiogenesis and collagen production. Both M1 macrophages and M2 macrophages are critical in cardiac repair, and ablation of either of healing phase can disturb proper scar formation and tissue regeneration.[106]

Classically activated M1 macrophages secrete pro-inflammatory cytotoxic cytokines such as tumor necrosis factor-α (TNF-α) and interleukin 6 (IL-6), while

alternatively activated M2 macrophages produce anti-inflammatory proteins such as interleukin 4 (IL-4) and interleukin 10 (IL-10).[75,107,108] Tissue regenerative phase by M2 macrophages occurs after the resolution of inflammation by M1 macrophages, hence, the regulation of M1 macrophages is critical in regulating infarct size and left ventricular remodeling. Imbalance between M1 and M2 macrophage population can prolong inflammation, and impair proper tissue reconstruction.[6,71,104] In such respect, previous studies focused on M2 macrophage populations, and demonstrated their importance in cardiac repair.[6,73,74,76,77,104] To control inflammation by M1 macrophages, or to polarize M1 to M2 macrophages, various kinds of supplements have been utilized.[109-115] To better target the cells of interests and deliver therapeutic cargos into the cells, nanomaterials such as alginate,[116] chitosan,[117] cell-based exosomes,[118] or hyaluronic acid[119] gathered much attention. More recently, other molecules that can differentially polarize macrophages and improve cardiac function were introduced. Jeong *et al.* has demonstrated that 5AZA can modulate interferon regulatory factor 1 in macrophages to polarize cardiac tissue resident macrophages toward M2 phenotype.[78] This study showed that M2 macrophage propagation can exert cardioprotective effect to improve cardiac function. Similarly, Kim *et al.* also showed that natural product derivative significantly inhibited the expression of inflammatory factors in macrophages, and increased M2 macrophage population to reduce fibrosis and enhance cardiac performance. Direct polarization of inflammatory M1 macrophages to M2 macrophages were also demonstrated previously.[77] Phosphatidylserine-based liposomes were preferentially uptaken by M1 macrophages at the myocardium and mimicked anti-inflammatory effects of apoptotic cells. Collectively, MI treatment *via* macrophage polarization has always accompanied biomaterials, hence the design of nanomaterials that can better elucidate macrophage modulation has attracted more interests.

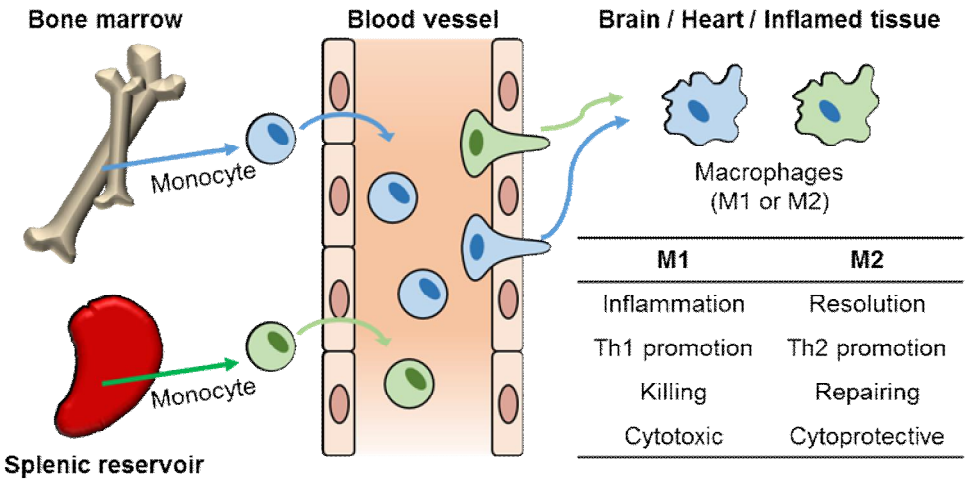

Figure 1.2. Polarization of macrophages for tissue regeneration

1.3. Nanomaterial-mediated cell therapy for MI

To better elucidate and potentiate the therapeutic efficacy of stem cells or target and polarize macrophages for MI treatment, researches regarding nanomaterials have made much advances recently. Biocompatible nanomaterials have previously been utilized to better deliver cells and enhance their survival at the infarct region to promote cardiac repair. Additionally, implantation of functionally designed nanomaterials with cells exploited synergistic effect for the treatment of MI. These nanomaterials could not only enhance the engraftment and survival of the implanted stem cells *in vivo*, but also modulate their functions in a more cardiac repair-favorable manner. More recently, nanomaterials that can modulate intracellular signaling *via* their genuine physicochemical properties have also been introduced. In the following sections, an overview of nanomaterial-mediated cell therapy for cardia repair is provided.

Approach and materials	Cells or biomolecules	Species	Major observations
Cell delivery materials			
Self-assembling peptide [57]	CSC	Mouse	Cardiac function ↑ Fibrosis ↓
Collagen patch [120]	MSC	Rat	MSC engraftment ↑ Cardiac function ↑
PLCL patch [121]	MSC	Rat	Infarct size ↓ Cardiac function ↑
Self-assembling peptide [122]	MNC	Pig	Cardiac function ↑ Cell engraftment ↑ Capillary density ↑
Self-assembling peptide [123]	MSC	Rat	Cardiac function ↑ Infarct size ↓ Capillary density ↑
Self-assembling peptide [124]	CSC	Rat	Vascular enlargement ↑ Cardiac function ↑ Capillary

			density ↑
Nanomaterials with topographical cues			
Nanofibers [97]	MSC / CMC co-culture	N/A	Conduction velocity ↑ Gap junction protein ↑
PCL nanofibers [125]	MSC	Rat	Cardiac function ↑ Infarct size ↓ Fibrosis ↓
Nanofibers [126]	MSC with 5AZA	N/A	Cardiac-specific protein ↑ Gap junction protein ↑
Nanomaterials with electrical conductivity			
Carbon nanotube [67]	MSC	N/A	Cardiac-specific protein ↑ Gap junction protein ↑
Gold nanoparticle [127]	MSC with 5AZA	N/A	Gap junction protein ↑ Cardiac-specific protein ↑
graphene oxide [55]	MSC spheroids	Mouse	Gap junction protein ↑ Cardiac function ↑
Nanomaterials with chemical cues			
Self-assembling peptide [128]	MSC-conditioned medium	Mouse	Contractility ↑ Revascularization ↑ Cardiac function ↑
Graphene [129]	MSC	N/A	Cardiac differentiation ↑ Gap junction protein ↑

Table 1.1. Results of biomaterials and biomaterials-integrated stem cell therapy for MI in animals or *in vitro* studies.

1.3.1 Nanomaterial-mediated stem cell delivery

Although stem cell therapy has emerged as a promising tissue regenerative treatment for cardiac repair, its therapeutic benefit is limited due to poor engraftment and long-term survival of the transplanted cells.[130] Functional engraftment and prolonged survival of the injected stem cells have always been one of the major challenges in stem cell's translational application for cardiac repair.[88] Therefore, the development of biomaterials that can enhance cell survival and extend its reparative action at the infarcted region has been proposed as the critical factor that promotes the beneficiary outcomes of the stem cells.[131] Various types of nanobiomaterials have been introduced as efficient cell delivery systems, and their therapeutic effects for MI have been investigated.

To improve stem cell retention at the infarct, nanostructured cardiac patches and injectable peptides have been studied.[13,132-134] Cardiac patches are placed on the epicardial surface of the infarcted heart, hence, these patches require unique structural and physicochemical properties that are compatible with the native heart tissue. Therefore, natural protein that is predominant at the heart tissue, such as collagen, has drawn much attention.[13] Simpson *et al.* have previously demonstrated that collagen-based cardiac patches seeded with MSCs improved MSC survival *in vitro*, and successfully restored cardiac function after implantation.[120] Compared to the cells delivered without collagen patch, which exhibited less than 11 % of cell engraftment, MSCs delivered with patches showed 23 % cell engraftment for cardiac function improvement. Cardiac patches without MSCs showed no significant improvements in cardiac function, suggesting that the major therapeutic efficacy was attributable to the increased survival of the stem cells. Along with collagen, synthetic materials have also been investigated for cardiac patch development.[13] Synthetic polymer poly(lactide-co-ε-caprolactone) has shown elasticity and biodegradability required for cardiac patch, and has been vigorously investigated.[13] Poly(lactide-co-ε-caprolactone)-based cardiac patch seeded with MSCs exhibited enhanced MSC survival and improved cardiac

function after implantation *in vivo*.[121] Injection of MSCs alone also showed partial improvement in cardiac function, while scaffold provided fertile microenvironment for MSCs to increase their viability and improve cardiac repair. Similar to the previous studies, cardiac function enhancement was not observed with cardiac patch alone. Even though aforementioned studies showed no beneficial effect of cardiac patch alone for cardiac function,[120,121] contradictory results have also been reported in other studies.[13] Further studies are required to better elucidate the efficacy of cardiac patches for cardiac repair.

Along with cardiac patches, self-assembling peptide nanofibers has also been utilized as cell delivery vehicle for MI treatment.[122,123,135] Previous studies demonstrated that self-assembling peptides greatly improved the viability of the implanted cells and significantly facilitated cardiac repair when implanted with MSCs, skeletal myoblasts, or bone marrow mononuclear cells.[122,123,135] Guo *et al.* have further integrated self-assembling peptides with CSCs and demonstrated their therapeutic applications in rat MI model.[124] Upon transplantation at the infarcted region, self-assembling peptide bundled into nanofibrous scaffolds and provided suitable microenvironment for cell survival to inhibit cellular apoptosis and necrosis caused by anoxia. Subsequently, increased survival of the stem cells resulted in enhanced cardiac differentiation of CSCs. Compared to the groups treated with stem cells or self-assembling peptides alone, the combination of stem cells with the peptides significantly improved cardiac function.

1.3.2 Topographical cues of nanomaterials for stem cell and macrophage behavior modulation

Previous studies further elaborated the physicochemical properties of biomaterials, and elucidate the roles of nanotopographical cues on modulating cell behaviors, such as cell differentiation, function, and gap junction expression. Previous researches have mainly focused on the innate properties of the heart, because application of cardiac-mimetic characteristics on therapeutic biomaterials may pose significant effects on the cells.[10,11,13] For efficient cell signal transduction and synchronous contraction of the cardiac muscles, cardiac cells need to be aligned for proper gap junction protein distribution.[43] To mimic such property of the heart, nanotopography-associated approaches have been introduced to modulate cell behaviors for better cardiac repair.

A previous study demonstrated that aligned topography or electrical field stimulation for cell alignment is crucial for orientation and elongation of cardiomyocytes.[58] The study showed that both topographical cue and electrical field stimulation are critical to preserve cardiac cell properties, while a combination of these two factors further promoted the contractile property of cardiomyocytes. Thereafter, to further evaluate the effect of nanotopography on cardiac cell behavior, a number of researches introduced aligned nanofibers, which mimic the nanostructures of natural extracellular matrices of the heart tissue,[59] that can improve alignment[60] and beating of cardiomyocytes.[62] Cardiomyocytes cultured on aligned nanofibers showed higher beating frequency compared to those cultured on randomly-oriented nanofibers. Upon transplantation *in vivo*, cardiomyocyte-seeded aligned cardiac patch greatly improved cardiac performance, while randomly-oriented patch exhibited serious cardiac deterioration for exacerbated cardiac function.[62] This study indicated that the anisotropic characteristics of the biomaterials can greatly regulate the behaviors of cardiac cells and proper design of biomaterials can be integrated into the development of translational cell therapy for

better cardiac tissue engineering. Kim *et al.* have further showed that aligned nanotopography could enhance the adhesion, proliferation, and cardiomyogenic differentiation of CSCs.[61] Implantation of stem cell-seeded scaffolds with proper alignments demonstrated better tissue integration attributable to the anisotrophic structure of the biomaterials. Subsequently, these cardiac patches reduced cardiac fibrosis and improved cardiac performance. Kang *et al.* have recently demonstrated that MSCs cultured on aligned polycaprolactone nanofibers exhibited enhanced expression of angiogenic and cardio-protective genes.[125] Furthermore, this study exhibited that MSCs cultured on anisotropic nanofibers demonstrated aligned cell phenotypes similar to native cardiac tissue, and the transplantation of such cardiac patch with aligned MSCs significantly improved cardiac function in rat MI model. Pijnappels *et al.* showed that alignment of MSCs in the patterned substrate can significantly improve cardiac differentiation of MSCs and their integration with cardiac cells in co-culture.[97] Alignment of MSCs also greatly improved conduction velocity generation in MSCs and the expression gap junction protein, connexin 43 (Cx43), necessary for intercellular crosstalk.

Topographical cues have also showed cell behavior modulation in macrophages as well. A previous study showed that macrophage shape change using nanotopographical cue can polarize inflammatory M1 macrophages to inflammation-resolving M2 macrophages.[136] Elongation of macrophages on micropatterned substrate greatly changed extracellular matrix architecture within the macrophages, and inhibited inflammatory cytokine secretion. Chen *et al.*[137] and Refai *et al.*[138] have further introduced the topographical effects on macrophage phenotype modulation and regulation.

1.3.3 Electrical properties of nanomaterials for stem cell behavior modulation

In addition to the anisotropic property, electrical conductivity is another genuine property of the cardiac tissue that is critical in developing therapeutic biomaterials for MI. Cardiac cells need gap junction-based intercellular coupling for electrical signal transduction and proper heart function. Therefore, previous approaches with electrochemically unsuitable treatments posed electrophysiological inharmony and caused arrhythmic risks upon application.[43] Hence, previous studies have focused on developing conductive nanobiomaterials that can further be integrated with original cardiac therapeutics to induce tissue compatible treatments.[139-141]

Integration of carbon nanofibers or carbon nanotubes with polymer scaffolds showed promising therapeutic potentials, and promoted the adhesion and proliferation of cardiomyocytes[63] and cardiac progenitor cells[64]. In addition, carbon-based nanomaterials significantly promoted the expression of Cx43 in these cardiac cells and stimulated electrical coupling among the cells. Cx43 is particularly important because it is essential for intercellular coupling, arrhythmic risk reduction, and functional differentiation of MSCs.[43,91,100,142] Martines *et al.* and Kharaziha *et al.* have observed improvements in the electrophysiological functions of cardiac constructs decorated with carbon nanofibers[68] and carbon nanotubes[70], respectively. In addition to carbon-based materials, gold nanomaterials have also gathered much attention for their excellent conductivity, and further been utilized to improve Cx43 expression and therapeutic efficacy of the cell therapy. Previous studies demonstrated that cardiomyocytes cultured in hydrogel scaffolds integrated with gold nanoparticles[65] or gold nanowires[66] can significantly increase Cx43 expression. Additionally, cardiac tissues grown on conductive hydrogels exhibited synchronous contraction upon electrical stimulation, demonstrating the importance of conductivity in heart function.[66] Such conductive properties of biomaterials have further been integrated to stem cell therapies for cardiac repair. Mooney *et al.* have

showed that electrical stimulation of carbon nanotube-embedded MSC-laden scaffolds significantly enhanced cardiomyogenic differentiation of MSCs.[67] Electrical stimulation repolarized MSCs perpendicular to the direction of the current, and greatly augmented the expression of cardiac biomarkers. Crowder *et al.* further investigated the effect of carbon nanotube-containing scaffolds without electrical stimulation on cardiac differentiation of MSCs,[69] demonstrating that electrically conductive nanobiomaterials alone can promote the cardiac differentiation of MSCs. Conductive materials have also been utilized together with conventional cardiac differentiation methods to stimulate MSCs differentiation. Ravichandran *et al.* demonstrated that 5AZA treatment on MSCs seeded on gold nanoparticle-decorated nanofibrous scaffold greatly stimulated MSC differentiation toward cardiomyogenic lineage.[127] Furthermore, Park *et al.* have recently demonstrated conductive nanomaterials can also participate in MSCs function modulation.[55] This study showed that electrically conductive reduced graphene oxides (rGO) incorporated in MSC spheroids significantly enhanced Cx43 expression of MSCs, while insulating graphene oxide flakes reduced the expression of Cx43. Ultimately, injection of MSC spheroids integrated with rGO significantly reduced cardiac fibrosis and improved cardiac performance.

1.3.4 Intrinsic properties of nanomaterials for stem cell and macrophage behavior control

Recently, the intrinsic chemical properties have been applied to regulate and modulate the functions stem cells and macrophages for the treatment MI. Carbon-based nanomaterials also showed much potential in stimulating cell behaviors. Park *et al.* have recently showed that graphene substrate can stimulate cardiac differentiation of MSCs.[129] Graphene substrate stimulated the expression of extracellular matrix in MSCs and further initiated signaling transduction related to cardiomyogenic differentiation.

Nanomaterial-based cell function modulation has also been introduced in macrophages for immunotherapy of MI. A number of particles showed anti-inflammatory effects within the macrophages to better inhibit M1 differentiation of macrophages, and reduce inflammatory cytokine secretion.[77,113-115,143,144] Hirst *et al*. demonstrated the cerium nanoparticles can significantly downregulate the generation of reactive oxygen species (ROS) within the inflammation stimulated macrophages.[113] Similarly, anti-inflammatory effects of nanomaterials were also demonstrated using gold nanoparticles.[114,115] Previous studies exhibited that pre-incubation of macrophages with gold nanoparticles can greatly reduce inflammation-related signal transduction within the cells to prevent inflammatory differentiation. Harel-Adar *et al*. have further demonstrated macrophage-polarizing nanoparticle *in vivo*. Uptake of phosphatidylserine-based nanoliposomes by the macrophages at the cardiac infarction area successfully mimicked the anti-inflammatory effects of apoptotic cells, and polarized local M1 macrophages to M2 macrophages to reduce cardiac fibrosis and improve cardiac function.

1.4. Limitations of previous cell or nanomaterial-mediated therapy

Previous studies achieved significant advances in the development biomaterial-assisted cell therapeutics for the treatment of MI. Major approaches using stem cells for the treatment of MI focused on their cardiac differentiation prior to *in vivo* transplantation, while macrophage-oriented treatment development focused on inflammation regulation at the infarcted region. Even so, limitations in combinatorial approaches between biomaterials and cell therapies remain.

Stem cell treatments for MI mainly focused on the cardiac differentiation of MScs prior to *in vivo* transplantation. Proteins or chemicals have mostly been used to initiate MSC differentiation, and cell behavior modulation using cell microenvironment has rarely been studied. Co-culture of MSCs with cardiac cells has been proposed as the cardiac mimetic microenvironment that stimulates MSC differentiation, however, their efficiency needs much improvements. Additionally, the paracrine activity needs better to be elucidated as the major therapeutic mechanism for cardiac repair, hence, therapeutic approaches that can integrate stem cell paracrine effects are required.

Macrophage-oriented MI treatments accompany inflammation regulation and inhibition of inflammatory cytokines. Nanoparticles of drugs have been utilized to directly reduce inflammatory cytokine downregulation or convert M1 macrophages to M2 macrophages. However, regulation of cardiac fibrosis and improvements in tissue regeneration need not only the regulation of M1 macrophages, but also the propagation of M2 macrophages for anti-inflammatory cytokine production. Treatment options that can inhibit M1 differentiation of resident macrophages, while improve M2 differentiation of these cells during the inflammatory phase need better elucidation as an efficient MI therapy.

1.5. Iron oxide nanoparticles (IONPs) and graphene oxide (GO) for cell modulation and tissue engineering applications

Iron oxide nanoparticle (IONP) is one of the most widely used nanoparticles for cell labeling or drug delivery, and the use of IONPs in cell studies has been shown safe and effective.[145,146] In spite of their plasticity in biomedical applications, IONP's innate properties have rarely been spotlighted. More specifically, how IONPs can influence intracellular signaling pathway has not been clarified, and the role of IONPs within the cells has not been studied. IONP can be decomposed into ferric ions under low pH condition and function as an ion delivery carrier. Previously, metal ion delivery for cell function control has been introduced,[147] and some studies have integrated IONPs to control cell behaviors *in vitro*,[148-150] but no studies integrated nanoparticles' innate properties into therapies. Also, the signaling transduction for nanoparticle-induced cell behavior modulation need clarification for potential application.

Graphene oxide (GO) has recently been utilized in biomedical engineering field as a gene or drug delivery carrier.[151-155] Similar to IONP, GO has majorly been used as a delivery tool and their physicochemical properties have not been clearly elucidated in cell studies. More specifically, GO has unique chemical structure with carbon atoms in hexagonal lattice form, however, how this innate property of GO can affect intracellular behaviors has not been closely studied. Recently, GO and many other graphene derivatives have been shown to possess antioxidant characteristic based on their sp^2 chemistry, yet their role in biomedical application has been limited. The functionality of GO as a gene carrier has well been introduced, hence, elucidating the natural properties of GO and applying them in tissue engineering therapeutics can synergize with current treatment options for efficient cardiac repair.

1.6. Research objectives

For the treatment of MI, therapeutics using cells and biomaterials have made great advances. Stem cells with differentiation plasticity, or macrophages with differential polarization phenotype showed promising results in treating cardiac infarction. Moreover, these therapeutic potentials of stem cells and macrophages have further been promoted using biomaterials. Nanoparticles, in particular, have exhibited excellent delivery capabilities and demonstrated synergistic therapeutic potentials when combined with cell therapies. For majority of nanoparticle-based treatment options for MI, however, previous studies mostly focused on passive role of nanoparticles and the effects of innate properties of nanoparticles in cell behavior modulation have not been studied. More specifically, previous studies rarely focused on potentiating the biological role of nanoparticles and the studies about how nanoparticles can regulate intracellular mechanism transduction and influence cell behaviors have been scarce.

In this dissertation, novel biological roles of nanoparticles and their synergistic effects with cell therapeutics for the treatment of cardiac infarction are introduced. First, I investigated how IONPs can function as a natural metal ion delivery carrier and transport ferric ions within the cells to modulate intracellular signaling transduction. More specifically, I investigated how IONP internalization can regulate gap junction protein expression in cardiac cells and improve intercellular crosstalk in stem cell co-culture system to potentiate cardiac priming of MSCs. Secondly, the innate chemical property of GO within the cells have been examined to better elucidate anti-inflammatory role of GO in macrophage immune modulation. Additionally, such genuine properties of GO was combined with gene delivery therapy for better cardiac regeneration. Collectively, the therapeutic efficacy of IONP and GO in treating MI was evaluated using mouse or rat infarction models.

Chapter 2.

Experimental procedures

2.1. Preparation of iron oxide nanoparticle (IONP)

Iron (III) acetylacetonate (0.706 g, Acros, 99 %) was dissolved in benzyl ether (10.40 g, Aldrich, 99 %) solution containing oleic acid (1.27 g, Aldrich, 90 %) and 4-phenylcarboxylic acid (0.4 g, Acros, 95 %). The solution was degassed under vacuum for 1 hour, refilled with argon, and heated to 290 ^{o}C with a heating rate of 20 ^{o}C/minute. After maintaining 290^{o}C for 30 minutess, the solution was cool to room temperature. To precipitate the resulting nanoparticles, acetone or ethanol was added to the solution, which was centrifuged at 1700 rpm for 10 minutess. The separated precipitate was dispersed in nonpolar chloroform. The shape and size of the nanoparticles were confirmed using transmission electron microscope operating at 200 kV. To make the nanoparticles hydrophilic, they were then encapsulated using 1, 2-distearoyl-sn-glycero-3-phosphoethanolamine-N-[methoxy(polyethylene glycol)-2000] (DSPE-mPEG) and 1, 2-distearoyl-sn-glycero-3-phosphoethanolamine-N-[amino(polyethylene glycol)-2000] (DSPE-PEG-NH2, Avanti Polar Lipids, Inc., Alabaster, AL). Typically, 10 mg of DSPE-mPEG and DSPE-PEG-NH2 was added to 2 ml of IONP solution in chloroform. After evaporating the solvent, 2 ml of sterilized water was added and sonicated to disperse the nanoparticles. Excess PEGylated phospholipids were removed using ultracentifugation at 20,000 rpm for 1 hour. Subsequently, aggregates or contaminants were removed using a cellulose acetate syringe filter (Advantec, Japan). To conjugate fluorescence dyes, nanoparticles with amine groups were dispersed in phosphate buffer saline. 1 mg of rhodamine B isocthiocyanate (RITC) was added, and the solution was stirred for 6 hours. Excess RITC was removed using a desalting column (PD-10, GE Healthcare Life Sciences, Pittsburgh, PA, USA).

2.2. Characterization of IONP

IONPs were characterized by transmission electron microscopy (TEM), dynamic light scattering (DLS), and inductively coupled plasma mass spectrometry (ICP-MS). TEM analysis was conducted using TEM (JEOL 2100, JEOL, Japan) operated at 100 kV. Size of IONP was analyzed using DLS (DLS-7000, Otsuka, Japan). Iron contents within the H9C2 cells after IONP uptake was analyzed using ICP-MS (ICP-7500, Shimadzu, Kyoto, Japan).

2.3. Cell preparation and IONP-based cell culture

2.3.1. MSC and H9C2 culture using IONP and nanoparticle toxicity

Human bone marrow MSCs were purchased from Lonza (Walkersville, MD, USA), and rat cardiac myoblast cell line H9C2 cells were purchased from Korean Cell Line Bank (Seoul, Korea). Both MSCs and H9C2 cells were cultured in growth medium consisting of low-glucose DMEM (Gibco, NY, USA) supplemented with 10 % (v/v) FBS, 100 units/ml penicillin, and 100 μg/ml streptomycin. To prepare IONP-internalized IONP(+) H9C2 cells, nanoparticles were added into the medium at a concentration of 40 μg/ml. After 24 hours, the cells were washed thoroughly with PBS. For the detection of internalized IONPs, the cells were analyzed using TEM and fluorescent microscopy (Model IX71, Olympus, Tokyo, Japan). The cytotoxicity of IONP was measured using cell counting kit (CCK) and quantitative reverse transcriptase polymerase chain reaction (qRT-PCR). Intercellular iron contents were then measured using inductively coupled plasma mass spectrometry (ICP-MS; ICPS-7500, Shimadzu, Kyoto, Japan). To compare the cytotoxicity of IONPs to direct iron ion delivery, H9C2 were treated with 40 μg/ml IONPs, or with the same molar concentration of $Fe^{2+/3+}$ in 40 μg/ml IONPs, and CCK assay was performed after 24 hours. To evaluate the intracellular signaling cascade upon IONP uptake, western blot analysis was performed.

2.3.2. IONP-based MSC co-culture

To prepare the IONP(+) H9C2 feeder layer, H9C2 cell proliferation was first inhibited with mitomycin-C (MMC; Sigma, USA) at a concentration of 10 μg/ml for 2 hours. The cells were washed with PBS and the media was switched to fresh growth medium. IONPs were then added into the medium. After 24 hours of incubation, the cells were washed with PBS and plated at a density of 3000 cells/cm^2 in 150-mm culture dishes. Two days later, $2x10^5$ MSCs were seeded into the IONP(+) H9C2 cell-plated 150-mm culture dishes. Cell number ratio of 2:1 between IONP(+) H9C2 and MSCs was used in this study because when 1:1 ratio was used for co-culture, mitomycin-C-treated, non-proliferating IONP(+) H9C2 were overwhelmed by proliferative MSCs after 1 week, limiting cell-cell crosstalk. When cell number ratio of 3:1 was used, on the other hand, there were comparatively too many IONP(+) H9C2 compared to MSC, resulting in non-effective cell-cell crosstalk. To maximize cellular contacts between IONP(+) H9C2 and MSCs, we optimized the cell number ratio to 2:1 between IONP(+) H9C2 and MSCs.

2.3.3. IONP-mediated cell sorting after co-culture

After 7 and 14 days of co-culture, the mixture of MSCs and IONP(+) H9C2 cells were collected by trypsinization, resuspended in growth medium and collected into Eppendorf tubes. A neodymium magnet was placed right next to the tube to induce cell sorting while the cell suspension was continually gently mixed for dispersion. After 2 minutes of sorting, macroscopically dark colored IONP(+) H9C2 cells were magnetized to the magnet and accumulated at the bottom of the tube. Only the top suspension of the cells was collected and resuspended in growth medium. Magnet-induced cell sorting was repeated 5 more times. After the 6^{th} sorting, the homogenous MSC suspension was collected, and the purity was evaluated by immunofluorescent staining for HNA and by fluorescence activated cell sorting (FACS; FACS Aria II; BD Bioscience, San Jose, CA, USA).

2.4. *In vitro* analysis

2.4.1. TEM analysis

H9C2 cells internalized with IONPs were first fixed with Karnovsky's solution (EMS Hatfield, PA, USA) for 24 hours at 4°C, then washed three times with 0.05 M sodium cacodylate buffer. Samples were fixed with 2 % osmium tetroxide (Sigma) for 2 hours at 4°C washed three times with distilled water, dehydrated through a series of graded ethanol (50, 60, 70, 80, 90, 95, and 100 %) and propylene oxide rinses, and finally embedded in Suppr's resin (Agar Scientific, Essex, UK). Samples were polymerized at 60°C for 24 hours and sliced into slices using ultramicrotome (MTX, RMC, Arizona, USA). TEM sections were observed with Libra 120 microscopy (Carl Zeiss, Oberkochen, Germany).

2.4.2. Fluorescent images

Uptake of RITC-conjugated IONP by H9C2 cells were analyzed using fluorescent microscopy (Model IX71, Olympus, Tokyo, Japan). IONP-internalized H9C2 cells were fixed with 4 % paraformaldehyde (PFA) for 15 minutes at room temperature. Samples were then washed two times with PBS and counterstained with 4,6-diamidino-2-phenylindole (DAPI, Vector Laboratories, USA) for nuclear staining.

2.4.3. Quantitative reverse transcriptase polymerase chain reaction (qRT-PCR)

Total RNA was extracted from the cells using 1 mL of TRIzol regent (Invitrogen, USA) and 200 μL of chloroform. Extracted samples were then centrifuged at 12,000 rpm at 4^{o}C for 10 minutes. Collected RNA pellets were washed with 75 % (v/v) ethanol and dried. Dried RNA samples were dissolved in RNase-free water. To prepare cDNA for qRT-PCR, 800 ng RNA from each samples was reverse-transcribed using GoScript Reverse Transcriptase (Promega, USA). Expression of genes were measured using StepOnePlus real-time PCR system (Applied Biosystems, Foster city, CA, USA) with FAST SYBR Green PCR master mix (Applied Biosystems) for 45 cycles. All of the data were analyzed using $2^{-\Delta\Delta Ct}$ method. Four samples were analyzed per each group.

2.4.4. Western blot assay

Cell lysate was prepared using sodium dodecyl-sulfate (DS) sample buffer (62.5 mM Tris-HCl (pH6.8), 2 % (w/v) SDS, 10 % (v/v) glycerol, 50 mM dithiothreitol, and 0.1 % (w/v) bromophenol blue). The total concentration of the protein was determined with bicinchninic acid protein assay (Pierce Biotechnology, Rockford, IL) and further performed through 10 % (w/v) SDS-polyacrylamide gel electrophoresis. Proteins were transferred to Immobilon-P membrane (Millipore Corp., Bedford, MA) and probed with antibodies against c-Jun N-terminal kinases (JNK; Abcam, Cambridge, UK), phosphorylated JNK (*p*-JNK; Abcam), c-Jun (Abcam), phosphorylated c-Jun (*p*-c-Jun; Abcam), connexin 43 (Cx43; Abcam) and beta actin (ß-actin; Abcam). Proteins were incubated with horseradish peroxidase-conjugated secondary antibody (Santa Cruz Biotechnology, Santa Cruz, CA) for 1 hour at room temperature, and blots were developed using chemiluminescence detection system (Amersham Bioscience, Piscataway, NJ, USA).

2.4.5. Calcein-AM dye transfer assay

H9C2 cells were first internalized with IONPs and further stained with 10 μM DiI and 10 μM Calcein-AM. After through washing, IONP(+) H9C2 were co-cultured with MSCs for 48 hours. Transferred calcein-AM fluorescent dye was evaluated using fluorescent microscopy.

2.4.6. Immunocytochemistry

cMSCs from IONP-mediated co-culture were first stained with primary antibodies against human nuclear antigen (HNA) or Cx43 (Abcam), and the signal was visualized with FITC or rhodamine-conjugated secondary antibodies, respectively (Jackson ImmunoResearch Laboratories, USA). The slides were counterstained with DAPI to stain the nuclei of the cells.

2.4.7. Paracrine profile analysis

To evaluate the paracrine molecule secretion activity of cMSCs after 1 week time point, 2-week-co-cultured cMSCs were sorted and plated to a 100 mm culture dish. One week later, the conditioned medium was collected for angiogenesis array. For the paracrine secretion activity characterization, initial number of the plated cells was kept the same for all groups (Unmodified MSCs, MSCs co-cultured with IONP(-)H9C2, cMSCs 2 days and cMSCs 1 week). Quantitative analysis for angiogenesis array was performed with densitometry using ImageJ software from National Institutes of Health.

2.5. Rat MI model and cMSC treatment

Myocardial infarction was induced in 8-week-old Sprague-Dawley rats (240±10 g) obtained from Samtako Bio (Osan, Korea), as previously described.[156] Briefly, after general anesthesia, the rat heart was exposed at the left costal rib through incision. Then, the left anterior descending artery (LAD) was ligated with a 6-0 silk suture (Ethicon, Cincinnati, OH) for 1 hour and then reperfused. Infarction was macroscopically visualized as blanching in the left ventricle. For sham-operated Normal groups, no ligation was performed. For intramyocardial injection of MSCs and cMSCs, $1x10^6$ cells were injected in a total volume of 60 μl PBS using a 30-guage needle (BD Bioscience) 1 hour after artery occlusion. Injections were made at the anterior and lateral aspects of the infarction border zone. For saline injection, 60 μl of saline was injected at the same sites. The use of animals was in accordance with the International Guide for the Care and Use of Laboratory Animals. The experimental protocol was approved by the Animal Research Committee of Yonsei University College of Medicine (IACUC No. 2012-0202-2).

2.6. *In vivo* assessment

2.6.1. Histological and immunohistochemical assessment

Two weeks after cell transplantation, the animals were sacrificed and the heart tissues were fixed with 10 % (v/v) formaldehyde, embedded in paraffin, and sliced into 5 μm sections. To assess fibrotic tissue formation after infarction, the heart sections were stained with Masson's trichrome. The area of fibrotic tissue was measured using MetaMorph software (Molecular Devices, Sunnyvale, CA), and further expressed as the percentage to the total left ventricle.

To measure the infarct size of the myocardium, hearts were sectioned transaxially and incubated in TTC (Sigma) for 20 minutes under 37 ^{o}C, followed by 10 % formalin fixation at 2-8 ^{o}C overnight. Infarcted region appeared yellow-white, and viable myocardium appeared red. Heart sections were photographed with a digital camera, and the area was measured with densitometry using ImageJ software. Infarction area was expressed as the percentage of yellow-white tissue to the total left ventricle.

Vessel density at peri-infarct was evaluated by staining tissue sections with anti-vWF antibody (Abcam) and anti-SMA-α antibody (Abcam). Fluorescent detection of vWF and SMA-α was visualized by FITC or Rhodamin-conjugated secondary antibody, respectively. Vessel structures positive for vWF or SMA-α expression were quantified for 4 animals per group, 2 slides per animal and 3 to 4 fields per slide.

To evaluate tissue apoptosis, TUNEL (Chemicon, Billerica, MA) was used according to the manufacturer's instruction. The number of apoptotic cells was counted for 4 animals per group, 2 slides per animal and 3 to 4 fields per slide. For the detection of Cx43 at the borderzone, anti-Cx43 antibody (Abcam) was used and detected with FITC-conjugated secondary antibody. Quantitative analysis was performed with densitometry using ImageJ software.

2.6.2. Evaluation of cardiac performance

Two-dimensional transthoracic echocardiography was performed at baseline (Normal) and for all experimental groups (n=6 per group) 2 weeks after treatment. Assessments were carried out by an experienced cardiologist, blinded to the identity of the experimental groups. Images were acquired with a 14 MHz linear-array transducer interfaced with an ultrasound system (Vivid q, GE, Vigmed Ultrasound, Horten, Norway). Left ventricular internal diameters at end-systole (LVIDs) and at end-diastole (LVIDd) were measured from M-mode echocardiography in the midpapillary short axis view.

2.7. Preparation of GO and GO derivatives

Branched PEI with molecular weight of 25 kDA was purchased from Sigma-Aldrich (USA), and N-(3-dimethylaminopropyl-N′-ethylcarbodiimide) hydrochloride (EDC) was purchased from TCI Co.,Ltd. (Japan). PEG was purchased from Sunbio (Korea), and FA-PEG was purchased from Nanocs (USA). GO was synthesized from graphite powders based on Hummers method[157] with some modifications. 1.0 g of graphite powders and 0.5 g of P_2O_5 were added into 6 mL of 98 % H_2SO_4. The mixture was kept at 85°C for 5 hours. Deionized water (200 mL) was then added to the mixture and left overnight, followed by the filtration through anode aluminum oxide (AAO) membrane with 0.2 μm pore size. The solid was dried in vacuum at 35°C overnight after through wash with deionized water. Thereafter, 1.0 g of dried product and 0.5 g of $NaNO_3$ were added to 23 mL of 98 % H_2SO_4 in ice bath and kept for 40 minutes without stirring. Then, 6.0 g of $KMnO_4$ was slowly added with stirring to keep the temperature below 10°C. Then, the mixture was heated to 35°C and stirred for 18 hours, followed by the addition of 140 mL of deionized water and 10 mL of 30 % H_2SO_4. The mixture was centrifuged for 30 minutes at 10,000 rpm and the supernatant was decanted. The solid was washed with deionized water and centrifuged with 250 mL of 10 % HCL at least 3 times until the pH reached 7. Mixture was vacuum filtered and the solid was dried overnight at 35°C. For the preparation of GP, GPP or MGC, EDC and NHS mixture was added to GO solution (5 mg/mL) under sonication for 10 minutes. PEI (0.1 mg/ml) was then added into the mixture dropwise, followed by 30 minutes of sonication and stirring at room temperature for 24 hours. Thereafter, FA-PEG (5 mg/ml) was activated with EDC and NHS and added into PEI-GO solution under sonication for 30 minutes, followed by stirring at room temperature for 24 hours. The solid was washed 3 to 5 times with deionized water under vacuum filtration. After the filtration, solid was dried overnight at 35°C. For the preparation of GP, no PEG was added after PEI conjugation. For the preparation of

MGC, FA-PEG was used instead of PEG, and the whole procedure was performed identically.

2.8. Characterization and DNA conjugation of GO derivatives

GO and GO derivatives were characterized by Raman spectroscopy, ultraviolet-visible spectrometer (UV-Vis), transmission electron microscopy (TEM), fourier transform infrared spectroscopy (FT-IR), dynamic light scattering (DLS), electrophoretic scattering light (ELS), and thermogravimetric analysis (TGA). The chemical structural characteristics of GO and various types of GO derivatives were investigated using Rama spectroscopy (RM 1000-Invia, Renishaw, UK). Raman spectra were recorded using an argon ion layer as the excitation source, and the scan range was set from 1000 to 2500 cm^{-1}. The optical transmittance of GO derivative for antioxidant chemistry activity was measured using UV-Vis spectrometer (Nanodrop 2000C, Thermo Scientific, USA). TEM analysis was conducted using TEM (JEOL 2100, JEOL, Japan) operated at 100 kV. Evaluation of chemical modification on GO was assessed using FT-IR (Nocolet 6700 spectrometer, Thermo Scientific, USA). Size and zeta potential of GO derivatives were analyzed using DLS (DLS-7000, Otsuka, Japan) and ELS (ELS-8000, Otsuka, Japan). To evaluate DNA conjugation, 1.5 % agarose gel electrophoresis was performed for various N/P ratios

2.9. Cell preparation and uptake of GO derivatives

2.9.1. Culture of mouse bone marrow-derived macrophages

Mouse bone marrow-derived macrophages (mBMDM) were isolated and differentiated from 6-week-old female BALB/c mice.[158] Primary macrophages were differentiated for 7 days in macrophage differentiation media (high-glucose DMEM (Gibco) supplemented with 10 % (v/v) FBS), 100 units/mL penicillin, 100 μg/mL streptomycin, and 30 % L929 cell-conditioned medium L929 cell-conditioned medium was prepared by growing L929 cells in high-glucose DMEM containing 10 % FBS, 100 units/mL penicillin, 100 μg/mL streptomycin for 10 days. The medium containing macrophage colony stimulating factor secreted by L929 cells was harvested and filtered through a 0.22 mm filter. At day 3, 3 mL extra macrophage differentiation media was added to mBMDM culture, and mBMDMs were collected at day 7 for further *in vitro* analysis.

To prepare MGC-positive mBMDMs, nanoparticles were added into the cell culture medium at a concentration of 10 μg/mL. After 4 hours, the cells were washed thoroughly with PBS. MGC-laden macrophages were further used for *in vitro* assays. For the detection of internalized GO nanoparticles, macrophages were analyzed using TEM and fluorescent microscopy (Model IX71, Olympus, Tokyo, Japan). The cytotoxicity of GPP and MGC was measured using MTT 24 or 72 hours after the treatments.

2.9.2. Uptake and cellular affinity of GO derivatives

Rat cardiomyocytes and cardiac fibroblasts were purchased from Lonza (Walkersville, MD). Cardiomyocytes, cardiac fibroblasts and BMDMs were labelled with green fluorescent DiO, while GPP and MGC were labelled with DiI for 4 hours. Cells were treated with GPP or MGC at 10 μg/mL for 30 minutes, and cellular uptake was analyzed using a fluorescent microscopy. Quantitative analysis for cellular uptake efficiency was performed with ImageJ software from National Institutes of Health.

2.10. *In vitro* analysis

2.10.1. Metal chelating assay

Metal chelating activities of GO or MGC were evaluated using the method of previous studies with some modifications.[159,160] GO or MGC dispersed in deionized water at various concentrations (0, 10, 50, 100, 200, or 500 μg/mL) was separately added to 2.8 mL of deionized water, followed by mixing with 50 μL of 2 mM $FeCl_2 \cdot 4H_2O$ and 150 μL of 5 mM ferrozine (Sigma). The control group contained all the reagents without the sample. The mixture was shaken vigorously and left at room temperature for 15 minutes. Absorbance levels of the solutions were then measure using a spectrophotometer at 562 nm. All measurements were run in triplicate and averaged. The percentage of inhibition activity of Fe^{2+} complex formation was calculated using the formula given below:

Fe^{2+} formation inhibition (%) = $[(A_{NT} - A_{562}) / A_{NT}] \times 100$, where A_{NT} denotes the absorbance of the control group, and A_{562} implies the absorbance of the samples.

2.10.2. Intracellular reactive oxygen species (ROS) generation

To further measure intracellular ROS level, mBMDMs were pre-incubated with or without MGC for 2 hours, and then treated with 200 ng/mL LPS for 24 hours. After washing the cells with PBS, the medium was changed to serum-free DMEM containing H_2DCFDA 20 μM (Invitrogen, Carlsbad, CA, USA) at 37^{o}C. Thirty minutes after the treatment, cells were washed and collected to be analyzed using FACS installed at the National Center for Inter-university Research Facilities (NCIRF) at Seoul National University (FACS Aria II, Seoul, Korea).

2.10.3. qRT-PCR and western blot assay

qRT-PCR and western blot analysis of MGC-polarized macrophages were performed using previously noted experimental procedures.

2.10.4. Paracrine secretion analysis

Cytokine secretion was analyzed using Quantikine (R&D systems, Minneapolis, MN, USA) according to the manufacturer's directions. For antioxidant property evaluation, macrophages were pretreated with 10 μg/mL MGC for 2 hours, followed by the treatment of 200 ng/mL LPS for 24 hours. For macrophage polarization analysis, macrophages were pretreated with 200 ng/mL LPS for 24 hours, followed by the treatment of 10 μg/mL MGC+ for 2 days. Conditioned medium was collected and centrifuged at 1500 rpm for 10 minutes to remove cell debris for Quantikine analysis. Proteome profiler assay was performed following the instructor's manual for cell culture conditioned medium.

2.10.5. Fluorescent imaging

Morphological changes after MGC uptake was evaluated using fluorescent images. Macrophages were first stained with DiO fluorescent dye for 3 hours. Thereafter, these cells were treated with 200 ng/mL LPS for 24 hours, followed by the treatment of 10 μg/mL MGC. Morphological changes in macrophages were assessed using fluorescent microscopy.

2.10.6. Co-culture of macrophages and cardiomyocytes

To assess the Cytoprotective efficacy of MGC/IL-4 pDNA -polarized macrophages, cardiomyocyte co-culture was performed. Two days after cardiomyocyte seeding on 6-well cell culture plate, 100 mM H_2O_2 was added into the cell culture medium to induce in vivo-mimicking cell death. After 4 hours, transwell inserts seeded with M1 macrophages or M1 macrophages treated with MGC/IL-4 pDNA (10 μg/mL MGC solution, 5ug IL-4 pDNA) for 72 hours, were placed within the 6-well cell culture plate and the medium was changed to H_2O_2-free medium. Viability of the cardiomyocytes was assessed using MTT assay after 24 hours of co-culture.

2.11. Mouse Model and MGC injection

Animal experimental protocol was approved by the Chonnam national University Animal Care and Use Committee (CNU IACUC-H-2016-37). MI was induced in 8-week-old male BALB/c mice (Central Lab Animal Inc., Seoul, Korea) by occlusion of the coronary artery. Briefly, the mice were anesthetized with an intramuscular injection of ketamine (50 mg/kg) and xylazine (10 mg/kg), and the left coronary artery was occluded within the myocardium between the left atrial appendage and the right ventricular outflow tract using a curved needle and a 5-0 silk suture. After ligation, 50 μL PBS, MGC (20 μg MGC) in 50 μL PBS, or MGC/IL-4 pDNA (10 μg DNA-conjugated 20 μg MGC) in 50 μL PBS was injected into the border zone. The mice were sacrificed 1, 4, or 14 days after the treatments.

2.12. *In vivo* assessment

2.12.1. Histological assessment and evaluation of genes and proteins

For immunohistochemical and H&E staining, heart tissues 1 or 4 days after the treatments were fixed with formaldehyde, embedded in paraffin, and sliced into 4 μm-thick sections. Tissue sections were analyzed using TUNEL assay for apoptotic cell evaluation, H&E staining for inflammatory cell infiltration assessments, and immunohistochemical staining against CD206 to visualize M2 macrophages. Images were quantified using ImageJ software.

Two weeks after the treatments, the animals were sacrificed and the heart tissues were fixed with formaldehyde, embedded in paraffin, and sliced into 4 μm-thick sections. To assess infiltration of inflammatory macrophages, the heart sections were stained with H&E. To evaluate fibrotic tissue formation after infarction, sections were stained with Masson's trichrome. Quantitative analysis for H&E staining and Masson's trichrome staining was performed with densitometry using ImageJ software, and further expressed the percentage to the total left ventricle.

For immunohistochemical analysis of M1 and M2 macrophages, heart sections were retrieved 14 days after the treatments. For immunohistochemical analysis of vessel density and cardiac remodeling, heart sections 14 days after the treatments were obtained. Sections were first treated with proteinase K for 15 minutes at 37°C for antigen retrieval. After nonspecific binding was blocked with 5% normal goat serum (Sigma), the slides were incubated with primary antibodies against Cx43 (Abcam), vWF (Abcam), and SMA-α (Abcam) for 18 hours at 4 °C. The sections were washed three times with PBS and incubated for 1 hour with FITC or Rhodamine-conjugated secondary antibodies. After washing, the slides were mounted with a mounting medium (VectaMount mounting medium, Vector Labs Inc., Burlingame, CA, USA). Images were obtained and digitized on a

computer using an Olympus CX31 microscope (Olympus) equipped with an Infinity 1 camera (Lumenera Scientific, Ottawa, Canada). Four samples per group were analyzed.

For qRT-PCR, RNA was isolated from heart tissue using TRIzol (Life Technologies, CA, USA) according to manufacturer's instructions. cDNA was synthesized using Applied Biosystems High-Capacity cDNA Reverse transcription Kit (Invitrogen, MA, USA) according to the manufacturer's instructions. PCR was performed using QuantiTect SYBR Green PCR kit (Qiagen, Valencia, USA) and Corbett Research Rotor-Gene RG-3000 Real Time PCR System. The sequences of primer pairs are described in Supplementary Table S1. All reactions were normalized using eukaryotic 18s rRNA endogenous control (Applied Biotechnologies).

For western blot, isolated hearts were snap-frozen in liquid nitrogen. Lysates were generated by pulverizing cardiac tissue on ice in RIPA Buffer (150 mM NaCl, 50 mM Tris-Cl pH 8.3, 0.5 % wt/vol sodium deoxycholate, 0.1 % wt/vol SDS) together with additional protease inhibitors (complete ULTRA mini tablet, Roche). After centrifugation at 10,000 g for 10 minnutes, the supernatant was prepared as a protein extract. Equal concentrations of proteins were fractionated by electrophoresis on 8-12 % acrylamide gels and were transferred onto a polyvinylidene fluoride membrane (Merck Millipore, Darmstadt, Germany), followed by blotting with antibodies for iNOS (Cell Signaling Technology, MA, USA), Arg1 (Cell Signaling Technology, MA, USA), BAX (Santa Cruz Biotech, Dallas, TX, USA), and glyceraldehyde 3-phosphoate dehydrogenase (GAPDH, Santa Cruz Biotech, Dallas, TX, USA) followed by incubation with horseradish peroxidase-conjugated secondary antibody (Cell Signaling Technology, MA, USA). Protein expression was detected by using an Image Reader (LAS-3000 Imaging System, Fuji Photo Film, Tokyo, Japan).

2.12.2. Evaluation of cardiac performance

Left ventricular function was assessed by transthoracic echocardiography. Two weeks after the treatments, the mice sere anesthetized, and echocardiography was performed with a 15-MHz linear array transducer system (iE33 system, Philips Medical Systems; Amsterdam, Netherland) by an expert who was not aware of the experimental conditions to exclude bias.

2.13. Statistical analysis

The quantitative data are expressed as the means ± standard deviations. The statistical analysis were performed through one-way analysis of variance (ANOVA) with Tukey's significant difference post hoc test using the SPSS software (SPSS Inc., USA). A value of $P<0.05$ was considered to be statistically significant. .

Chapter 3.

Iron oxide nanoparticle-mediated development of cellular gap junction crosstalk to improve mesenchymal stem cells' therapeutic efficacy for myocardial infarction

3.1. Introduction

Mesenchymal stem cells (MSCs) can repair myocardium damaged by MI.[161-163] There are largely two mechanisms of action for the repair; one mechanism suggesting MSCs directly differentiate into functional cardiac cells,[164-167] and the second mechanism addressing MSCs secrete therapeutic paracrine molecules.[34,167,168] Although the multipotency of MSCs is promising, their cardiac differentiation *in vivo* is controversial,[35,161,169] and the lack of cardiac phenotypes in naïve MSCs poses an electrophysiological challenge for MI repair.[41-44] Previous studies have showed that MSCs expressing cardiac-specific biomarkers can reduce arrhythmic risks and improve cardiac function *in vivo*,[91,170,171] suggesting that cardiac phenotype development of MSCs can improve the therapeutic efficacy. Along with the cardiac phenotypes, the salutary effects of the paracrine molecules secreted from MSCs have been demonstrated in a number of studies,[84,172,173] and the enhanced paracrine secretion resulted in better reparative efficacy of the MSC therapies.[99-101] Hence, both cardiac phenotype development for myocardium compatibility and paracrine signaling improvements may improve the therapeutic potential of MSCs for MI.

To induce cardiac phenotype development of MSCs *in vitro*, exogenous supplements, such as transforming growth factor beta 1 (TGF-β1) and 5AZA, have been used in MSC cultures.[89,174,175] Co-culture with cardiomyocytes or cardiomyoblasts has also been proposed as a method for cardiac lineage differentiation that requires no exogenous supplements.[94,176] Primary cardiomyocytes, however, pose challenges for co-culture, because these cells have limited life span and do not proliferate *in vitro*.[175] Moreover, the limited accessibility to the primary cardiomyocytes causes another difficulty for the co-culture. To overcome these problems, cardiomyoblast cell line, H9C2, has been used in previous co-culture studies.[176,177] Although H9C2 cells provide excellent accessibility and quality assurance, they rarely express connexin 43 (Cx43), a gap

junction protein,[178] which is responsible for intercellular gap junction coupling and cell-to-cell crosstalk in co-culture, which are previously known to play major roles in MSC modification.[93,170] Thus, H9C2 with enhanced Cx43 expression may provide active intercellular interactions with MSCs in co-culture, which could promote cardiac lineage development of MSCs.

Aside from direct cardiac phenotype development of MSCs, improvement in indirect paracrine mechanism of MSCs was studied using various culture conditions. MSCs are known to repair damaged organs through a broad spectrum of reparative paracrine molecules.[35,84,172] To improve the paracrine secretion of MSCs, previous studies introduced hypoxic culture conditions or mild hypoxia generated from MSC spheroids.[99-101] Even so, no previous studies have investigated whether both cardiac phenotype development and paracrine profile improvement of MSCs could be achieved simultaneously and orchestrated into one solution for MI. Recently, iron oxide nanoparticle (IONP)-mediated cell labeling or drug delivery has been extensively studied, and the use of IONPs in cell studies has been shown safe and effective.[145,146] In spite of their plasticity in biomedical applications, the effect of IONPs as ion-delivering carriers has rarely been studied, and their use in cell biology or stem cell-based therapy needs more exploration. While some studies have integrated IONPs to control cell behaviors *in vitro*,[148-150] approaches with IONP-induced gap junctional communication improvements have not been reported. Additionally, the mechanisms behind the nanoparticle-induced cellular behavior changes need better clarification for potential application of IONPs in the biomedical field.

In the present study, we demonstrate new biofunctional properties of IONPs in gap junctional cell-cell crosstalk, and focus on the generation of therapeutic potential-improved MSCs using IONP-induced co-culture with H9C2 (Figure 3.1). The major therapeutic mechanisms of MSC therapies for MI, namely the cardiac phenotype development and reparative paracrine molecule secretion, were targeted to be improved from the IONP-based co-culture system. When

uptaken by H9C2, IONPs are partially ionized into iron ions, which may trigger gap junctional signaling cascade to develop Cx43 expression. To address the development of Cx43 by IONPs and subsequent cellular crosstalk in co-culture, we analyzed the gene and protein expression of Cx43 in IONP-harboring H9C2 (IONP(+) H9C2), and evaluated Cx43-based crosstalk of these H9C2 with MSCs in co-culture. Consequently, we investigated cardiac phenotype development of MSCs influenced by Cx43-mediated cellular crosstalk in co-culture with IONP(+) H9C2. Additionally, we assessed the modification of MSCs' reparative paracrine profile after co-culture through gene expression and protein secretion analysis. To address the therapeutic efficacy of IONP(+) H9C2 co-cultured MSCs (cMSCs), we injected cMSCs into rat MI models, and evaluated cardiac tissue repair and cardiac functional recovery. Here, we demonstrate a new application of IONPs in developing cellular gap junction, and propose a new window for the generation of therapeutic potential-improved MSCs from IONP-based co-culture.

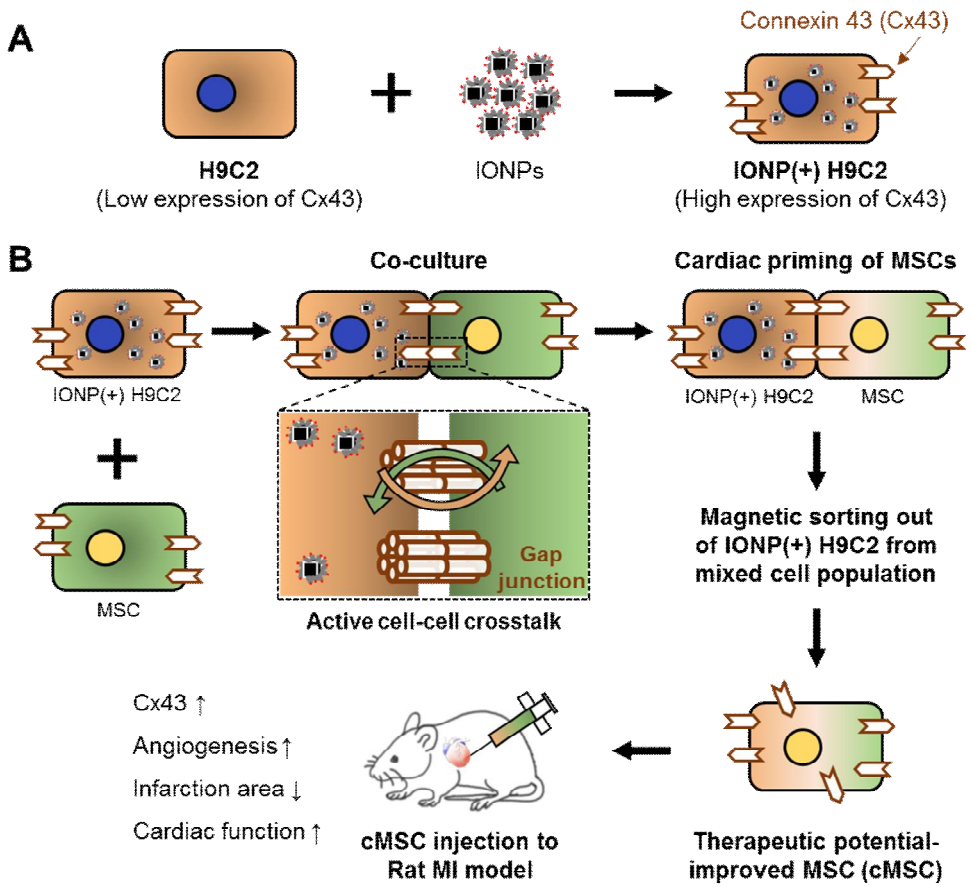

Figure 3.1. Schematic illustration of IONP-induced Cx43 expression enhancement in H9C2, and the assessments of IONP effects in co-culture for better *in vivo* therapeutic efficacy. (A) Cx43 expression enhancement in H9C2 by IONP uptake. (B) Generation of therapeutic potential-improved MSCs (cMSCs) from IONP-induced active cell-cell crosstalk between IONP(+) H9C2 and MSCs in co-culture, and the improved therapeutic efficacy of cMSCs *in vivo*.

3.2. Results and discussion

3.2.1 Internalization of IONP and H9C2 behavior modulation

The physiological properties of IONP, and the effects of IONP-internalization in H9C2 were evaluated (Figure 3.2). We have utilized nanocubes rather than nanospheres to maximize the high magnetization while maintaining the colloidal stability. Since the responsiveness of IONPs to external magnetic field is proportional to their volume, larger nanoparticles is desirable for effective magnetic cell sorting. However, iron oxide nanoparticles larger than 20 nm exhibit ferromagnetic property and easily form large aggregates owing to their strong magnetic attraction to each other. Interestingly, a previous report showed that iron oxide nanocube with an edge length of 22 nm, which were encapsulated with PEG-phospholipid, exhibited high colloidal stability while maintaining high magnetization.[179] Therefore, iron oxide nanocubes with a similar size were employed in this study. The size and shape of IONP, along with the cellular uptake of nanoparticles, were assessed using transmission electron microscopy (TEM; Figure 3.2B). When treated with 40 μg/ml of fluorescent dye-labeled IONPs for 24 hours, H9C2 showed efficient uptake of nanoparticles and IONP clusters were observed only within the cells. IONP uptake was further visualized with a fluorescent microscope, and IONP-uptaken H9C2 (IONP(+) H9C2) expressed strong fluorescent signal compared with untreated H9C2 (IONP(-) H9C2) after 24 hours (Figure 3.2C). To quantitatively evaluate iron contents within H9C2, both IONP(-) H9C2 and IONP(+) H9C2 were assessed with inductively coupled plasma mass spectrometry (ICP-MS; Figure 3.2D). When compared with IONP(-) H9C2, IONP(+) H9C2 showed significantly increased iron contents within the cells.

To evaluate whether IONP uptake affected the inherent gene expressions of H9C2, IONP(+) H9C2 were analyzed with quantitative real-time reverse transcription-polymerase chain reaction (qRT-PCR; Figure 3.2E). The data showed that IONP uptake did not affect the expression levels of H9C2-inherent apoptosis-

regulatory (Bcl-2/BAX) or cardiac-specific genes when compared with no IONP uptake. Interestingly, IONP(+) H9C2 showed significantly improved gap junction protein Cx43 gene expression compared to IONP(-) H9C2 (Figure 3.2E), and its protein expression was further assessed with immunocytochemistry (Figure 3.2F).

Next, we examined the intracellular signaling mechanisms for the improved expression of Cx43 after IONP uptake (Figure 3.2G). To assess the stability of IONPs at low pH, a condition that resembles cell endosomes, IONPs were added and incubated in pH 4 or pH 7 solution for 24 hours. After 24 hours, pH 4 solution showed better transparency compared with pH 7 solution, suggesting IONPs are partially ionized into Fe^{2+} or Fe^{3+} ions at low pH condition (Figure 3.2H),[180] and IONPs would generate metal ions upon endosomal uptake. Interestingly, when the same molar concentration of iron ions, were directly added into the H9C2 culture, instead of using IONPs, significant cytotoxicity was observed (Figure 3.2I). To further evaluate the intracellular signaling cascades upon IONP uptake (Figure 3.2G), IONP(+) H9C2 were analyzed with western blots (Figure 3.2J). When treated with IONPs, H9C2 uptake nanoparticles through endocytosis and these IONPs are retained in the intracellular endosomes.[180] Upon internalization in the endosomes, which have comparatively low pH level as low as 4,[181] IONPs are partially ionized into iron ions in the endosomes, and the metal ions are released into the cytosol.[180] These free metal ions promote JNK activation, c-Jun phosphorylation and ultimately JNK-mediated Cx43 expression as expected from the previous study (Figure 3.2G).[182] Twenty four hours after the IONP treatment, IONP(+) H9C2 exhibited great upregulation in the phosphorylated protein forms of JNK (*p*-JNK) and c-Jun (*p*-c-Jun) relative to the non-phosphorylated protein forms compared with untreated H9C2 (Figure 3.2J). Increase in *p*-JNK and *p*-c-Jun consequently activated Cx43 expression in IONP(+) H9C2.

Next, the functional role of enhanced Cx43 expression was evaluated using dye transfer assay (Figure 3.2K). Cx43 is known to induce intercellular

coupling among the adjacent cells, and a previous study demonstrated Cx43-overexpressing cells show active gap junctional communication with the nearby cells and transfer biomolecules to these cells.[170] To investigate whether IONP-induced Cx43 expression in H9C2 successfully formed functional gap junctions with the adjoining MSCs and transferred cellular biomolecules, IONP(+) H9C2 or IONP(-) H9C2 were co-cultured with MSCs for 48 hours. Before co-cultured with MSCs, both IONP(+) H9C2 and IONP(-) H9C2 were dual-labelled with DiI (red), which cannot pass through gap junctions, and calcein-AM (green), which can only pass through gap junctions. Only when H9C2 formed functional gap junctions with MSCs, calcein-AM, not DiI, would be transferred to unlabeled MSCs. When dye transfer was evaluated with fluorescence microscopy 48 hours after co-culture, more MSCs having calcein-AM without DiI were observed in co-culture with IONP(+) H9C2 compared with the IONP(-) H9C2 co-culture (Figure 3.2K), suggesting IONP(+) H9C2 formed more functional gap junctions with MSCs compared with IONP(-) H9C2. Quantitative analysis also showed the calcein-AM transfer from H9C2 to MSCs were significantly more frequent when H9C2 were pre-treated with IONPs. This data suggests that IONP uptake can not only enhance Cx43 expression of H9C2 but also develop functional gap junction communications with MSCs in co-culture.

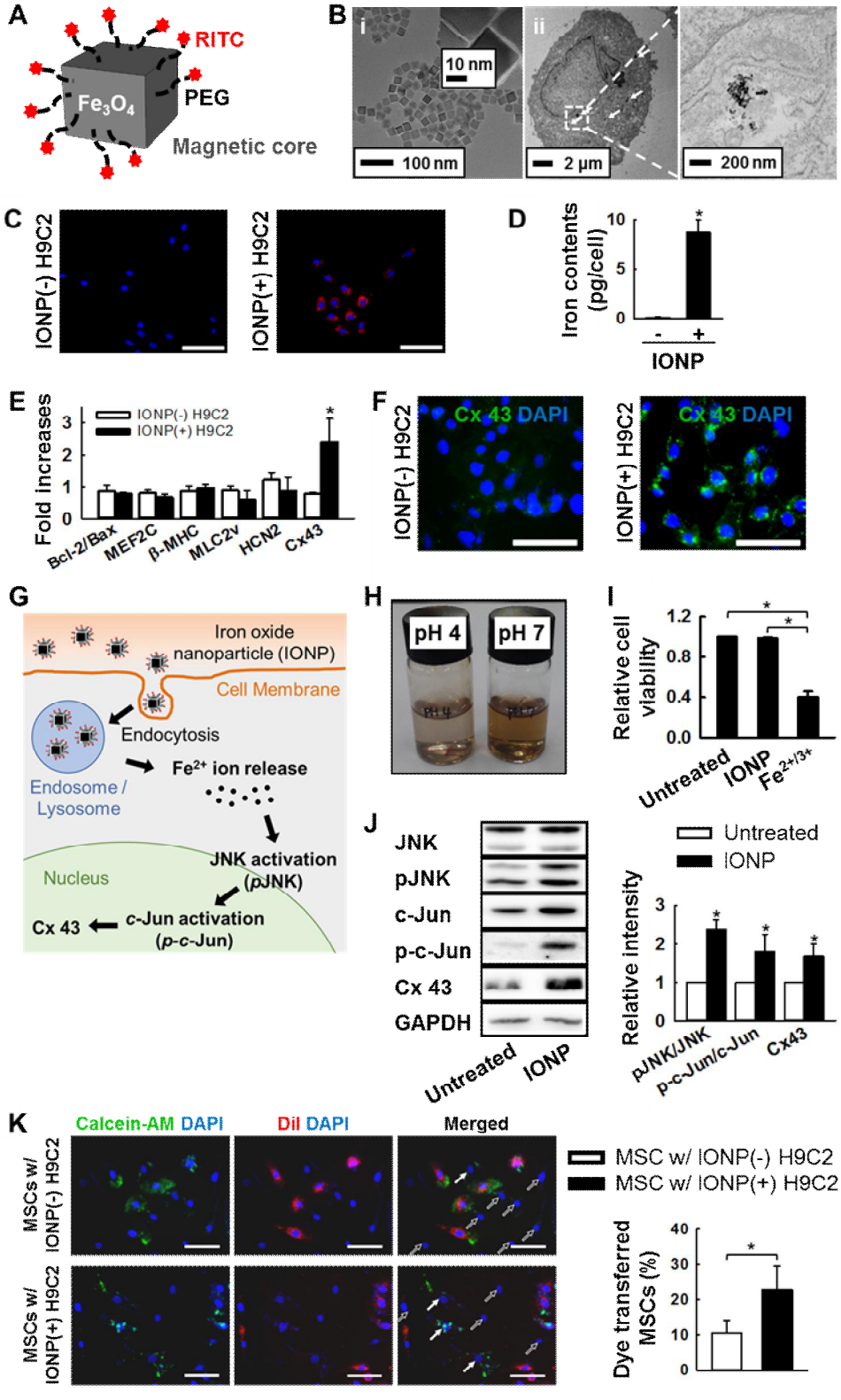
A
RITC
Fe_3O_4
PEG
Magnetic core
B
i
10 nm
100 nm
ii
2 μm
200 nm
C
IONP(-) H9C2
IONP(+) H9C2
D
Iron contents (pg/cell)
10
5
0
*
-
+
IONP
E
IONP(-) H9C2
IONP(+) H9C2
Fold increases
3
2
1
0
*
Bcl-2/Bax
MEF2C
β-MHC
MLC2v
HCN2
Cx43
F
IONP(-) H9C2
Cx 43 DAPI
IONP(+) H9C2
Cx 43 DAPI
G
Iron oxide nanoparticle (IONP)
Cell Membrane
Endocytosis
Fe^{2+} ion release
Endosome / Lysosome
JNK activation (pJNK)
Nucleus
Cx 43
c-Jun activation (p-c-Jun)
H
pH 4
pH 7
I
Relative cell viability
1.2
0.8
0.4
0.0
*
*
Untreated
IONP
$Fe^{2+/3+}$
J
JNK
pJNK
c-Jun
p-c-Jun
Cx 43
GAPDH
Untreated
IONP
Untreated
IONP
Relative intensity
3
2
1
0
*
*
*
pJNK/JNK
p-c-Jun/c-Jun
Cx43
K
Calcein-AM DAPI
DiI DAPI
Merged
MSCs w/ IONP(-) H9C2
MSCs w/ IONP(+) H9C2
MSC w/ IONP(-) H9C2
MSC w/ IONP(+) H9C2
Dye transferred MSCs (%)
40
30
20
10
0
*

Figure 3.2. IONP-induced Cx43 upregulation in H9C2 and its functional role in gap junctional crosstalk in co-culture with MSCs. (A) Schematic representation of IONP. (B) TEM images of (i) IONPs (iron oxide nanoparticles) and (ii) IONPs uptaken by H9C2. IONPs are marked with white arrows. (C) Fluorescent images of H9C2 after IONP (red) treatment for 24 hours. Bars, 100 μm. (D) Quantification of iron contents within H9C2 after IONP uptake. ICP-MS was performed 24 hours after IONP treatment. **P*<0.05. (E) Expressions of H9C2-inherent cardiac and apoptosis-regulatory genes before and after IONP treatment. Gene expressions were normalized to the levels of IONP(-) H9C2. **P*<0.05 *vs*. IONP(-) H9C2. (F) Expression of a gap junction protein, Cx43 (green), in H9C2 after IONP uptake. Blue indicates nuclei. Bars, 100 μm. (G) Schematic illustration of IONP-mediated signaling cascades within the cells. (H) Visualization of IONP ionization at low pH. For visualization, 40 μg/ml of IONPs were added into pH 4 or pH 7 solution and the images were taken after 24 hours. (I) The cytotoxicity of exogenous iron ions or IONPs added in H9C2 culture. 40 μg/ml of IONPs or the same molar concentration of iron ions were added directly into H9C2 culture. For cell viability evaluation, MTT assay was performed 24 hours after IONP or $Fe^{2+/3+}$ treatment. **P*<0.05. (J) Western blot analysis and the quantification of intracellular signaling cascades for enhanced Cx43 expression triggered from IONP uptake. n=3, **P*<0.05 *vs*. Untreated. (K) Fluorescent images and quantitative analysis showing active dye (calcein-AM, green) transfer after 48 hours of co-culture. Before co-culture, IONP(+) H9C2 were labeled with calcein-AM and DiI (red), while MSCs were unlabeled. After 48 hours of co-culture, cells having green fluorescence without red (calcein-AM^+/DiI^-; solid arrow) denote MSCs that received calcein-AM through functioning gap junction. Cells having no fluorescence but DAPI (calcein-AM^-/DiI^-; hollow arrow) denote MSCs that did not receive calcein-AM during 48 hours of co-culture. Bars, 100 μm. **P*<0.05.

3.2.2. IONP-based magnetic H9C2 sorting post co-culture

The efficiency of IONP-assisted MSC sorting was assessed (Figure 3.3). Two week-co-cultured cells, consisting of MSCs and IONP(+) H9C2, were trypsinized and collected in a tube and IONP(+) H9C2 were magnetized to a neodymium magnet (Figure 3.3A). IONP-based magnetic cell sorting induced high-density accumulation of IONP(+)H9C2 after 2 minutes, and was evaluated with a fluorescent microscope (Figure 3.3B). To further assess the cell population contents, cell populations attracted to the magnet (magnet(+) population) and those not attracted to the magnet (magnet(-) population) were both stained for human nuclear antigen (HNA) to assess MSC purity (Figure 3.3C). HNA staining only stained human MSCs from the cell suspension. As shown in Figure 3.3C, counterstaining with 4,6 diamidino-2-phenylindole (DAPI) displayed IONP(+) H9C2 cells as DAPI+ (blue)/HNA- blue, and MSCs as DAPI+/HNA+ (green) blue-green. After magnetic cell separation, no IONP(+) H9C2 was observed in the magnet(-) population (Figure 3.3C). Similarly, almost no MSCs was observed in the magnet(+) population. The immunofluorescent images were then quantitatively evaluated. To further confirm pure MSC population in the magnet(-) population, the cell population for *in vivo* injection, the MSC purity was evaluated using fluorescent-activated cell sorting (FACS; Figure 3.3D). FACS result demonstrated over 99% pure MSCs in the magnet(-) population. Facile separation of MSCs after co-culture is particularly intriguing, because conventional cell sorting method after co-culture faces several challenges. For cardiac differentiation of MSCs or endothelial progenitor cells, direct cell-to-cell contact with cardiomyocytes or cardiomyoblasts was shown pivotal.[94,176] Even so, cell separation following co-culture necessitates costly cell-specific antibodies, sorting equipment, and expertise, thereby limiting simple, efficient, and clinical-scale cell sorting. Moreover, the inability to eliminate cell-conjugated antibodies after antibody-induced cell sorting could be problematic for the transplantation of the co-cultured cells. Likely for this reason, *in vivo* administration of the co-cultured MSCs for MI has rarely been

reported. In contrast, IONP-based co-culture facilitated a simple, cost-effective, easily scalable, and efficient cell sorting following co-culture, allowing for the separation of transplantable dosages of MSCs for *in vivo* applications.

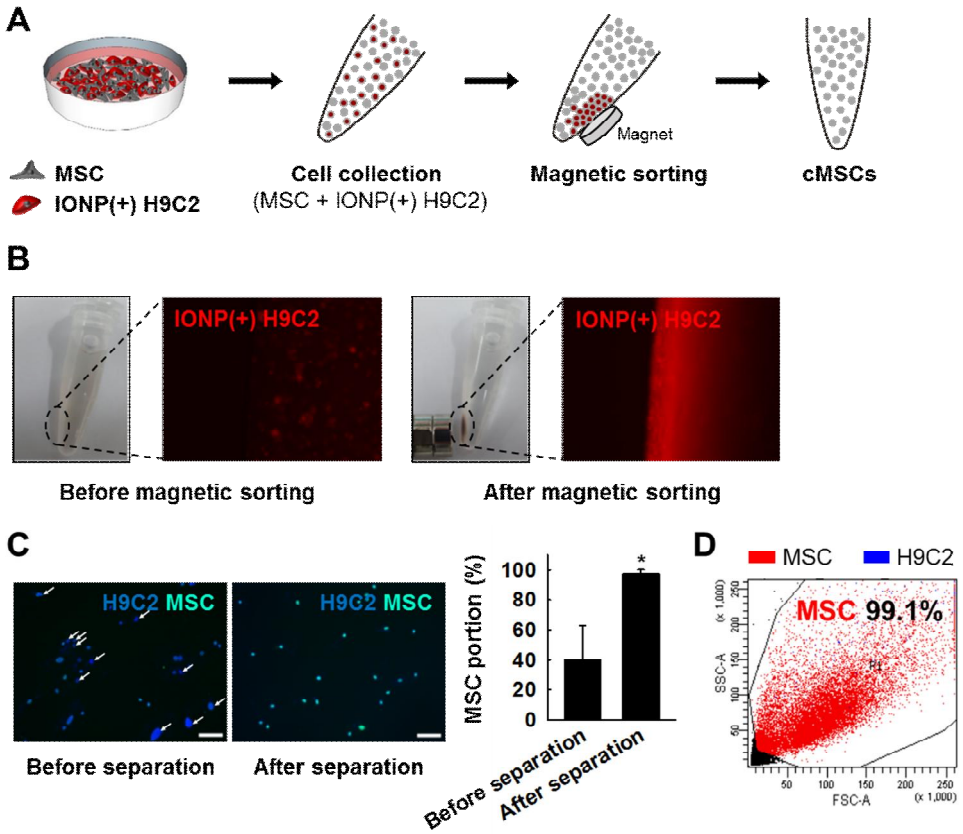

Figure 3.3. Facile separation of cMSCs following co-culture by magnetically removing IONP-harboring H9C2 from the co-cultured cell population. (A) Representative illustration of the cell sorting method. (B) Macroscopic fluorescent visualization of IONP(+) H9C2 (red) sorting using a magnet. (C) Efficiency of IONP-induced cell sorting. DAPI+ (blue)/ HNA- H9C2 were visualized as blue, and DAPI+/ HNA+ (green) human MSCs were visualized as blue-green. Fluorescent images were taken and quantified for both magnet(-) and magnet(+) populations. H9C2 are marked with white arrows in the first image (before separation). Bars, 100 μm. *P<0.05 vs. before separation. (D) FACS result of the IONP-based cell sorting.

3.2.3. Cardiac phenotype development in MSCs after co-culture

Cellular phenotype changes in the co-cultured MSCs were evaluated by analyzing the expression of cardiac-specific biomarkers (Figure 3.4). MSCs were co-cultured with IONP(+) H9C2 or IONP(-) H9C2, and sorted by neodymium magnet or FACS, respectively. After 7 days of co-culture, MSCs co-cultured with IONP(-) H9C2 showed no significant changes in their cardiac genes compared with unmodified MSCs. However, MSCs co-cultured with IONP(+) H9C2 showed significant increase in cardiac-specific genes including ß-MHC, MLC2a and MLC2v (Figure 3.4A). This data suggests that the improved gap junctional communication from IONP uptake (Figure 3.2J-K) successfully induced cardiac phenotype development of MSCs after co-culture.

To further compare the cardiac phenotype development efficacy of IONP-based co-culture with the conventional cardiac differentiation methods, a number of groups were analyzed with qRT-PCR (Figure 3.4B). After 7 and 14 days of culture, qRT-PCR was performed for unmodified MSCs, MSCs treated with cardiac differentiation supplements, such as TGF-β1 or 5-AZA, and MSCs co-cultured with IONP(+) H9C2. As shown in Figure 3.4B, only the MSCs co-cultured with IONP(+) H9C2 showed distinctively increased mRNA expression of cardiac-specific proteins compared with the other groups. Co-cultured MSCs exhibited increased expression levels of a cardiac transcription factor, MEF2C, as well as the mid-late cardiac structural genes ß-MHC and MLC. Increase in cardiac structural gene expressions was dependent to the co-culture period, and the similar tendency was observed in cardiac ion channel marker expressions (Figure 3.4C). A significant increase in the mRNA expression of ion channel proteins was observed in 2 week-co-cultured MSCs (cMSCs) compared with unmodified or 1 week-co-cultured MSCs (Figure 3.4C). Based on these data, the optimal co-culture period needed for MSCs to develop cardiac phenotypes was set to 2 week.

Immunocytochemistry and western blot analysis were then performed to evaluate the expression of Cx43 in cMSCs compared with unmodified MSCs (Figure 3.4D). Cx43 expression is particularly important, because Cx43 plays a critical role in gap junctional communications in the myocardium.[183,184] After acute myocardial infarction, severe loss of healthy myocardium impairs intercellular communications at the peri-infarct and induces cardiac conduction disturbances.[183-185] Administration of naïve MSCs at this phase faces compatibility issues and may pose arrhythmic risks.[42,43] Previous studies addressed that abnormal cardiac conduction and arrhythmogenic remodeling after MI could be worsened by low Cx43 expression, immature ion channel activity, or even a physiological incompatibility of naïve MSCs.[41,43,186] Interestingly, injection of MSCs expressing cardiac biomarkers or genetically modified cells that overexpress Cx43 conferred a better reparative effect post-infarct.[41,91,170] Previous studies also showed that overexpression of Cx43 in MSCs or skeletal muscle cells can greatly improve the therapeutic efficacy of the cell therapy in MI regardless of the cellular arrangement of Cx43.[41,91,170,171,187]

MSC overexpression of cardiac structural genes, ion channel biomarkers, as well as Cx43, from the IONP-based co-culture could associate with enhanced therapeutic efficacy *in vivo*. A number of previous studies tried terminal cardiac differentiation of MSCs, however, developing functional cardiac behaviors such as action potential generation or calcium transient was limited.[89,91,93,94,170,174,188,189] Hence, the present study did not address action potential generation or calcium transient in MSCs. On the other hand, adaptation of electrophysiological biomarkers showed promising results in MI treatment.[91,170,171]

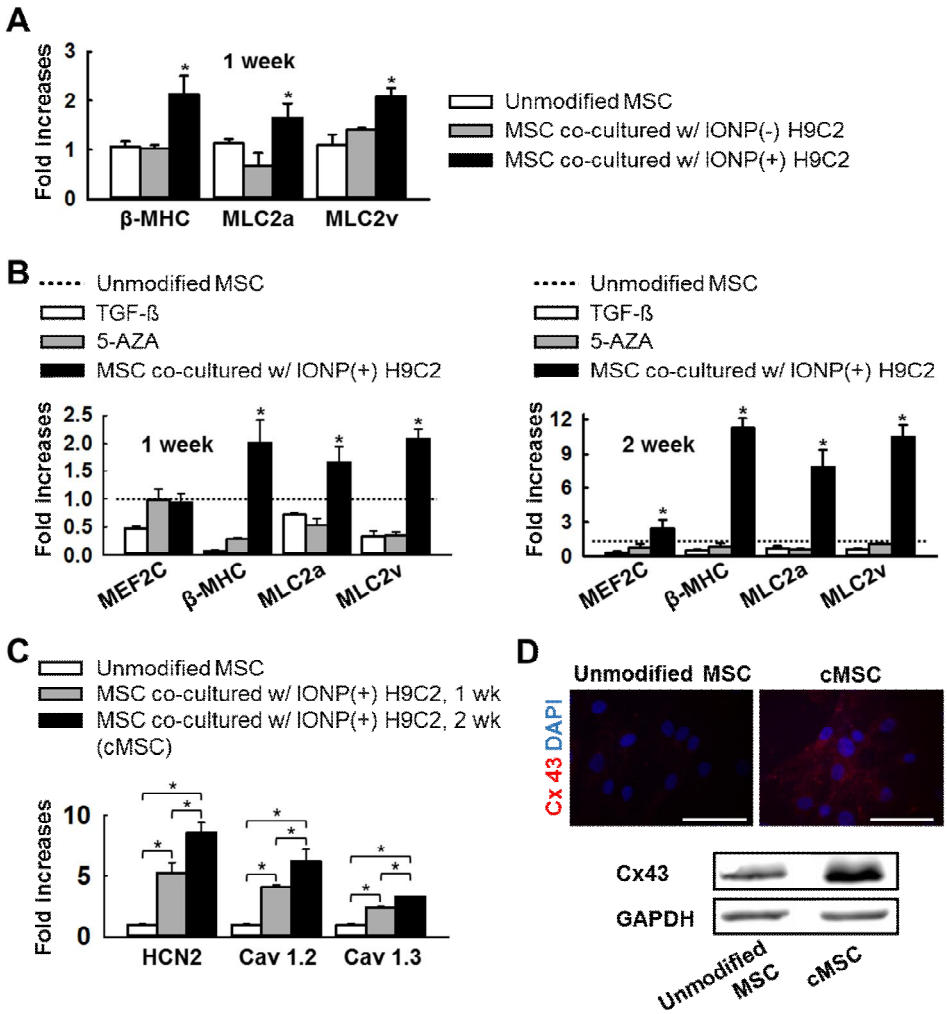

Figure 3.4. Effective development of cardiac phenotype in MSCs by co-culture with IONP(+) H9C2. (A) IONP-dependent cardiac phenotype development of MSCs. **P*<0.05 vs. any group. (B) Enhanced cardiac phenotype development of MSCs by IONP-induced co-culture compared with the conventional cardiac differentiation methods, treated with TGF-β or 5AZA. **P*<0.05 vs. any group. (C) Culture period-dependent expression of ion channel genes in cMSCs (MSCs co-cultured with IONP(+) H9C2). **P*<0.05. (D) Immunocytochemistry staining and western blot analysis for Cx43. Bars, 100 μm.

3.2.4. Cardiac repair-favorable paracrine profile in MSCs after co-culture

The alteration of the cellular paracrine profile in MSCs after IONP-based co-culture was assessed by qRT-PCR and protein array analysis (Figure 3.5). Angiogenic and cardioprotective proteins that are inherently expressed in MSCs were first evaluated with qRT-PCR (Figure 3.5A). Interestingly, cMSCs exhibited augmented gene expression of angiogenic proteins such as basic fibroblast growth factor (bFGF), hepatocyte growth factor (HGF) and vascular endothelial growth factor (VEGF) compared with unmodified MSCs or MSCs co-cultured with IONP(-) H9C2 (Figure 3.5A). bFGF and VEGF are known to promote angiogenesis and induce proliferation of endothelial cells,[35,101,163] while HGF has cytoprotective and anti-apoptotic effects.[34,35] This finding is particularly interesting because co-culture of MSCs with IONP(+) H9C2 affected not only the cardiac-specific gene expression (Figure 3.4) but also the angiogenic gene expression in MSCs. Additionally, upregulation of these therapeutic genes was IONP-dependent, suggesting that IONP-induced gap junctional coupling was critical in developing cardioprotective gene expression in MSCs during co-culture.

To further evaluate the paracrine profile improvement by co-culture with IONP(+) H9C2, we performed protein array analysis for the conditioned media of unmodified MSCs, MSCs co-cultured with IONP(-) H9C2 and cMSCs. Co-cultured MSCs were first sorted and re-plated to a culture plate. Initial number of the plated cells was kept the same for all groups (Unmodified MSCs, MSCs co-cultured with IONP(-) H9C2 and cMSCs). Figure 3.5B demonstrates representative dot blots and quantitative analysis of the assay 2 days after the MSC re-plating. MSCs co-cultured with H9C2, regardless of their IONP uptake, produced large number of cytokines compared with unmodified MSCs. Proteins that are known to repair damaged myocardium, such as angiopoietin 1 (Ang-1) and urokinase-type plasminogen activator (uPA) that reduce infarct size[190-192], along with placental

growth factor (PlGF) and monocyte chemoattractant protein-1 (MCP-1) that help collateral perfusion[193] showed significant upregulation in both MSCs co-cultured with IONP(-) H9C2 and cMSCs compared with unmodified MSCs. Surprisingly, the secretion of plasminogen activator inhibitor-1 (PAI-1), pigment epithelium-derived factor (PEDF) and VEGF was shown IONP-dependent, and was significantly increased in cMSCs compared to MSCs co-cultured with IONP(-) H9C2. PAI-1 is known to promote angiogenesis by stimulating endothelial cell migration,[194] and is expected to protect damaged myocardium from extensive fibrosis.[195] Also, PEDF and VEGF have been suggested to have a protective role in MI and reduce collagen deposition for improved cardiac function, respectively.[196,197] After magnetic cell sorting, cMSCs remained active for 1 week to secrete the paracrine molecules (PLGF, MCP-1, PEDF and VEGF), and showed increased cytokine secretion compared to unmodified MSCs. This suggests that the enhancement in paracrine profile was not transient. Upregulation in paracrine molecules is beneficial in myocardium regeneration, as a number of studies have previously emphasized the reparative and long-term effect of paracrine signaling of MSCs.[198-200] Our study demonstrates that cMSCs show higher levels of therapeutic gene expression and protein secretion compared with unmodified MSCs or MSCs co-cultured with IONP(-) H9C2. Although we could not specify which type of molecules were transferred from H9C2 to MSCs, IONP-dependent developments of therapeutic gene expression and paracrine profile were clearly demonstrated. Significant enhancements in MSC's innate cytokine profile could augment the therapeutic efficacy of stem cell therapy.[170]

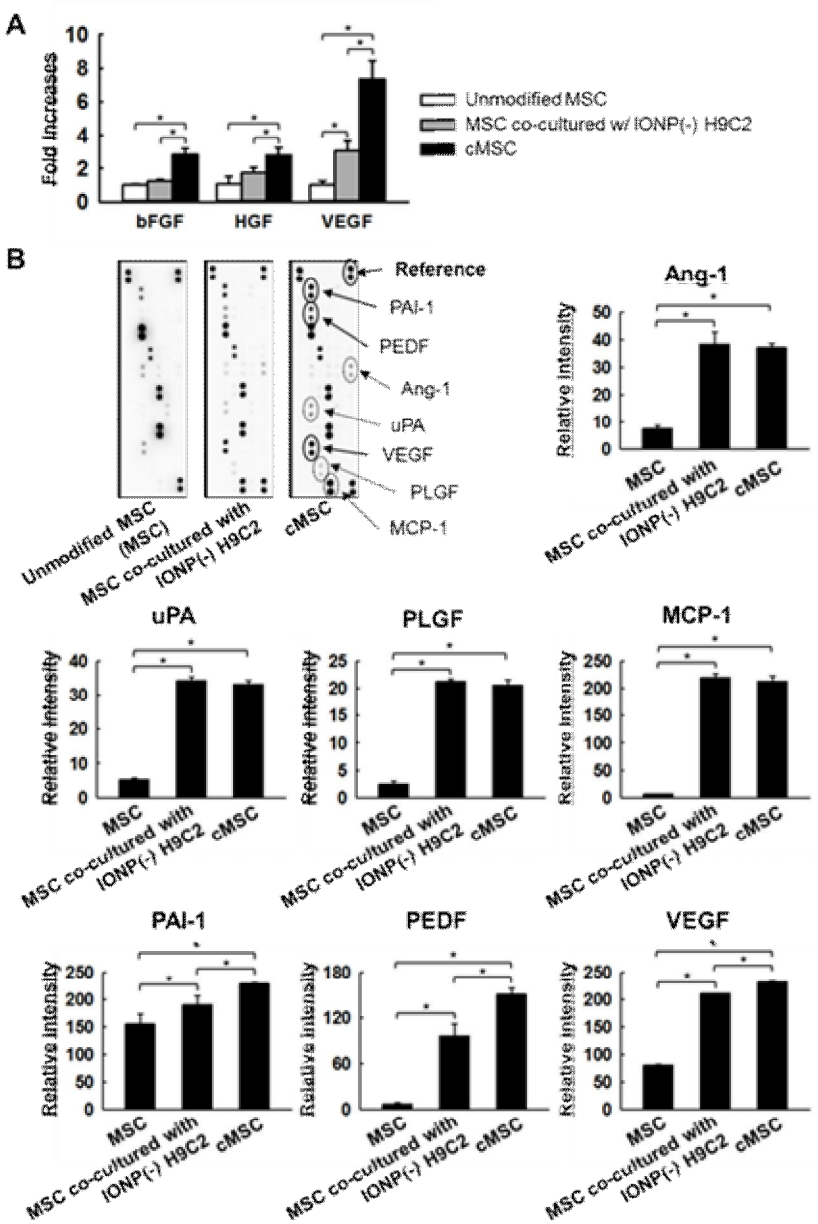

Figure 3.5. Cardiac repair-favorable paracrine profile of cMSCs. (A) Enhanced gene expressions of angiogenic proteins in MSCs, as evaluated by qRT-PCR. **P*<0.05. (B) Representative images and quantitative analysis of the protein array. Paracrine molecules with significant differences in pixel densities compared to unmodified MSCs or MSCs co-cultured with IONP(-) H9C2 labelled with dotted or solid lines, respectively. n=3, **P*<0.05.

3.2.5. Attenuation of left ventricular remodeling

Attenuation of ventricular remodeling by cMSC administration *in vivo* was assessed (Figure 3.6). Rats were treated with no operation as a positive control, with saline as a negative control, with MSCs as a conventional MI treatment, and with cMSCs as the experimental group. Two weeks after the treatments, Masson's trichrome staining was performed to assess the area of collagen-containing fibrous tissue. Longitudinal sections of the heart showed markedly low levels of blue-colored fibrotic tissue area in the cMSC group (Figure 3.6A). Quantitative analysis showed that the injection of cMSCs significantly reduced fibrotic tissue formation compared with the injection of saline or MSCs (8.9±3.6 *versus* 22.6±4.5 and 18.2±5.6 %, respectively; $P<0.05$). The administration of cMSCs was also associated with superior infarct size suppression (Figure 3.6B). Infarct size was analyzed by triphenyl tetrazolium chloride (TTC) staining and quantitatively assessed by measuring the ratio of infarcted myocardium in the left ventricle. The degree of infarct size was significantly lower in the cMSC group compared with the saline or MSC groups (15.7±3.2 *versus* 33.0±9.9 and 28.2±2.6 %, respectively; $P<0.05$).

Regulation of cardiac remodeling was further assessed with myocardium apoptosis and endogenous gap junction protein expression (Figure 3.6C). ApopTag Fluorescein *In Situ* Apoptosis Detection Kit (TUNEL) assay and immunohistochemistry for Cx43 were performed 2 weeks after the treatments. The administration of cMSCs decreased peri-infarct apoptotic cell numbers compared with the injection of saline or MSCs (20.9±3.2 *versus* 41.9±11.1 and 33.9±6.2 cells/mm^2, respectively; $P<0.05$). Consequently, the densitometry ratio of Cx43 to DAPI at the peri-infarct was higher in the cMSC group compared with the saline or MSC groups (3.9±1.6 *versus* 0.6±0.5 and 1.4±0.5, respectively; $P<0.05$). This data suggests that cMSC injection salvaged dying cardiac cells and better preserved Cx43 expression.

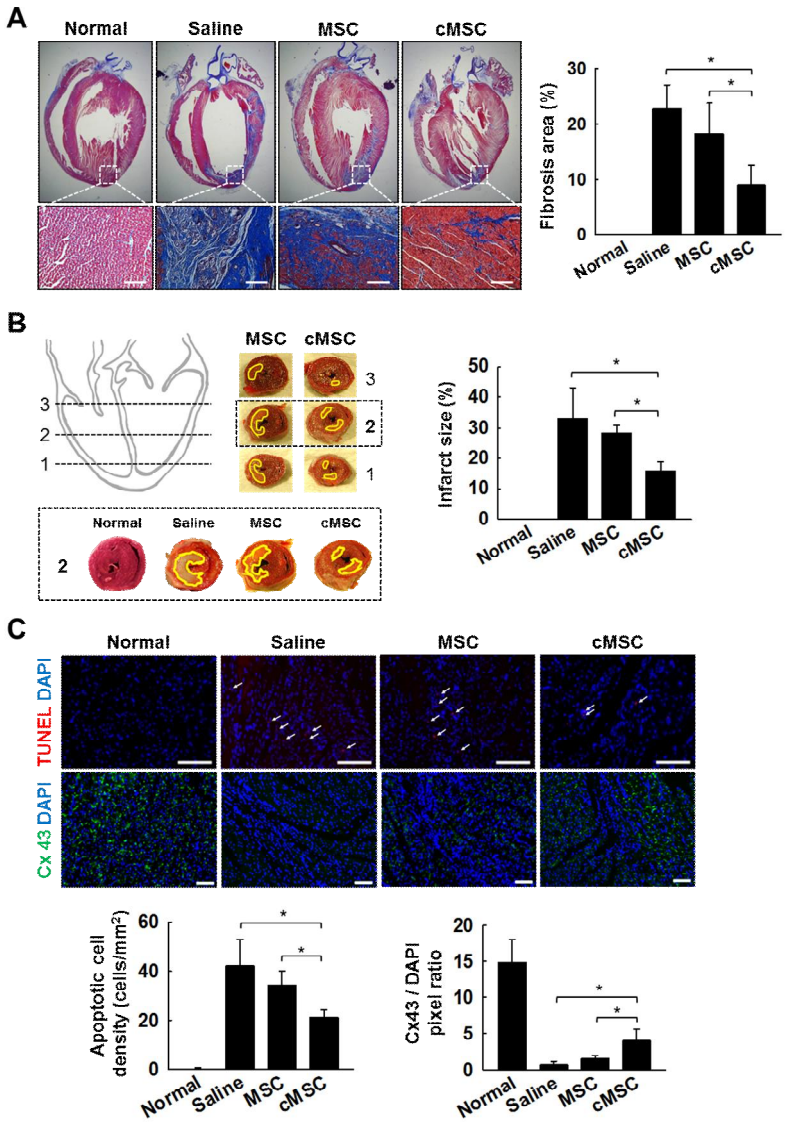

Figure 3.6. Injection of cMSCs attenuates left ventricular remodeling. (A) Histological sections of myocardium stained with Masson's Trichrome, and their quantitative analysis. n=4 animals, **P*<0.05. Bars, 200 μm. (B) Images of TTC stained heart sections, and the quantitative analysis. The infarcted area is marked with a yellow line. n=4 animals, **P*<0.05. (C) Immunohistochemistry images of apoptotic cells and gap junction proteins. $TUNEL^+$ apoptotic cells (red) are marked with white arrows. Apoptotic cells were quantified using densitometry and evaluated relative to $DAPI^+$ expression. Bars, 100 μm. n=4 animals, **P*<0.05.

3.2.6. Improved vessel density

To confirm that the increased vascular growth was involved with the improvement in cardiac remodeling, the heart sections were stained 2 weeks after the treatments for the expression of von Willebrand Factor (vWF) and smooth muscle actin alpha (SMA-α) (Figure 3.7). Capillary density was notably higher in the cMSC group compared with the saline or MSC groups (20.3±4.3 *versus* 2.6±0.9 and 12.3±5.1 vessels/mm^2, respectively; P<0.05). The cMSC group also showed higher arteriole density at the border zone compared with the saline or MSC groups (36.3±6.2 *versus* 11.7±2.6 and 20.8±6.8 vessels/mm^2, respectively; P<0.05). Our observations demonstrate that the suppression of physiological remodeling of the heart was accompanied with enhanced capillary and arteriole growth.

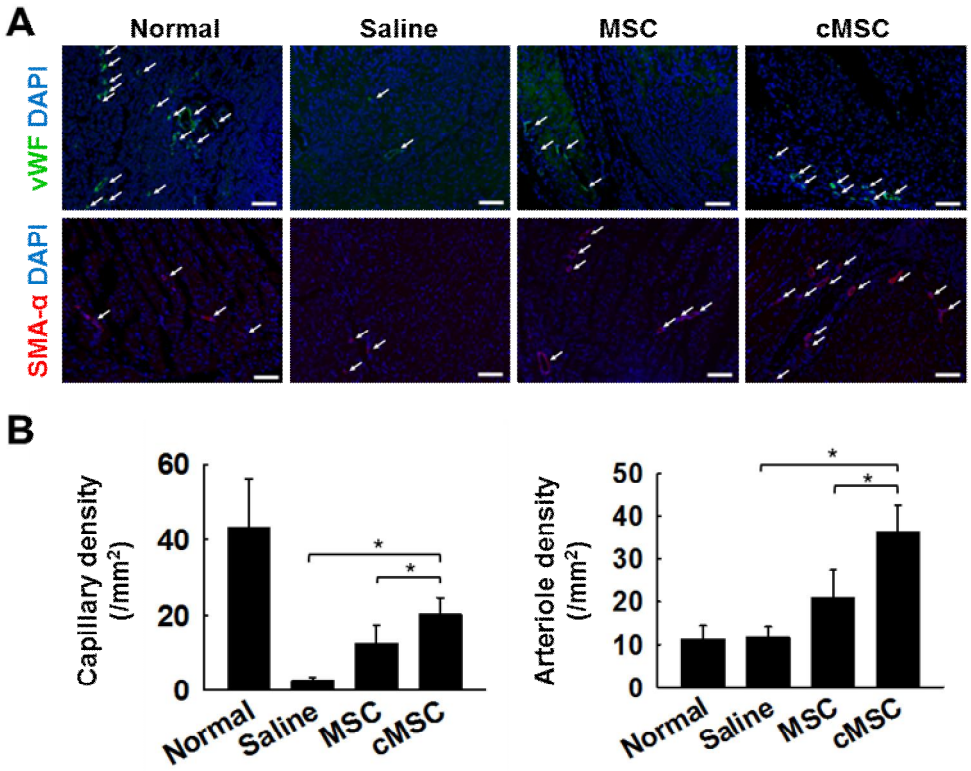

Figure 3.7. Injection of cMSCs increases vessel density. (A) Expression of vWF (upper images; white arrows) and SMA-α (lower images; white arrows) at the peri-infarct, 2 weeks after the treatments. Bar, 100 μm. (B) Quantification of capillary and arteriole density. Vascular densities were quantified as vWF+ or SMA-α+ vessels per mm2. n=4 animals, **P*<0.05.

3.2.7. Enhancement in animal survival and cardiac function

Improvements in animal survival and cardiac function after cMSC injection were evaluated (Figure 3.8). The cumulative animal survival rate was analyzed with Kaplan-Meier analysis (n=6 animals for Normal, 27 for Saline, 21 for MSC and 22 for cMSC; Figure 3.8A). The cMSC group displayed the highest animal survival compared with the other groups. The MSC group showed an increase in survival, but not significant, compared with the saline group (P>0.05). The cMSC group, on the other hand, showed a significant increase in animal survival compared with the saline group (P<0.05). Interestingly, a notable change in animal survival was detected only within 72 hours after treatment. Previous studies showed the ventricular arrhythmias are most likely observed within 48-72 hours after infarction, and they can be regulated with increased expression of cardiac ion channel genes and gap junction protein of the injected cells.[41,43,201] Thus, the improved survival in cMSC-treated animals at the initial phase of MI could have been mediated by the cardiac electrophysiological properties of cMSCs.

To further investigate the functional recovery of the ischemic myocardium, transthoracic echocardiography was performed and quantified (Figure 3.8B). Two weeks after the treatments, both left ventricular internal diameter at end diastole (LVIDd) and at end systole (LVIDs) were markedly decreased in the cMSC group (LVIDd = 6.2±0.5; LVIDs = 3.4±0.5mm) compared with the saline (7.6±0.6; 5.9±0.7mm; P<0.05) or MSC (7.0±0.7; 4.6±1.1mm; P<0.05) groups. The improvements in LVIDd and LVIDs collectively affected the contractility of the heart and greatly recovered the ejection fraction (EF) ratio and fractional shortening (FS) in the cMSC group (EF = 80.3±5.9; FS = 44.7±5.7 %) compared with the saline (50.9±10.4; 22.6±5.7%; P<0.05) or MSC (67.4±14.2; 34.0±10.2%; P<0.05) groups (Figure 3.8B). A previous study has shown that MSCs that express cardiac biomarkers can reduce early animal sudden death, and MSCs' paracrine signaling results in prolonged myocardium protection.[91] We expect the developments of cardiac phenotype and reparative paracrine profile in cMSCs from

the IONP-based co-culture functioned cooperatively to prevent physiological remodeling of the heart, and resulted in cardiac function recovery.[91,100,202]

Long-term engraftment of MSCs, however, was not observed in this study, conforming to the previous studies that showed improved cardiac function with insignificant long-term survival of the injected MSCs.[121,203-206] Injection of human-derived MSCs into rat models could have attributed to the low MSC survival, but a previous study also reported that allogenic injection of rat MSCs also showed rapid cell clearance with improved cardiac function.[203,205,207] Even so, the physiological properties of cMSCs that were previously known to be beneficiary for MI treatment, including Cx43 overexpression (Figure 3.4),[41,171,187] cardiac electrophysiological gene expression (Figure 3.4),[42,43,91] and paracrine signaling (Figure 3.5),[34,36,101,167,168] contributed to the remarkable improvement in cardiac tissue repair and function.

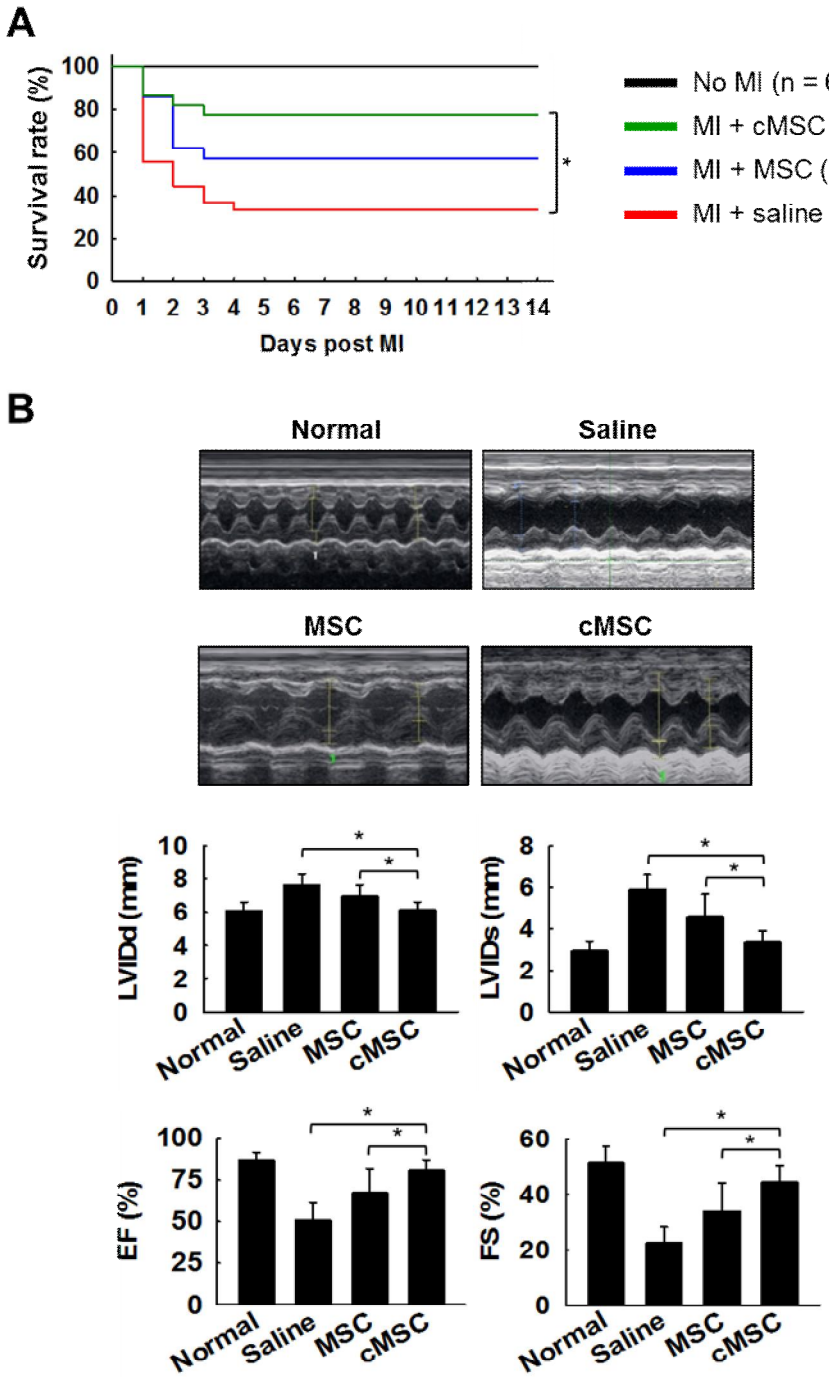

Figure 3.8. Injection of cMSCs improves animal survival and cardiac functions. (A) The cumulative animal survival rate. **P*<0.05, log-rank analysis. (B) Representative images and the quantitative analysis of echocardiography. n=6 animals, **P*<0.05.

Chapter 4.

Dual Roles of Graphene Oxide to Attenuate Inflammation and Elicit Timely Polarization of Macrophage Phenotypes for Cardiac Repair

4.1. Introduction

Cardiac diseases are the leading causes of death worldwide,[1,2] and myocardial infarction (MI) contributes to majority of cardiac-associated disorders.[1,4,5] MI occurs from coronary artery occlusion, resulting in low blood supply and oxygen deprivation at the downstream myocardium,[6] inducing necrosis and apoptosis of resident cardiomyocytes, infiltration of inflammatory macrophages, initiation of inflammation and progression of cardiac tissue remodeling.[6] Left untreated, these remodeling events lead to cardiac fibrosis and electrophysiological challenge in the myocardium for heart failure.[3] Recently, significant advances have been made in MI treatment using mesenchymal stem cells (MSCs) with their angiogenic, anti-apoptotic, anti-inflammatory, and cardioprotective effects.[17-20,38-40] Even so, stem cell therapy faces a number of problems including invasive autologous cell isolation procedure, time-consuming and expensive *ex vivo* cell-manipulation, low cell-grafting efficiency and electrophysiological challenge after implantation.[41,42,44,208-210] More recently, implantation of primed dendritic cells (DCs) has been utilized to improve wound remodeling and preserve cardiac function after MI *via* modulating regulatory T cells and macrophages.[211] However, the DC therapy requires *ex vivo* manipulation of DCs and modulates systemic immune system.[211] Hence, timely modulation of local inflammatory macrophages in MI region with off-the-shelf materials may provide a novel therapeutic approach that can overcome the shortcomings of the current cell therapies for cardiac repair.

Macrophages are the primary and integral responders of the body immune system after MI.[6,71,73,74] There are largely two types of macrophages involved in cardiac repair; classically activated M1 macrophages that secrete pro-inflammatory cytokines such as tumor necrosis factor-α (TNF-α) and interleukin 6 (IL-6), and alternatively activated M2 macrophages that produce anti-inflammatory cytokines including interleukin 4 (IL-4) and interleukin 10 (IL-10).[75,107,108] After MI, resident macrophages and peripheral monocytes/macrophages targeted to the infarct region

differentiate into M1 macrophages to remove necrotic cells and debris, further initiating inflammatory reactions (phase 1).[71,104,105] Thereafter, during the inflammation resolution stage (phase 2), cardiac tissue-dominant macrophage populations become reparative M2 macrophages that propagate cardiac repair.[71,104,105] Both phase 1 and 2 are required for successful tissue repair, where the extent of inflammatory phase 1 is particularly critical in regulating infarct size and left ventricular remodeling because uncontrolled adjustment of macrophage phenotypes and prolonged inflammation can impair proper tissue reconstruction.[6,71,104] Recently, earlier phenotype shift of M1 to M2 macrophages has demonstrated significant improvements in MI wound modeling and cardiac function.[211] Inflammatory phase 1 is closely related to the generation of reactive oxygen species (ROS),[212,213] which are known to initiate inflammatory activation of macrophages and facilitate inflammatory cell migration to the infarct.[72,78,79] Hence, modulation of ROS in inflammation-stimulated macrophages and earlier shift of macrophage phenotype have become a major therapeutic target for MI treatment.[72,78,79,211]

The therapeutic efficacy of M2 macrophages has been demonstrated previously, [76,77,211] hence, various kinds of supplements, such as IL-4, IL-10, cerium oxide nanoparticle, and gold nanoparticle, have been utilized previously to polarize M1 to M2 macrophages. [109-115] Among a number of supplements, recombinant proteins have been most widely used and served as golden standards for macrophage polarization. However, the difficulties in the preservation of their bioactivity *in vivo* and local delivery of the proteins[214-216] limited their utilization. To overcome these problems, targeted delivery of DNAs, RNAs and siRNAs to the cells of interests using nanomaterials, such as alginate,[116] chitosan,[117] cell-based exosomes,[118] or hyaluronic acid,[119] has been introduced for macrophage polarization. Additionally, nanomaterials with natural anti-inflammatory properties have also been introduced.[113-115,217,218] However, the effect of nanoparticles in cell function modulation has rarely been elucidated, and the potential synergistic effects

between nanomaterials and gene delivery have not been clarified.

Recently, graphene oxide (GO) has been spotlighted as an efficient gene carrier.[151-155,219] Previous studies highlighted the facile manipulation of GO in conjugating polyethyleneimine (PEI) and polyethylene glycol (PEG) that are necessary for gene carrying and long circulation in blood, respectively, demonstrating the effectiveness of GO as a biocompatible gene delivery carrier.[152,155] Additionally, previous studies have reported that the implantation of GO did not exhibit *in vivo* toxicity even after 90 days in mice,[220] and GO dosage less than 100 mg/kg does not elicit *in vivo* toxicity.[221] Even so, previous studies did not elucidate the biological role of GOs within the cells. Furthermore, GOs have been introduced to possess antioxidant property based on sp^2 chemistry,[222] but their radical scavenging effect within the cells has not been clarified. Such natural antioxidant function and gene-deliverable property may potentiate the therapeutic application of GO, and this modality can lead to an off-the-shelf therapy for inflammation-mediated diseases such as MI.

Here, we demonstrate that GOs can function as natural antioxidants to attenuate inflammatory polarization of macrophages (M1) *via* ROS reduction within macrophages and can serve as a gene carrier to further polarize M1 macrophages to inflammation-resolving M2 macrophages for the synergistic treatment of MI (Figure 4.1). We modified GOs with PEI and folic acid-PEG (FA-PEG) to develop macrophage-targeting/polarizing GO complex (MGC, Figure 4.1A), and showed that MGC uptake can not only reduce ROS in immune-stimulated macrophages but also produce less amounts of inflammatory biomarkers (Figure 4.1B). Additionally, delivery of IL-4 plasmid DNA (pDNA) using MGC further polarized M1 macrophages to M2 macrophages, and significantly increased the expression of reparative biomarkers necessary for cardiac repair (Figure 4.1B). Thereafter, we injected MGC/IL-4 pDNA in MI mice and demonstrated regulation of local macrophage polarization, attenuation of cardiac fibrosis, increase in blood vessel density, and preservation of cardiac function (Figure 4.1B). In the present

study, we elucidate dual roles of GO in reducing ROS within the macrophages for inflammation attenuation and in delivering anti-inflammatory gene to elicit earlier shift to regenerative macrophages (M2) for the synergistic therapy of MI.

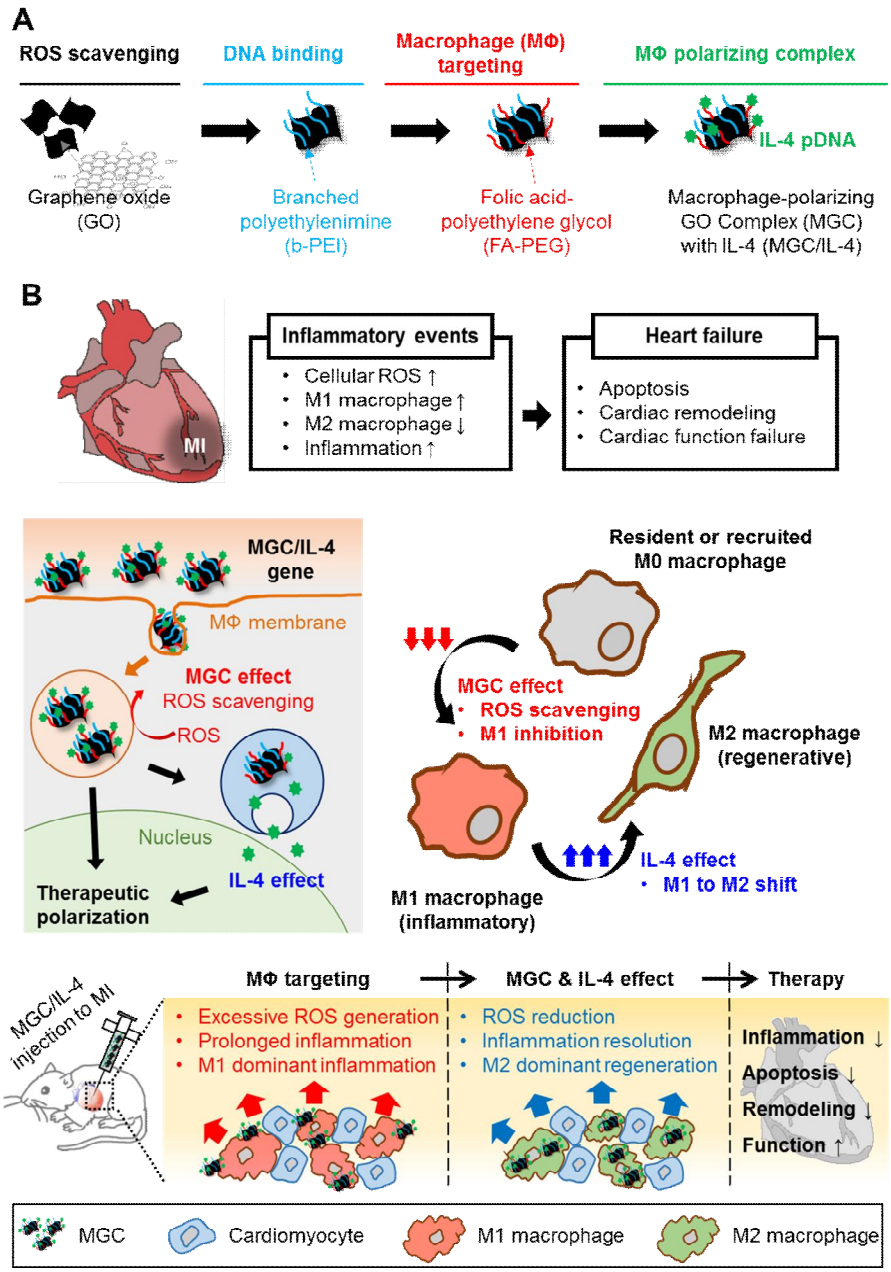

Figure 4.1. Schematic illustration of the preparation of macrophage-polarizing GO complex (MGC)/IL-4, progression of heart failure after MI and the therapeutic mechanisms of MGC/IL-4 pDNA in treating MI. (A) Stepwise preparation of MGC or MGC/IL-4 pDNA, and the role of each chemical conjugation. (B) Progression of heart failure after MI, and the therapeutic mechanisms of MGC/IL-4 pDNA in cardiac repair.

4.2. Results and discussion

4.2.1 Preparation and characterization of macrophage-targeting/polarizing graphene oxide complex (MGC)

MGC was prepared and characterized (Figure 4.2). Graphene oxides (GO) were first conjugated with DNA-conjugatable Polyethyleneimine (PEI), and further reacted with folic acid-conjugated polyethylene glycol (FA-PEG) for the generation of MGC. To evaluate the conjugation of PEI, PEG or FA-PEG individually, PEI-conjugated GO (GP) and PEI/PEG-conjugated GO (GPP) were also synthesized (Figure 2A). Fourier transform infrared (FT-IR) analysis demonstrated that GOs were successfully conjugated with PEI, PEI/PEG or PEI/FA-PEG for the generation of GP, GPP, or MGC, respectively (Figure 4.2A). The GO complexes were then characterized using Raman spectroscopy (Figure 4.2B) and thermogravimetric analysis (TGA: Figure 4.2C) to assess chemical property alterations after chemical conjugations. Raman spectrum analysis demonstrated that GO derivatives all exhibited intensity peaks at both D and G band, suggesting that there was no significant change in sp^2 carbon structure after chemical conjugations (Figure 4.2B). Additionally, TGA assessment showed similar weight loss profiles in GP, GPP and MGC (Figure 4.2C). Thereafter, GO derivatives were analyzed with dynamic light scattering (DLS) and electrophoretic light scattering (ELS) for their size determination and surface zeta potential evaluation, respectively (Figure 4.2D). Previous studies showed smaller-sized nanoparticles could enhance their cellular uptake,[223] and large-sized microparticles could provoke inflammatory responses in macrophages.[224] More importantly, it was reported that nanoparticles less than 100 nm were co-localized in lysosomes 24 hours after cellular uptake, while larger particles with 200 nm size showed relatively less lysosomal localization,[225] which implies that nanoparticles with the range of 100 and 200 nm are better suited for gene delivery. DLS data showed that GO complexes had relatively uniform size distribution with average size of

approximately 150 nm, which is proper for gene delivery. Additionally, all PEI-conjugated GO complexes (GP, GPP and MGC) exhibited positively charged surface potential, which is required for DNA conjugation (Figure 4.2D). Furthermore, to assess the functionality of PEG conjugation, the colloidal stability of the GO complexes in aqueous solution was evaluated (Figure 4.2E). Colloidal stability of nanoparticles under serum-present condition is particularly important because low aqueous stability and excessive protein fouling on the nanoparticle surface can dramatically change particle size, charge, and hydrophobicity.[226] The data demonstrated that GP, GPP and MGC all exhibited high colloidal stability in deionized water (DW). In serum-containing cell culture medium, however, GP showed particle precipitation at 2 hours, while GPP and MGC demonstrated better dispersion. The data suggested that PEG conjugation greatly improved the colloidal stability of GO complexes in *in vivo*-mimicking serum-present condition, and only GPP and MGC are suitable for further *in vitro* analysis and *in vivo* applications. Interestingly, conjugation of FA-PEG showed much better aqueous stability compared to PEG conjugation.

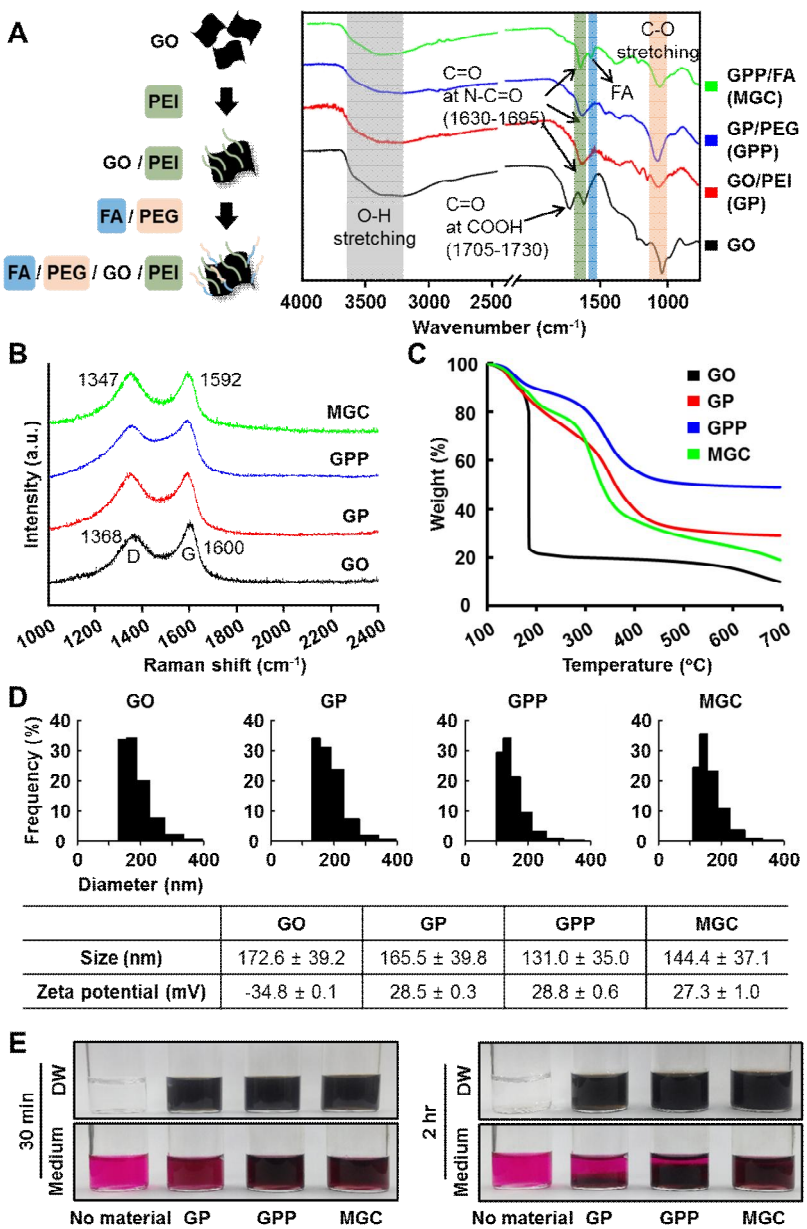

	GO	GP	GPP	MGC
Size (nm)	172.6 ± 39.2	165.5 ± 39.8	131.0 ± 35.0	144.4 ± 37.1
Zeta potential (mV)	-34.8 ± 0.1	28.5 ± 0.3	28.8 ± 0.6	27.3 ± 1.0

Figure 4.2. Characterization of GO derivatives (GP: GO/PEI, GPP: GO/PEI/PEG, and MGC: GO/PEI/PEG/FA). (A) FT-IR evaluation of GO derivatives to assess each step of chemical conjugation. (B) Raman spectra of GO derivatives. (C) TGA profiles of GO derivatives. (D) DLS and ELS assessment of GO derivatives. (E) Colloidal stability of GO derivatives dispersed in deionized water (DW) or serum-containing cell culture medium. Images were acquired after leaving each sample at room temperature for 30 or 120 minutes.

4.2.2. Selective cellular uptake and cytotoxicity of MGC

Selective cellular uptake and cytotoxicity of GO complexes were then evaluated. Mouse bone marrow-derived macrophages (mBMDM) were first treated with 200 ng/mL lipopolysaccharide (LPS) for 24 hours to induce M1 phenotype, followed by the treatment of DiI-conjugated GPP or MGC for 2 hours. Fluorescent images showed efficient uptake of nanoparticles regardless of FA conjugation after 2 hours (Figure 4.3A). Transmission electron microscopy (TEM) images further demonstrated that GO nanoparticles were internalized into the cells rather than on the surface of the cells (Figure 4.3A). Previously, it was reported that large-sized GOs that cannot be internalized into macrophages may induce M1 phenotype by stimulating membrane proteins.[227] In the present study, however, no GPP or MGC was observed on macrophage surfaces, and the nanoparticles were completely internalized into the cells (Figure 4.3A). Internalization of GPP or MGC exhibited no cellular toxicity 3 days after treatment, whereas naked PEI demonstrated notable cytotoxicity (Figure 4.3B).

Next, the functionality of folic acid (FA) in GO complexes was evaluated using cellular uptake assay. FA is known to bind to the receptors on activated macrophages, and previous studies demonstrated the efficacy of FA in macrophage targeting.[228-230] To demonstrate that MGC has more affinity toward inflammatory macrophages and are better uptaken by these cells compared with GPP, cellular uptake of MGC by various cell types were assessed. Three types of cells that are most abundant at cardiac infarction area, namely cardiomyocytes, cardiac fibroblasts and macrophages, were first labelled using green fluorescent dye DiO and treated with DiI-conjugated GPP or MGC. Thirty minutes after nanoparticle treatment, fluorescent images showed that both GPP and MGC were extensively detected in macrophages, whereas almost no nanoparticle uptake was observed in cardiomyocytes or cardiac fibroblasts (Figure 4.3C). Quantitative analysis further demonstrated that GPP and MGC showed more than 7-fold increased uptake in macrophages compared with other infarction-abundant cells, and MGC exhibited

notably more cellular uptake in macrophages compared to GPP. Collectively, the data suggest MGC has high affinity toward macrophages, and majority of MGC delivered *in vivo* would likely be internalized into macrophages rather than cardiomyocytes or cardiac fibroblasts. Hence, only the MGC group was further utilized in the subsequent *in vitro* and *in vivo* studies.

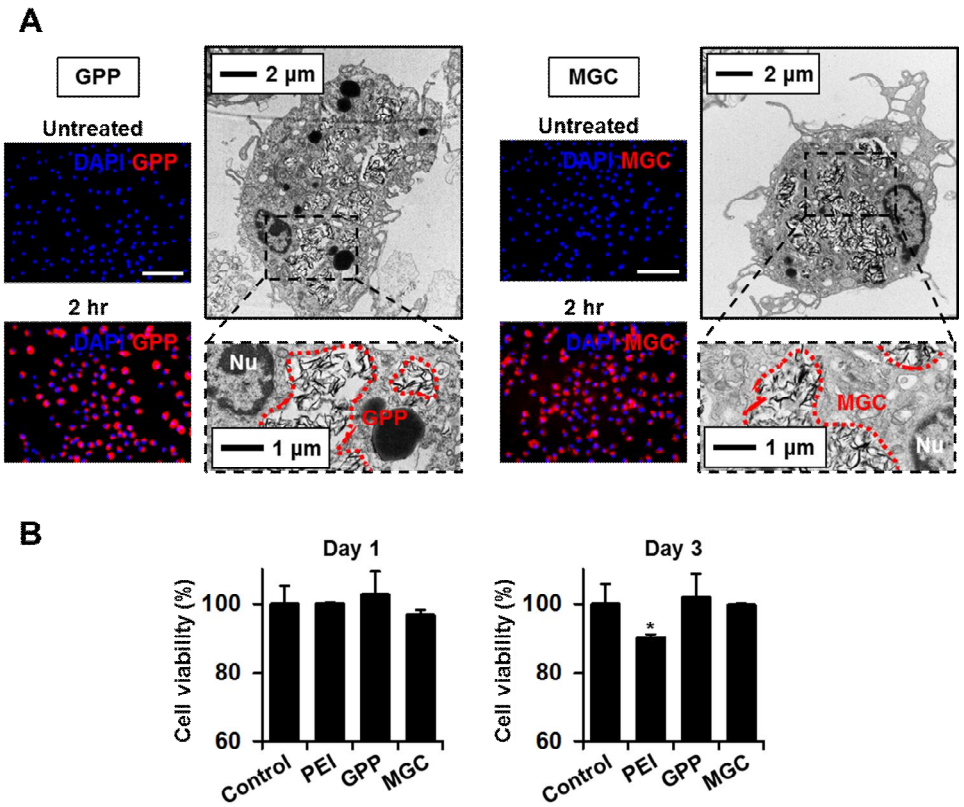

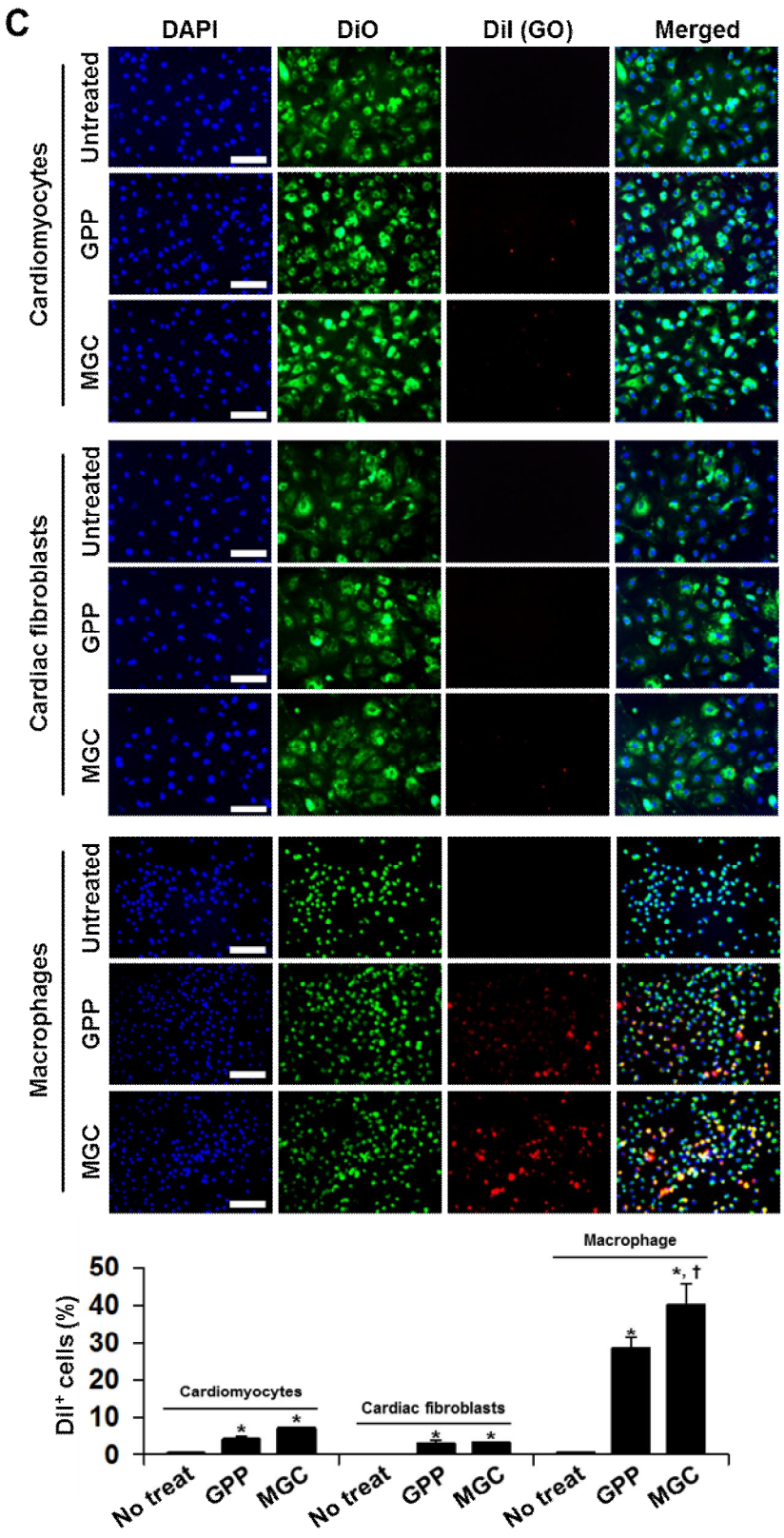
C
DAPI
DiO
DiI (GO)
Merged
Cardiomyocytes
Untreated
GPP
MGC
Cardiac fibroblasts
Untreated
GPP
MGC
Macrophages
Untreated
GPP
MGC
Macrophage
DiI+ cells (%)
50
40
30
20
10
0
Cardiomyocytes
Cardiac fibroblasts
*
*, †
No treat
GPP
MGC
No treat
GPP
MGC
No treat
GPP
MGC

Figure 4.3. Targeted cellular uptake and cytotoxicity of MGC in vitro. (A) Fluorescent and TEM images of GPP or MGC-uptaken macrophages 2 hours after the treatments. GPP and MGC were labeled with red fluorescent dye DiI prior to treatments. Bars, 100 μm in fluorescent images. (B) Viability of macrophages treated with either PEI, GPP or MGC for 1 or 3 days, as evaluated by MTT assay. Each group was treated with either 15 μg/mL PEI, 100 μg/mL GPP or 100 μg/mL MGC. *$p<0.05$ vs. Control. (C) Fluorescent images showing selective uptake of MGC in macrophages compared to other cell types abundant in the infarction region. Cardiomyocytes, cardiac fibroblasts, and macrophages were pre-labeled with green fluorescent dye DiO. Cells were treated with DiI-labeled GPP or MGC for 30 minutes at 37oC. Cells that did not uptake GPP or MGC were visualized as DiO+/DiI- (green), while the GPP or MGC-uptaken cells were visualized as DiO+/DiI+ (yellow). Bars, 100 μm. Fluorescent images were quantified for statistical evaluation. n=3. *$p<0.05$ vs. Control, and †$p<0.05$ vs. GPP.

4.2.3. Reactive oxygen species scavenging and inflammation modulation by MGC

The antioxidant effect MGC was next investigated (Figure 4.4). Quantification of Raman spectrum analysis demonstrated that the relative intensity ratio between D and G band of MGC was higher than that of GO (Figure 4.4A), indicating that smaller in-plane sp^2 domains were formed in MGC compared to GO.[231,232] Thereafter, metal chelating activity assay using ferric chloride and Ferrozine was performed (Figure 4.4B and C). Transition metal such as iron is a well-known factor that forms hydroxyl radicals and contributes to the generation of oxidative stress and reactive oxygen species (ROS) within the cells.[233,234] Hence, the functionality of antioxidant materials has been analyzed using the metal chelation methods.[159,235] Figure 4.4B demonstrates that both GO and MGC successfully disrupted Fe^{2+} complex formation, but MGC exhibited better metal chelation compared to GO at a concentration of 500 μg/mL. Further spectrophotometer assessment indicated that MGC showed better antioxidant function with the increase in the MGC concentration (Figure 4.4C).

Next, the ability of MGC to reduce ROS within the immune-stimulated cells was evaluated (Figure 4.4D). Infarction- or ischemia-mediated generation of ROS is an important signal that activates inflammation by recruiting inflammatory cells to the infarct,[236] promotes M1 differentiation[237] and increases the risks of cardiac arrhythmia[238]. Hence, timely reduction of both cellular ROS and inflammatory macrophages are critical for effective cardiac healing. To evaluate ROS scavenging effect of MGC, mBMDMs were pretreated with MGC at concentration of 10 μg/mL for 2 hours, followed by the treatment of 200 ng/mL LPS, which is previously known to induce intracellular ROS and promote M1 differentiation.[239-241] After 24 hours, the level of ROS was determined using H_2DCFDA fluorescence kit, and further analyzed with fluorescence-activated cell sorting (FACS: Figure 4.4D). When macrophages were treated with MGC alone,

approximately 8 % of mBMDMs exhibited ROS-positive green FITC fluorescence. Cells treated with LPS, however, exhibited more than 70 % FITC-positive cell populations. Surprisingly, the MGC pretreatment before LPS treatment dramatically reduced FITC-positive cell populations to less than 36 % (Figure 4.4D), indicating that MGC could suppress the production of ROS within the immune-stimulated macrophages. Moreover, the MGC pretreatment prior to LPS treatment greatly downregulated the expression of pro-inflammatory inducible nitric oxide synthase (iNOS) gene in macrophages (Figure 4.4E). Downregulation of iNOS expression was further evaluated using western blot assay, and the MGC pretreatment significantly reduced the protein expression iNOS in immune-stimulated macrophages (Figure 4.4F), conforming to the results of previous studies with immune-modulatory antioxidants.[113-115,242] Increased expression of inflammatory genes and proteins are closely related to the phosphorylation of Akt,[114] hence, the activation of Akt signaling pathway was examined using western blot assay (Figure 4.4F). The result indicates that LPS treatment induced significant phosphorylation of Akt signaling in macrophages, whereas the phosphorylation was reduced by the MGC pretreatment. Thereafter, the secretion of an inflammatory cytokine, tumor necrosis factor alpha (TNF-α), was evaluated (Figure 4.4G). mBMDM treated with MGC alone showed negligible secretion of TNF-α, whereas LPS treatment significantly increased TNF-α secretion. The MGC Pretreatment prior to LPS treatment, however, reduced TNF-α secretion by 20 %, which is partially attributable to the downregulation of iNOS expression and Akt phosphorylation. Collectively, the data suggest that MGC actively reduce ROS in immune-stimulated macrophages for inflammation modulation and prevention of inflammatory activation of the cells.

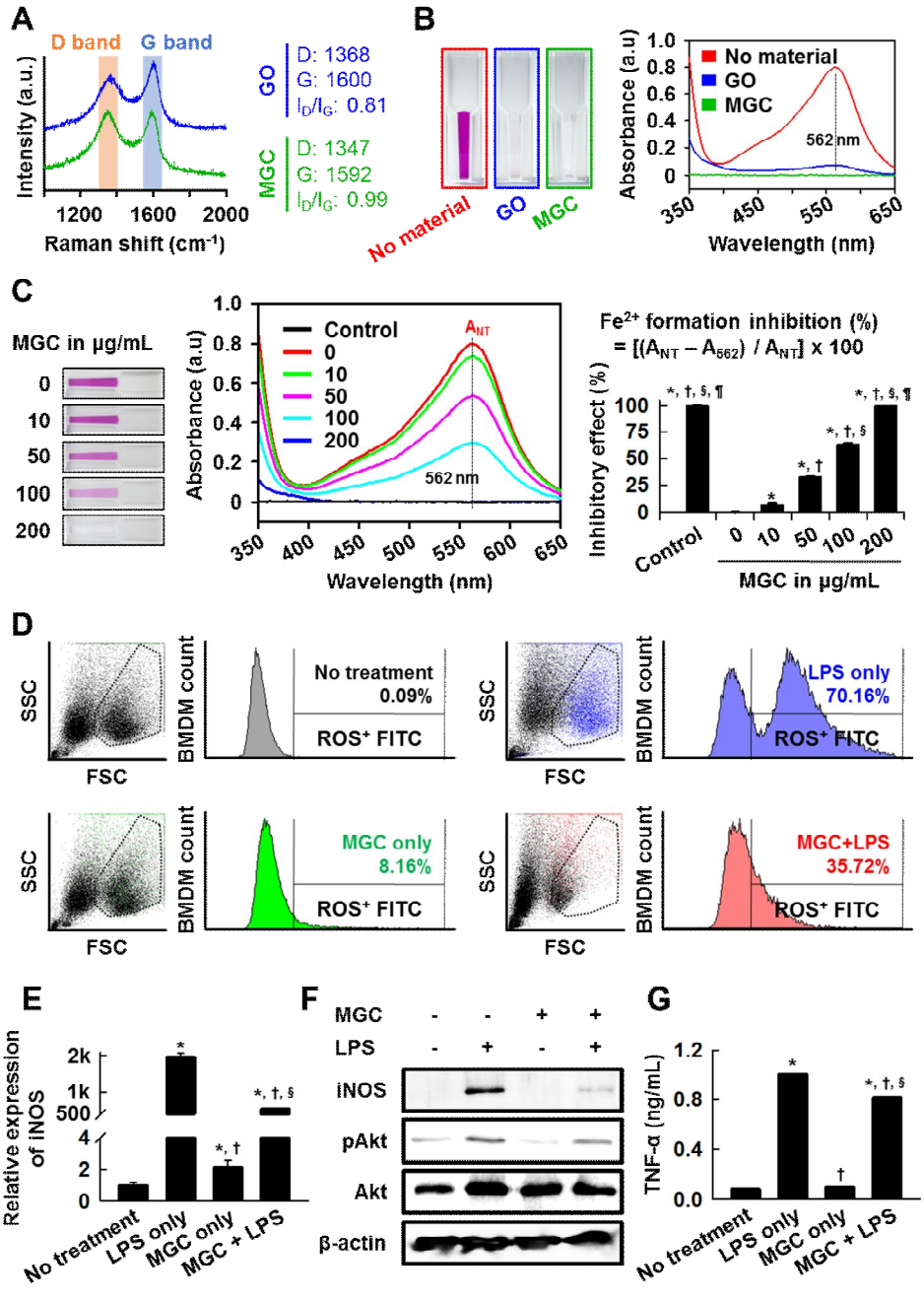
A
D band
G band
Intensity (a.u.)
1200
1600
2000
Raman shift (cm-1)
GO
D: 1368
G: 1600
ID/IG: 0.81
MGC
D: 1347
G: 1592
ID/IG: 0.99
B
No material
GO
MGC
Absorbance (a.u)
No material
GO
MGC
562 nm
Wavelength (nm)
C
MGC in μg/mL
0
10
50
100
200
Absorbance (a.u)
Control
0
10
50
100
200
ANT
562 nm
Wavelength (nm)
Fe2+ formation inhibition (%)
= [(ANT – A562) / ANT] x 100
Inhibitory effect (%)
Control
MGC in μg/mL
D
SSC
FSC
BMDM count
ROS+ FITC
No treatment
0.09%
LPS only
70.16%
MGC only
8.16%
MGC+LPS
35.72%
E
Relative expression of iNOS
No treatment
LPS only
MGC only
MGC + LPS
F
MGC
LPS
iNOS
pAkt
Akt
β-actin
G
TNF-α (ng/mL)
No treatment
LPS only
MGC only
MGC + LPS

Figure 4.4. Metal chelation, intracellular ROS scavenging, and inflammation modulation by MGC. (A) Intensity peak ratio evaluated by Raman spectra for GO and MGC. (B) Metal ion chelating activity of GO and MGC (concentration, 500 μg/mL). Representative macroscopic images were acquired 5 minutes after the treatments. Absorbance was measured at 562 nm. (C) Metal ion chelating activity of MGC at various concentrations. The inhibition of Fe^{2+} formation was calculated using absorbance at 562 nm. Representative macroscopic images were acquired 5 minutes after the treatments. n=3, *p<0.05 *vs.* 0 group, $^{\dagger}p$<0.05 *vs.* 10 group, $^{\S}p$<0.05 *vs.* 50 group, and $^{\P}p$<0.05 *vs.* 100 group. (D) FACS analysis of intracellular ROS in macrophages under various conditions, and the ROS scavenging effect of MGC pretreatment prior to LPS treatment to macrophages. Fluorescent signal of intracellular ROS was induced using H_2DCFDA kit. MGC pretreatment-mediated inhibition of the expressions of inflammation-involved (E) iNOS gene (qRT-PCR), (F) iNOS proteins and Akt phosphorylation (western blot), and (G) TNF-α (Quantikine) in macrophages treated with or without 200 ng/mL LPS for 24 hours. Expression levels of the gene were normalized to the control group (no treatment). n=3, *p<0.05 *vs.* No treatment, $^{\dagger}p$<0.05 *vs.* LPS only, and $^{\S}P$<0.05 *vs.* MGC only.

4.2.4. Polarization of M1 macrophages to M2 macrophages

Next, we delivered IL-4 pDNA using MGC to polarize M1 macrophages to M2 macrophages (Figure 4.5). Previous studies demonstrated that M2 macrophages actively participate in cardiac repair,[77-80,243] and depletion of M2 macrophages can result in cardiac failure by severely impairing left ventricular contractile function and increasing inflammatory cell population.[76,81] Hence, early shift from the inflammatory M1 phase to reparative M2 phase is essential for successful cardiac repair.[211] To assess the therapeutic potential of MGC as a gene carrier, DNA conjugation was first evaluated using 1.5 % agarose gel electrophoresis assay. Figure 4.5A shows that IL-4 pDNA was completely conjugated to MGC at a N/P ratio of 10. The IL-4 pDNA transfection to macrophages was evaluated and quantified using western blot assay (Figure 4.5B). Interestingly, treatment of MGC alone (the MGC group) also increased the expression of M2 biomarker IL-4 within the cells, whereas IL-4 pDNA-conjugated MGC (the MGC/IL-4 pDNA group) exhibited better protein expression of IL-4 (Figure 4.5B). To evaluate the cell morphological change after MGC/IL-4 pDNA treatment, mBMDMs were stimulated with 200 ng/mL LPS for 24 hours, followed by the addition of MGC or MGC/IL-4 pDNA for 48 hours. Fluorescent images showed that macrophages treated with MGC or MGC/IL-4 pDNA exhibited significant morphological change to elongated shape of M2 macrophages, conforming to the results of previous studies.[136,244] Two days after the treatment, quantitative polymerase chain reaction (qRT-PCR) analysis showed that MGC or MGC/IL-4 pNDA uptake significantly downregulated the expressions of inflammatory genes such as interleulkin-6 (IL-6), iNOS, and TNF-α (Figure 4.5D). Interestingly, downregulation in gene expression was observed regardless of IL-4 pDNA, while IL-4 pDNA delivery induced better inflammatory gene reduction. Significant downregulation in inflammatory genes in the MGC group could be attributed to the ROS scavenging effect of MGC (Figure 4.4). Meanwhile, both MGC and MGC/IL-4 pDNA significantly upregulated the expression of genes associated with reparative M2 macrophages, namely IL-10 and

mannose receptor (CD206: Figure 4.5D). Interestingly, uptake of MGC or MGC/IL-4 pDNA also increased the gene and protein expression of gap junction protein connexin 43 (Cx43: Figure 4.5D and E). Cx43 expression is particularly important in cardiac repair, because Cx43 plays a major role in intercellular gap junction communications in the myocardium.[45,183] Previous studies addressed that irregularity in cardiac conduction after MI could be exacerbated by low Cx43 expression at the infarct zone,[45,183,245] and that cardiac abnormalities can be mitigated when Cx43-expressing cells were delivered at the infarct.[41,45,91,170] The activation of c-Jun N-terminal kinase (JNK) can reduce Cx43 expression and develop arrhythmias,[246] hence, significant upregulation of Cx43 and inhibition of JNK phosphorylation (Figure 4.5E) by MGC or MGC/IL-4 pDNA treatment suggest that macrophages treated with MGC or MGC/IL-4 pDNA *in vivo* may participate in electrophysiological cardiac repair after MI. Cytokine secretion of macrophages treated with MGC or MGC/IL-4 pDNA was then analyzed using Quantikine assay (Figure 4.5F). Data showed that M1 macrophages treated with MGC or MGC/IL-4 pDNA exhibited decreased secretion of inflammatory cytokine IL-6 and TNF-α. Interestingly, uptake of MGC alone downregulated the secretion of the cytokines, while no significant increase in M2 cytokine IL-10 secretion was observed. MGC/IL-4 pDNA, however, increased IL-10 secretion, demonstrating that conjugation of IL-4 pDNA to MGC was vital in reparative cytokine secretion. IL-4 pDNA also played a critical role in the expression of angiogenic genes (Figure 4.5G). Data showed that M1 macrophages treated with MGC did not significantly affect the gene expression of basic fibroblast growth factor (bFGF) and transforming growth factor-beta (TGF-β3), while MGC/IL-4 pDNA exhibited increase in these angiogenic genes. Interestingly, MGC slightly increased vascular endothelial growth factor (VEGF) gene. Collectively, the data suggest that while MGC alone can regulate the expression of inflammatory genes and proteins of M1 macrophages, the delivery of Il-4 pDNA using MGC is vital in differentiating M1 macrophages to functional reparative M2 macrophages.

Next, the secretion of angiogenic or inflammation-regulatory cytokines was evaluated using protein array for the conditioned medium of non-treated M1 macrophages and MGC- or MGC/IL-4 pDNA-treated M1 macrophages (Figure 4.5H). The dot blot analysis 3 days after the treatments indicated that macrophages treated with MGC or MGC/-IL4 pDNA showed significant reduction in plasminogen activator inhibitor-1 (PAI-1), CXCL10, Amphiregulin, tissue inhibitor of metalloproteinase-1 (TIMP-1) and macrophage inflammatory protein-1 alpha (MIP-1α). On the other hand, the secretion of matrix metalloproteinase-8 (MMP-8) and interleukin-1 alpha (IL-1α) was increased in these groups. Secretion of PAI-1 and TIMP-1 is known to be higher in M1 macrophages compared to M2 macrophages.[247] PAI-1 activates macrophages to produce pro-inflammatory cytokines and skew M2 differentiation,[248,249] while silencing TIMP-1 in M1 macrophages can render them angiogenic.[250] M1-associated CXCL10[251] recruits monocyte-derived macrophages and aggravate inflammatory response,[252,253] where Amphiregulin and MIP-1α are mainly generated by M1 macrophages.[254,255] Amphiregulin is also known to promote pro-inflammatory activity,[256] and MIP-1α silencing exerts anti-inflammatory effects.[257] On the other hand, secretion of MMP-8, which is involved in M2 differentiation of macrophages,[258,259] was promoted in the MGC or MGC/IL-4 pDNA groups. Interestingly, the secretion of IL-1α was also promoted by MGC or MGC/IL-4 pDNA treatments. Similar to the gene expression alteration (Figure 4.5D), MGC could also improve the paracrine profile of the macrophages, while the IL-4 pDNA conjugation demonstrated superior secretion of cardiac repair-favorable cytokines. Collectively, this data suggest that macrophages polarized by MGC or MGC/IL-4 pDNA could augment cardiac repair *via* paracrine signaling pathways and the IL-4 gene conjugation can further improve the therapeutic efficacy of MGC. The functionality of these paracrine factors in salvaging ROS-mediated apoptotic cardiomyocytes was then evaluated (Figure 4.5I). Cardiomyocytes treated with 100 mM H_2O_2 for 4 hours showed extensive cell death, and co-culture of these cells with M1 macrophages further

aggravated cell viability. When M1 macrophages were polarized with MGC/IL-4 pDNA for 2 days, however, significant enhancement in cell viability was observed, suggesting the cytokines secreted from MGC/IL-4 pDNA-polarized macrophages were cardioprotective.

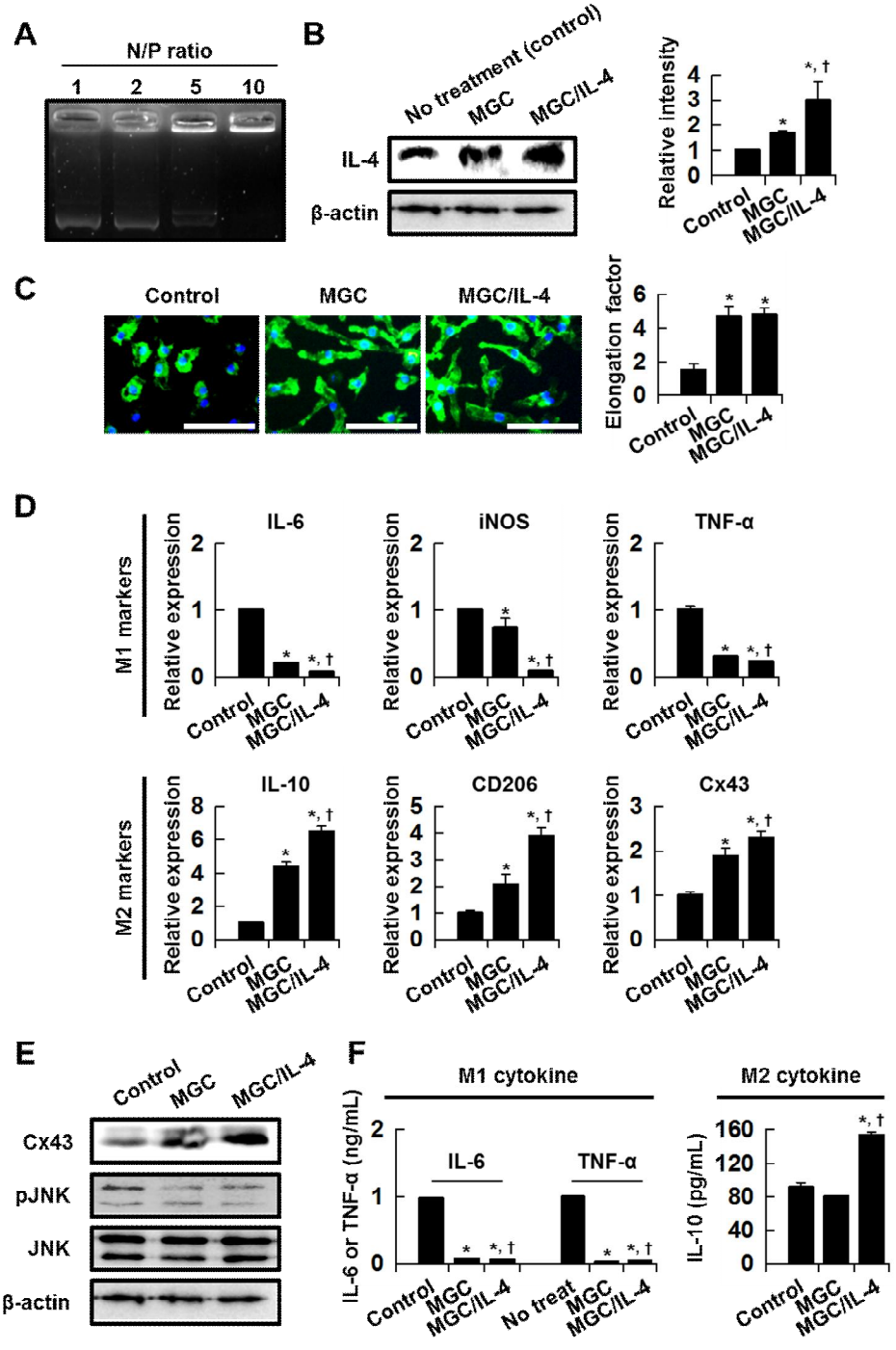
A
N/P ratio
1
2
5
10
B
No treatment (control)
MGC
MGC/IL-4
IL-4
β-actin
Relative intensity
Control
MGC
MGC/IL-4
C
Control
MGC
MGC/IL-4
Elongation factor
D
M1 markers
M2 markers
Relative expression
IL-6
iNOS
TNF-α
IL-10
CD206
Cx43
E
Control
MGC
MGC/IL-4
Cx43
pJNK
JNK
β-actin
F
M1 cytokine
M2 cytokine
IL-6 or TNF-α (ng/mL)
IL-10 (pg/mL)
IL-6
TNF-α
No treat

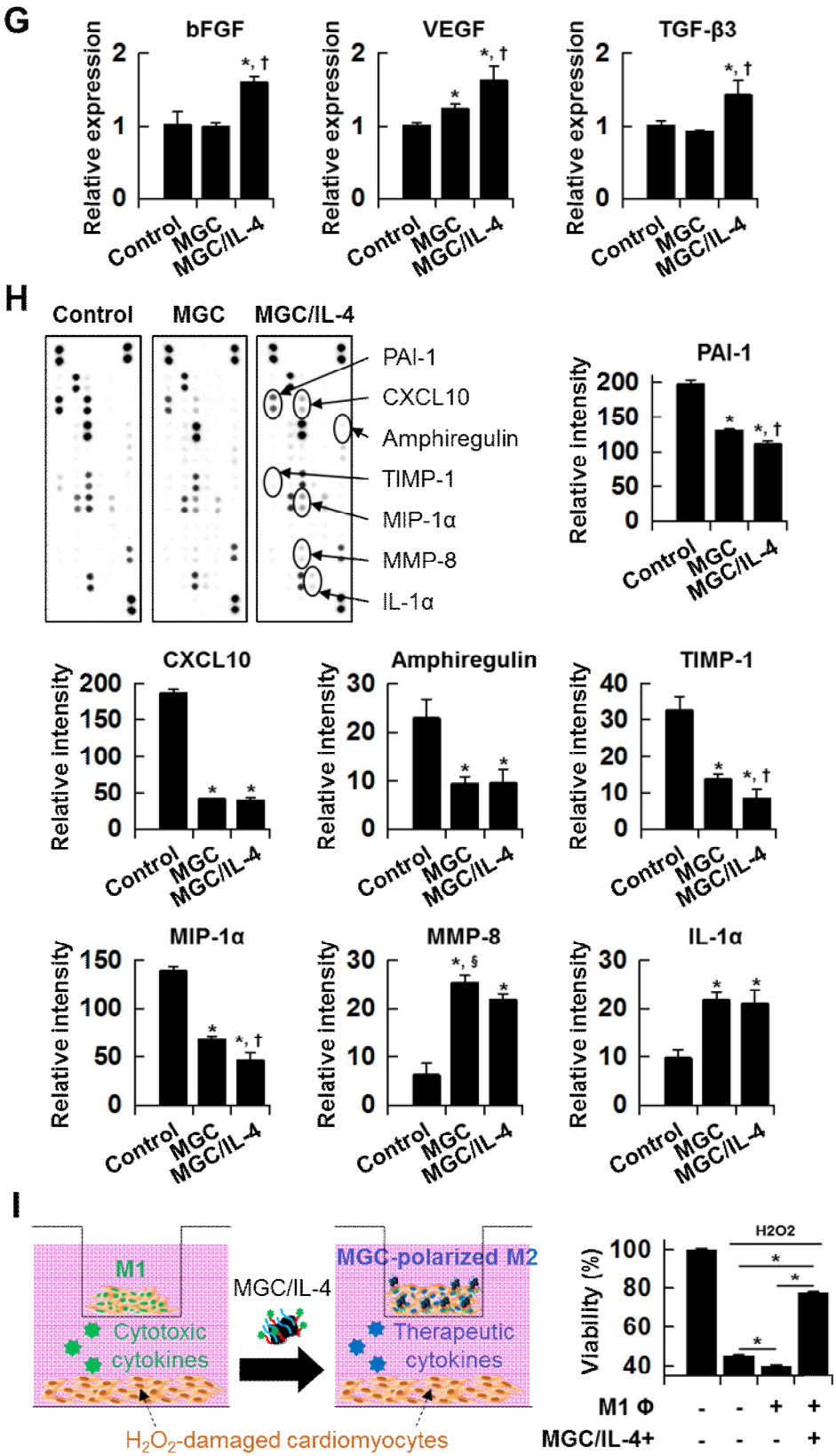
G
bFGF
VEGF
TGF-β3
Relative expression
Control
MGC
MGC/IL-4
H
Control
MGC
MGC/IL-4
PAI-1
CXCL10
Amphiregulin
TIMP-1
MIP-1α
MMP-8
IL-1α
Relative intensity
I
M1
Cytotoxic cytokines
MGC/IL-4
MGC-polarized M2
Therapeutic cytokines
H2O2-damaged cardiomyocytes
H2O2
Viability (%)
M1 Φ
MGC/IL-4+

Figure 4.5. *In vitro* M2 polarization of LPS-stimulated M1 macrophages by MGC or MGC/IL-4 pDNA and their differential profile assessment. The MGC/IL-4 group denotes MGC/IL-4 pDNA. (A) Gel retardation assay of MGC at different N/P ratio showing conjugation of MGC and IL-4 pDNA. (B) Protein expression of IL-4 in LPS-stimulated M1 macrophages after MGC or MGC/IL-4 pDNA treatment for 72 hours. n=3, *p<0.05 *vs.* Control (no treatment), and $^{\dagger}P$<0.05 *vs.* MGC. (C) Morphological change in LPS-stimulated M1 macrophages after MGC or MGC/IL-4 pDNA treatment for 72 hours and the assessment of cell elongation factor. Bars, 100 μm. n=3. *p<0.05 *vs.* Control. (D) The modulatory effects of MGC or MGC/IL-4 pDNA on the regulation of M1 genes and the promotion of M2 phenotype in LPS-stimulated M1 macrophages. n=3, *p<0.05 *vs.* Control, and $^{\dagger}p$<0.05 *vs.* MGC. (E) Western blot analysis for intracellular signaling molecules in LPS-stimulated M1 macrophages after MGC or MGC/IL-4 pDNA treatments for 72 hours. (F) ELISA assessment of inflammatory or anti-inflammatory protein secretion in LPS-stimulated M1 macrophages after MGC or MGC/IL-4 pDNA treatments for 72 hours. n=3, *p<0.05 *vs.* Control, and $^{\dagger}p$<0.05 *vs.* MGC. (G) Enhanced angiogenic gene expressions after MGC or MGC/IL-4 pDNA treatments for 72 hours. n=3, *p<0.05 *vs.* Control, and $^{\dagger}p$<0.05 *vs.* MGC. (H) Representative images and quantitative analysis of the angiogenic and inflammation-regulatory protein array. Paracrine molecules with significant differences in pixel densities compared to the control or MGC group are labelled. n=3, *p<0.05 *vs.* Control, and $^{\dagger}p$<0.05 *vs.* MGC. (I) Cardioprotective effect of MGC/IL-4 pDNA-polarized M2 macrophages as indicated by the viability of H_2O_2-treated cardiomyocytes after co-culture with M1 macrophages or MGC/IL-4 pDNA-polarized M2 macrophages for 48 hours. n=3, *p<0.05.

4.2.5. Attenuation of inflammation and early shift to reparative M2 phase after MGC/IL-4 pDNA injection i*n vivo*

Previous studies demonstrated that the circulating monocytes were infiltrated and differentiated to inflammatory macrophages one day after MI, and subsequent transition from the inflammatory phase to reparative phase occurs between 3 and 5 days after infarction.[260,261] Based on the previous studies, evaluation of inflammatory or reparative phases was performed on 1 and 4 days after MI (Figure 4.6). One and 4 days after the treatments, heart tissues were extracted and analyzed using qRT-PCR for the expression of M1 biomarkers [IL-6, iNOS, monocyte chemoattractant protein-1 (MCP-1), and toll-like receptor-2 (TLR-2)] and M2 biomarkers (IL-10, Ym-1, IL-4, and Fizz1). Figure 4.6A demonstrates that both MGC and MGC/IL-4 pDNA downregulated inflammatory genes 1 and 4 days after the treatments, while the MGC/IL-4 pDNA group exhibited greater downregulation of MCP-1 and TLR-2 genes compared to the MGC group. On the other hand, mice heart tissues demonstrated early inductions of M2 genes only when they were treated with MGC/IL-4 pDNA, implying that IL-4 gene delivery using MGC is crucial in the polarization of macrophages toward M2 type *in vivo*. Cardiac tissues were further evaluated using Western blot assay for the expression of inflammatory or reparative mediators (Figure 4.6B). Data showed that only the groups treated with MGC/IL-4 pDNA exhibited significant downregulation of iNOS, a representative marker of M1 macrophages, and pro-apoptotic BAX. Interestingly, both the MGC group and MGC/IL-4 pDNA group demonstrated enhanced expression of tissue-expression of arginase-1 (ARG1), another common marker for M2 macrophages.[262] We have also observed that the early induction of ARG1 was apparent only in the MGC/IL-4 pDNA group 1 day after MI (Figure 4.6B).

Next, cellular apoptosis (Figure 4.6C) and macrophage infiltration (Figure 4.6D) 1 and 4 days after the treatments were evaluated. One day after the injection of MGC or MGC/IL-4 pDNA, there was no significant improvements in cell

viability at the peri-infarct. Four days after the treatments, however, significant reduction in cellular apoptosis was observed in the MGC/IL-4 pDNA group compared to the saline or MGC group. Thereafter, hematoxylin and eosin (H&E) staining was performed to evaluate macrophage infiltration into the peri-infarct 1 and 4 days after the treatments (Figure 4.6D). Interestingly, the data showed that there was no significant difference in the macrophage infiltrated area among the groups, implying that the total population of macrophages at the infarction site was similar even after MGC or MGC/IL-4 pDNA treatments. Hence, the data showing the enhanced expression of M2 genes and proteins at the peri-infarct zone (Figure 4.6A and B) demonstrates that the majority of the infiltrated macrophages 4 days after MGC/IL-4 pDNA treatment were M2 macrophages. To further evaluate the population of M2 macrophages, heart tissues were analyzed 4 days after MI using immunohistochemistry for CD206, a M2 macrophage marker (Figure 4.6E). The analysis showed that MGC/IL-4 pDNA significantly raised the population of M2 macrophages at the peri-infarct zone compared to the control (PBS injection) and MGC injection group. This data suggests the total population of macrophages after infarction remained similar in each group (Figure 4.6D), Conforming to the previous studies,[76] while the ratio of M2 macrophages was significantly higher after MGC/IL-4 pDNA treatment (Figure 4.6E). Collectively, these data suggest that MGC/IL-4 pDNA can significantly downregulate inflammation at the infarcted region 1 and 4 days after the treatment, and facilitate effective transition of inflammatory phase to reparative phase to increase the population of M2 macrophages for better cardiac repair.

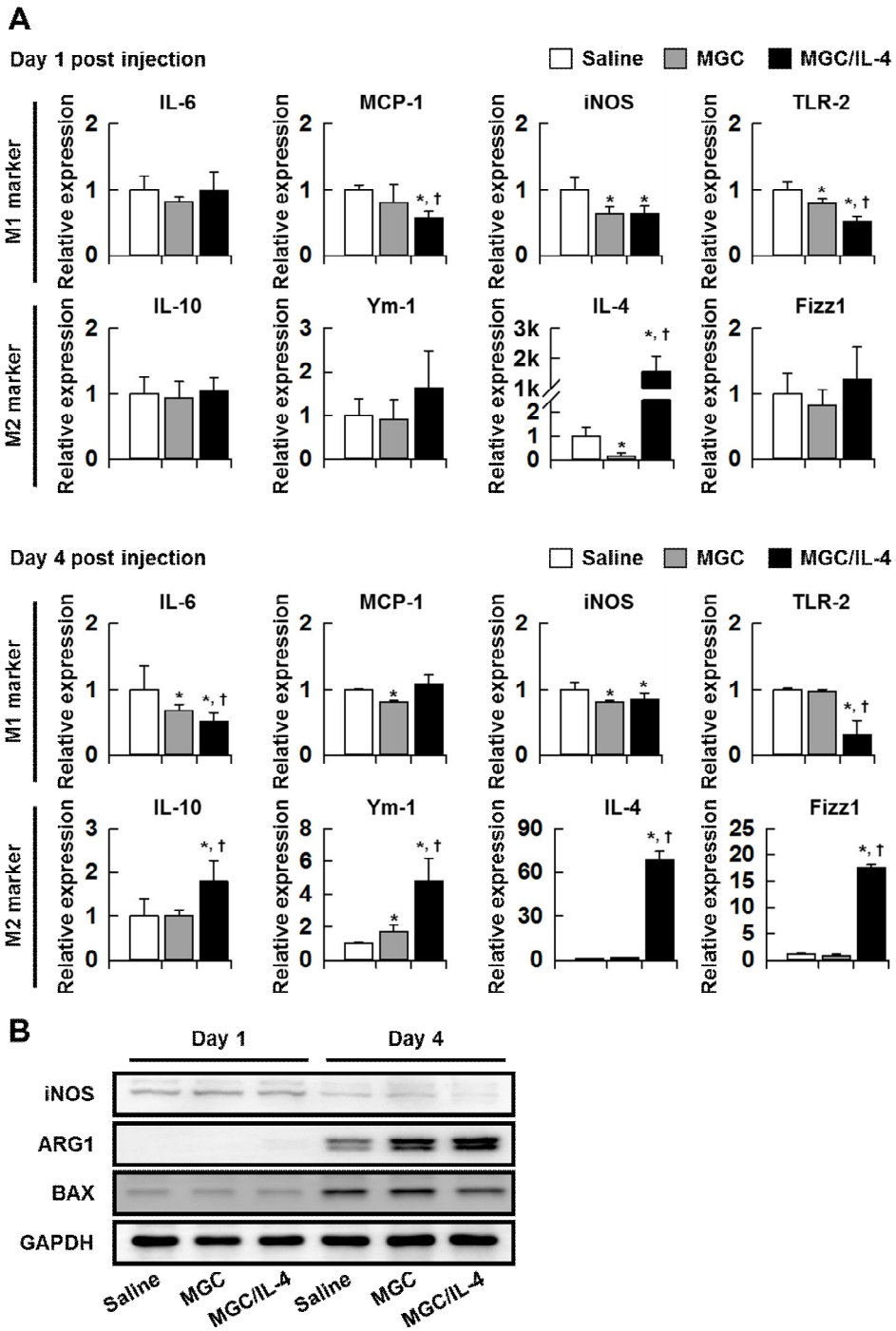
A
Day 1 post injection
Saline
MGC
MGC/IL-4
M1 marker
M2 marker
Relative expression
IL-6
MCP-1
iNOS
TLR-2
IL-10
Ym-1
IL-4
Fizz1
Day 4 post injection
B
Day 1
Day 4
iNOS
ARG1
BAX
GAPDH
Saline
MGC
MGC/IL-4

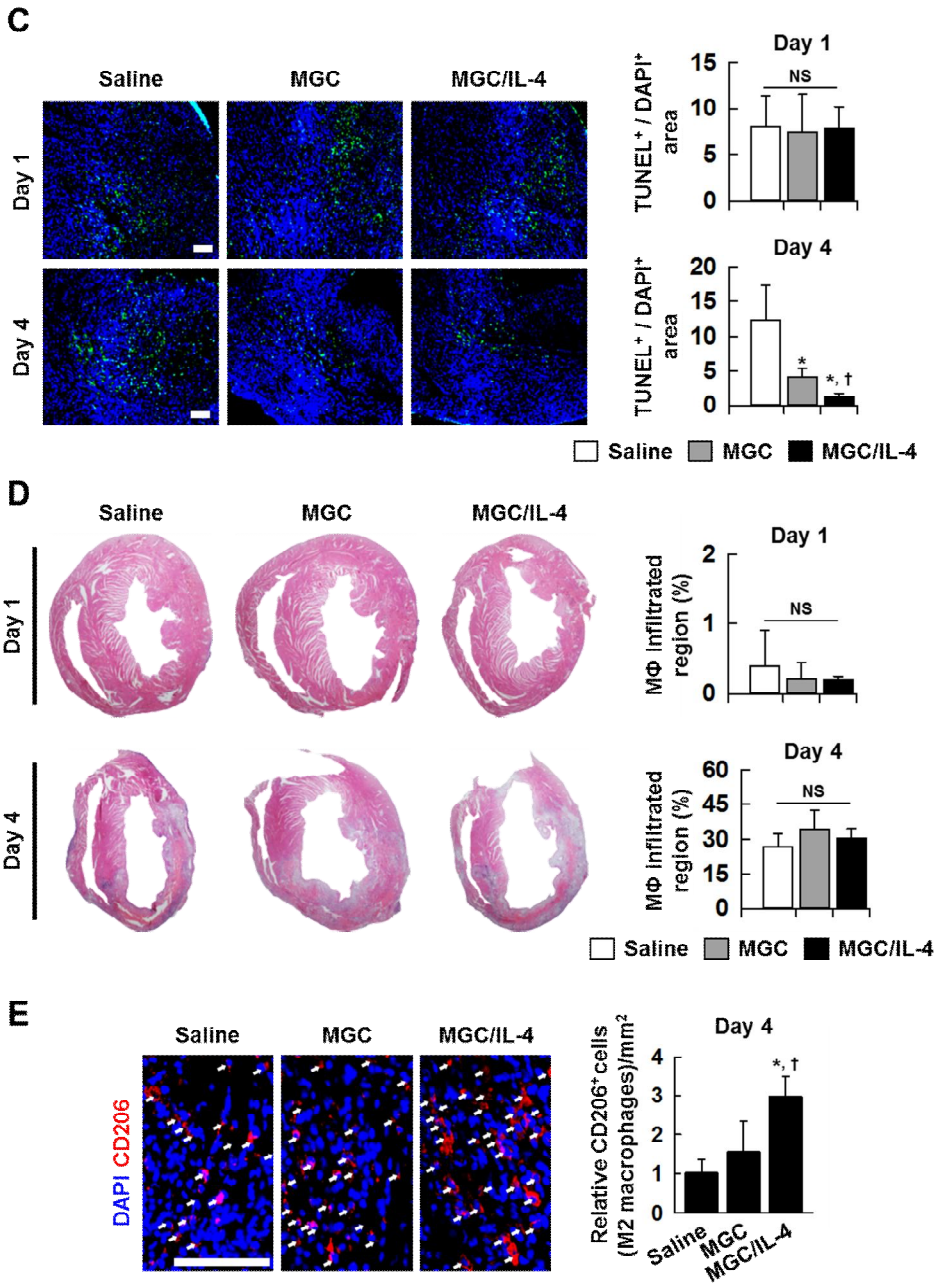
C
Saline
MGC
MGC/IL-4
Day 1
Day 4
Day 1
TUNEL+ / DAPI+ area
15
10
5
0
NS
Day 4
TUNEL+ / DAPI+ area
20
15
10
5
0
*
*, †
Saline
MGC
MGC/IL-4
D
Saline
MGC
MGC/IL-4
Day 1
Day 4
Day 1
MΦ infiltrated region (%)
2
1
0
NS
Day 4
MΦ infiltrated region (%)
60
45
30
15
0
NS
Saline
MGC
MGC/IL-4
E
Saline
MGC
MGC/IL-4
DAPI CD206
Day 4
Relative CD206+ cells (M2 macrophages)/mm2
4
3
2
1
0
*, †
Saline
MGC
MGC/IL-4

Figure 4.6. *In vivo* timely shift of M1 macrophages to M2 macrophages for the regulation of inflammation in MI mice. The MGC/IL-4 group denotes MGC/IL-4 pDNA. (A) Gene expression of M1 and M2 markers at the left ventricle 1 or 4 days after the treatments *in vivo*. n=3 animals, $*p<0.05$ *vs.* Saline, and $^{\dagger}p<0.05$ *vs.* MGC. (B) Western blot analysis of M1, M2 and pro-apoptotic protein of the left ventricle 1 or 4 days after the treatments. (C) Fluorescent images of apoptotic cells at the peri-infarct zone 1 or 4 days after the treatments, and their quantification analysis. n=3 animals, $*p<0.05$ *vs.* Saline, and $^{\dagger}P<0.05$ *vs.* MGC. (D) H&E staining of heart tissues 1 or 4 days after the treatments, and the quantification assessment. n=3 animals. No significant change (NS) in the macrophage infiltration area was observed. (E) Immunofluorescent images of M2 macrophages (CD206-positive cells, arrows) at the peri-infarct zone 4 days after the treatments, and their quantification. n=3 animals, $*p<0.05$ *vs.* Saline, and $^{\dagger}p<0.05$ *vs.* MGC.

4.2.6. Improved Left Ventricular Remodeling and Increased Vessel Density In Vivo

To further assess therapeutic efficacy of MGC/IL-4 pDNA treatment, inflammatory cell population, Cx43 expression and vessel density were evaluated 14 days after the treatments (Figure 4.7). H&E staining was performed to assess the area of inflammatory cell infiltration near the border zone (Figure 4.7A). Longitudinal sections of mouse hearts demonstrated extensively reduced inflammatory cell population at the border zone in the MGC/IL-4 pDNA groups. Interestingly, quantitative densitometry analysis demonstrated that the MGC group showed significant reduction in inflammatory cell population area compared with the saline group, while the MGC/IL-4 pDNA group significantly mitigated inflammatory cell population area compared with either the saline or MGC group 2 weeks after the treatment. Regulation of left ventricular remodeling was further evaluated by Cx43 expression at the border zone (Figure 4.7B). Fluorescent images showed that the injection of MGC/IL-4 pDNA significantly preserved Cx43 expression at the peri-infarct zone compared to the injection of saline or MGC. Densitometry analysis further demonstrated that the density ratio of Cx43 to DAPI at the peri-infarct zone was significantly higher in the MGC and MGC/IL-4 pDNA group compared to the saline group, while the MGC/IL-4 pDNA group showed the highest Cx43 to DAPI ratio.

Injection of MGC/IL-4 pDNA resulted in significant decrease in fibrous tissue area (Figure 4.7C). Masson's trichrome staining showed markedly smaller fibrotic tissues at both border and infarct zone for the MGC and MGC/IL-4 pDNA groups. Quantification evaluation exhibited the fibrosis area was significantly smaller in the MGC/IL-4 pDNA group compared with the saline or MGC group. Thereafter, vessel density at the peri-infarct zone was evaluated to determine whether the attenuation of cardiac remodeling was associated with the improvement in blood vessel density. Heart sections were stained for von

Willebrand factor (vWF) and smooth muscle actin alpha (SMA-α; Figure 4.7D). Capillary density, as evaluated by the expression of vWF, was significantly higher in the MGC/IL-4 pDNA group compared with the saline or MGC group. Additionally, MGC/IL-4 pDNA injection demonstrated higher arteriole density compared with saline or MGC administration. The data suggest the attenuation of left ventricular remodeling by MGC/IL-4 pDNA treatments may be attributable to increased vessel density.

Collectively, these data suggest the injection of antioxidant MGC alone can partially reduce inflammatory cell population and alleviate cardiac remodeling. Importantly, IL-4 pDNA delivery can exert synergistic effects with MGC and result in better attenuation of left ventricular remodeling.

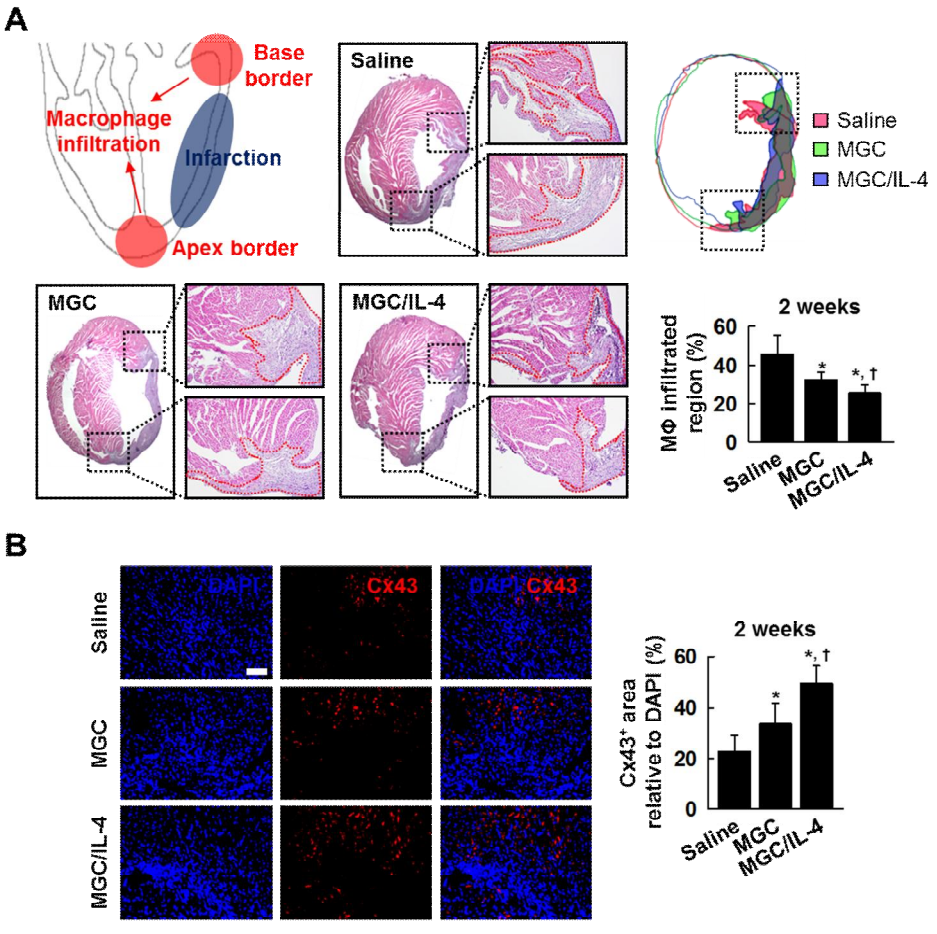
A
Base border
Macrophage infiltration
Infarction
Apex border
Saline
MGC
MGC/IL-4
Saline
MGC
MGC/IL-4
2 weeks
MΦ infiltrated region (%)
60
40
20
0
*
*, †
Saline
MGC
MGC/IL-4
B
Saline
MGC
MGC/IL-4
DAPI
Cx43
DAPI Cx43
2 weeks
Cx43+ area relative to DAPI (%)
60
40
20
0
*
*, †
Saline
MGC
MGC/IL-4

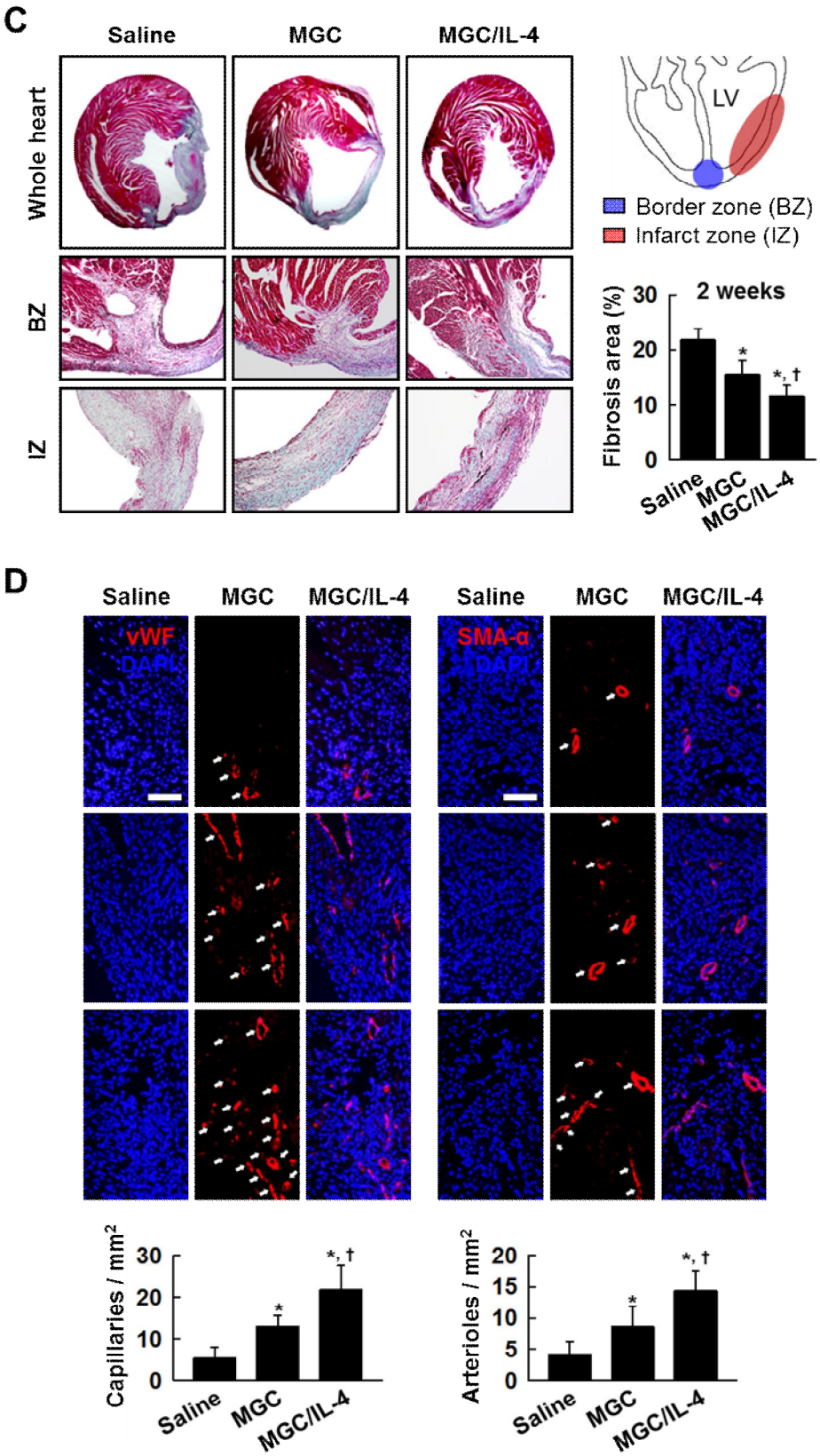
C
Saline
MGC
MGC/IL-4
Whole heart
BZ
IZ
LV
Border zone (BZ)
Infarct zone (IZ)
2 weeks
Fibrosis area (%)
30
20
10
0
*
*, †
Saline
MGC
MGC/IL-4
D
Saline
MGC
MGC/IL-4
Saline
MGC
MGC/IL-4
vWF
DAPI
SMA-α
DAPI
Capillaries / mm²
30
20
10
0
*
*, †
Saline
MGC
MGC/IL-4
Arterioles / mm²
20
15
10
5
0
*
*, †
Saline
MGC
MGC/IL-4

Figure 4.7. Attenuation of left ventricular remodeling and increase in blood vessel density in MI mice by injection of MGC/IL-4 pDNA. The MGC/IL-4 group denotes MGC/IL-4 pDNA. **(A)** H&E staining of the heart 2 weeks after the treatments, and their quantitative analysis. **(B)** Immunohistochemistry images of a gap junction protein, Cx43, at the border zone 2 weeks after the treatments. Cx43 expression (red) was quantified using densitometry and evaluated relative to $DAPI^+$ expression. Bars, 100 μm. **(C)** Histological sections of myocardium stained with Masson's Trichrome, and their quantitative analysis 2 weeks after the treatments. **(D)** Immunohistochemical images for vWF (red, arrows, capillaries) and SMA-α (red, arrows, arterioles) at the peri-infarct zone 2 weeks after the treatments, and their quantification analysis. Vascular densities were quantified as vWF^+ or $SMA\text{-}\alpha^+$ vessels per mm^2. **(A-D)** n=4 animals. $*p<0.05$ *vs.* Saline, and $^{\dagger}p<0.05$ *vs.* MGC.

4.2.7. Improved Recovery of Cardiac Function

Higher animal survival rate was observed in the MGC/IL-4 pDNA group compared with the other groups after 2 weeks (Figure 4.8A). Interestingly, a notable decrease in animal survival was detected 5 or 6 days after MI, when inflammatory phase declines and reparative phase progresses. The effective inflammation reduction and M2 macrophage shift in the MGC/IL-4 pDNA group (Figure 4.6) could contribute to the higher animal survival rate in the MGC/IL-4 pDNA group at this early time point. Interestingly, the MGC group did not show better animal survival at this time point. Thus, the improved animal survival after MI could be mediated by not only the regulation of M1 macrophage-based inflammatory phase but also the progression of M2 macrophage-based reparative phase.

To assess functional recovery of the infarcted myocardium, transthoracic echocardiography was performed (Figure 4.8B). Two weeks after the treatments, the MGC/IL-4 pDNA group demonstrated significant decrease in left ventricular internal diameter at end diastole (LVIDd), end-diastolic volume (EDV), and end-systolic volume (ESV) compared with the saline or MGC group. Additionally, ejection fraction (EF) and fractional shortening (FS) were significantly higher in the MGC/IL-4 pDNA group compared with the saline or MGC group. On the other hand, injection of MGC alone did not demonstrate functional recovery (EF and FS), suggesting that the recovery of left ventricular function may be associated with not only the regulation of inflammation by M1 macrophages but also the promotion of M2 macrophage population.

A

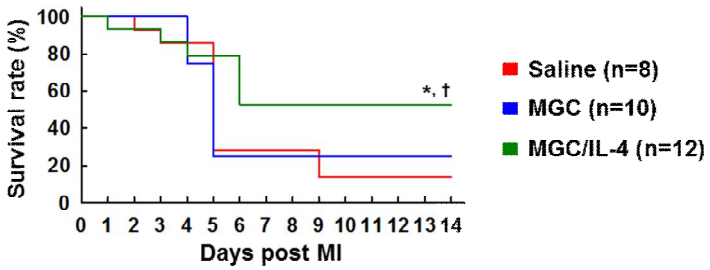

B

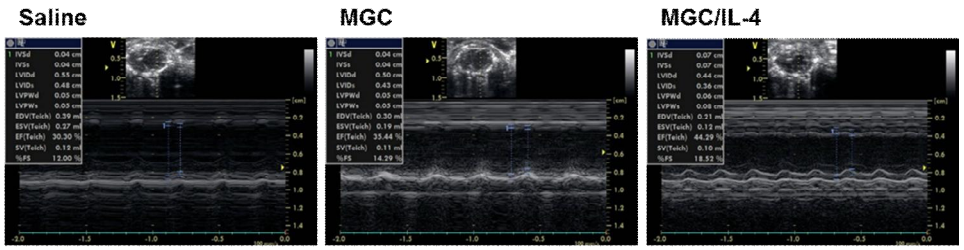

	LVIDd (mm)	LVIDs (mm)	EDV (μL)	ESV (μL)	EF (%)	FS (%)
Saline	4.8±0.4	4.2±0.4	27.3±6.9	18.3±5.1	33.1±3.0	13.2±1.4
MGC	4.4±0.3	3.8±0.3	21.3±4.9	13.8±3.0	35.3±2.0	14.2±0.9
MGC/IL-4	4.2±0.4	3.4±0.3	18.1±4.6	9.8±2.5	45.3±1.9	19.0±1.0

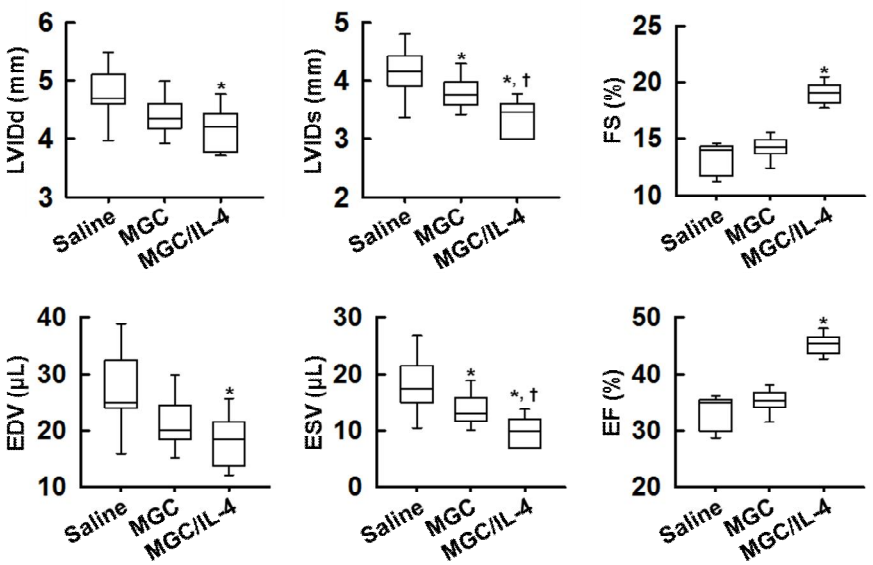

Figure 4.8. Improvement of animal survival and cardiac functions in MI mice by injection of MGC/IL-4 pDNA. The MGC/IL-4 group denotes MGC/IL-4 pDNA. (A) The cumulative animal survival rate. n=8 in the Saline group, n=10 in the MGC group, n=12 in the MGC/IL-4 group. *p<0.05 *vs.* Saline, and $^{\dagger}p$<0.05 *vs.* MGC. (B) Representative images and the quantitative analysis of echocardiography. n=5. *p<0.05 *vs.* Saline, and $^{\dagger}p$<0.05 *vs.* MGC.

Chapter 5.

Conclusions

This dissertation presents the studies on elucidating innate physicochemical properties of nanoparticles in modulating cellular behaviors of cardiac and immune cells for the treatment MI.

Chapter 3 provides the very first demonstration that iron oxide nanoparticles can greatly improve intracellular gap junction protein in H9C2 cardiac cells, and these cells can further be utilized in stem cell co-culture to generate cardiac primed MSCs with notably increased therapeutic potentials for MI treatment. Uptake of iron oxide nanoparticles in H9C2 cells triggered cell signaling cascade and enabled gap junctional coupling with MSCs for promoted intercellular biomolecule transfer. Subsequently, MSCs co-cultured with IONP-harboring H9C2 cells showed enhanced cardiac phenotype development that can reduce electrophysiological challenges posed by naïve MSCs, and exhibited unique paracrine profile that provided more cardiac repair-favorable cytokines. Thereafter, injection of these cardiac primed MSCs into rat MI models significantly improved cardiac tissue repair and performance. Our results suggest that iron oxide nanoparticles can serve as a metal ion delivering nanocarrier and greatly affect the development of cellular gap junction crosstalk. On the basis of our findings, the potential application of iron oxide nanoparticles can be extended in cell biology and cell-based therapeutics. For example, enhancement of cell behavior after IONP uptake can further be utilized in many other cell types. Current study focused on the effect of IONP in H9C2 only, hence, more studies on various other cell types can be performed to better elucidate the general therapeutic efficacy of IONPs. Additionally, the natural magnetic property of IONP can further be utilized *in vivo*. Current study used the magnetic property of IONP in the separation of the cells *in vitro*, however, such characteristic of IONP can further be used in *in vivo* to target the cells to the area of interest. Combined with the cell behavior-modulatory effect of IONP, magnetic targeting can exert synergistic effects in treating various types of diseases that require nanoparticle targeting. Additionally, IONP can also be used as an imaging tool and the validation of IONP's therapeutic effects can expand the

utilization of IONP in broader biomedical field.

Chapter 4 demonstrates the very first study evaluating graphene oxide can be utilized as a natural antioxidant within the cells, and further be utilized to modulate inflammatory activation of the macrophages for the treatment of MI. In this study, we demonstrate dual roles of GO in attenuating inflammation by ROS scavenging and in polarizing inflammatory macrophages to reparative macrophages *via* DNA delivery for MI treatment. GO-based MGC uptake by macrophages significantly prohibited ROS generation within the cells and downregulated M1 phenotype and inflammatory cytokine secretion *in vitro*. Conjugation of IL-4 pDNA to MGC demonstrated successful polarization of M1 macrophages to M2 macrophages and the expression of cardiac regenerative cytokines *in vitro*. Injection of MGC/IL-4 pDNA into MI mice mitigated inflammation and promoted timely polarization of M1 macrophages to M2 macrophages, resulting in alleviated cardiac remodeling and improved heart functional recovery. This study introduces a new biological role of GO in regulating macrophages for cardiac repair. At the same time, current study demonstrated the synergistic therapy of M1 regulation and M2 progression. Previous therapeutic approaches in treating inflammatory disorders majorly focused on eliminating inflammation and utilizing adjuvant to promote tissue regeneration. Current study using GO, however, introduced a new perspective of achieving these two goals with one off-the-shelf material. Therefore, current antioxidant therapies for MI can be combined with gene or cell therapy to better elucidate the cellular mechanisms at the infarct for cardiac repair. Moreover, further studies utilizing other GO-based materials, especially reduced GO with differential reduction ratio, are required to better elucidate the biomedical role of GO for the treatment of various disorders.

References

1. Mirotsou, M.; Jayawardena, T. M.; Schmeckpeper, J.; Gnecchi, M.; Dzau, V. J. Paracrine mechanisms of stem cell reparative and regenerative actions in the heart. *J. Mol. Cell. Cardiol.* 2011, 50, 280-9.
2. Writing Group, M.; Lloyd-Jones, D.; Adams, R. J.; Brown, T. M.; Carnethon, M.; Dai, S.; De Simone, G.; Ferguson, T. B.; Ford, E.; Furie, K., et al. Heart disease and stroke statistics--2010 update: a report from the American Heart Association. *Circulation* 2010, 121, e46-e215.
3. Burchfield, J. S.; Xie, M.; Hill, J. A. Pathological ventricular remodeling: mechanisms: part 1 of 2. *Circulation* 2013, 128, 388-400.
4. Park, H. J.; Yang, F.; Cho, S. W. Nonviral delivery of genetic medicine for therapeutic angiogenesis. *Adv. Drug Deliv. Rev.* 2012, 64, 40-52.
5. Aguirre, A.; Sancho-Martinez, I.; Izpisua Belmonte, J. C. Reprogramming toward heart regeneration: stem cells and beyond. *Cell Stem Cell* 2013, 12, 275-84.
6. Lambert, J. M.; Lopez, E. F.; Lindsey, M. L. Macrophage roles following myocardial infarction. *Int. J. Cardiol.* 2008, 130, 147-58.
7. McMurray, J. J.; Pfeffer, M. A. Heart failure. *Lancet* 2005, 365, 1877-89.
8. Bramucci, E.; Repetto, A.; Ferrario, M.; Canosi, U.; Boschetti, E.; Brambilla, N.; Gnecchi, M.; Merlini, P. A.; Ardissino, D.; Angoli, L., et al. Effectiveness of adjunctive stent implantation following directional coronary atherectomy for treatment of left anterior descending ostial stenosis. *Am. J. Cardiol.* 2002, 90, 1074-8.
9. Gnecchi, M.; Danieli, P.; Cervio, E. Mesenchymal stem cell therapy for heart disease. *Vascul. Pharmacol.* 2012, 57, 48-55.
10. Pascual-Gil, S.; Garbayo, E.; Diaz-Herraez, P.; Prosper, F.; Blanco-Prieto, M. J. Heart regeneration after myocardial infarction using synthetic

biomaterials. *J. Control. Release* 2015, 203, 23-38.

11. Reis, L. A.; Chiu, L. L.; Feric, N.; Fu, L.; Radisic, M. Biomaterials in myocardial tissue engineering. *J. Tissue Eng. Regen. Med.* 2016, 10, 11-28.
12. Han, J.; Park, J.; Kim, B. S. Integration of mesenchymal stem cells with nanobiomaterials for the repair of myocardial infarction. *Adv. Drug Deliv. Rev.* 2015, 95, 15-28.
13. Rane, A. A.; Christman, K. L. Biomaterials for the treatment of myocardial infarction: a 5-year update. *J. Am. Coll. Cardiol.* 2011, 58, 2615-29.
14. Christman, K. L.; Lee, R. J. Biomaterials for the treatment of myocardial infarction. *J. Am. Coll. Cardiol.* 2006, 48, 907-13.
15. Venugopal, J. R.; Prabhakaran, M. P.; Mukherjee, S.; Ravichandran, R.; Dan, K.; Ramakrishna, S. Biomaterial strategies for alleviation of myocardial infarction. *J. R. Soc. Interface* 2012, 9, 1-19.
16. Cutts, J.; Nikkhah, M.; Brafman, D. A. Biomaterial Approaches for Stem Cell-Based Myocardial Tissue Engineering. *Biomark. Insights* 2015, 10, 77-90.
17. Huikuri, H. V.; Kervinen, K.; Niemela, M.; Ylitalo, K.; Saily, M.; Koistinen, P.; Savolainen, E. R.; Ukkonen, H.; Pietila, M.; Airaksinen, J. K., et al. Effects of intracoronary injection of mononuclear bone marrow cells on left ventricular function, arrhythmia risk profile, and restenosis after thrombolytic therapy of acute myocardial infarction. *Eur. Heart J.* 2008, 29, 2723-32.
18. Meyer, G. P.; Wollert, K. C.; Lotz, J.; Pirr, J.; Rager, U.; Lippolt, P.; Hahn, A.; Fichtner, S.; Schaefer, A.; Arseniev, L., et al. Intracoronary bone marrow cell transfer after myocardial infarction: 5-year follow-up from the randomized-controlled BOOST trial. *Eur. Heart J.* 2009, 30, 2978-84.
19. Assmus, B.; Rolf, A.; Erbs, S.; Elsasser, A.; Haberbosch, W.; Hambrecht, R.; Tillmanns, H.; Yu, J.; Corti, R.; Mathey, D. G., et al. Clinical outcome

2 years after intracoronary administration of bone marrow-derived progenitor cells in acute myocardial infarction. *Circ. Heart Fail.* 2010, 3, 89-96.

20. Leistner, D. M.; Fischer-Rasokat, U.; Honold, J.; Seeger, F. H.; Schachinger, V.; Lehmann, R.; Martin, H.; Burck, I.; Urbich, C.; Dimmeler, S., et al. Transplantation of progenitor cells and regeneration enhancement in acute myocardial infarction (TOPCARE-AMI): final 5-year results suggest long-term safety and efficacy. *Clin. Res. Cardiol.* 2011, 100, 925-34.

21. Hodgson, D. M.; Behfar, A.; Zingman, L. V.; Kane, G. C.; Perez-Terzic, C.; Alekseev, A. E.; Puceat, M.; Terzic, A. Stable benefit of embryonic stem cell therapy in myocardial infarction. *Am. J. Physiol. Heart Circ. Physiol.* 2004, 287, H471-9.

22. Min, J. Y.; Yang, Y.; Converso, K. L.; Liu, L.; Huang, Q.; Morgan, J. P.; Xiao, Y. F. Transplantation of embryonic stem cells improves cardiac function in postinfarcted rats. *J. Appl. Physiol. (1985)* 2002, 92, 288-96.

23. Xie, C. Q.; Zhang, J.; Xiao, Y.; Zhang, L.; Mou, Y.; Liu, X.; Akinbami, M.; Cui, T.; Chen, Y. E. Transplantation of human undifferentiated embryonic stem cells into a myocardial infarction rat model. *Stem Cells Dev* 2007, 16, 25-9.

24. Ye, L.; Chang, Y. H.; Xiong, Q.; Zhang, P.; Zhang, L.; Somasundaram, P.; Lepley, M.; Swingen, C.; Su, L.; Wendel, J. S., et al. Cardiac repair in a porcine model of acute myocardial infarction with human induced pluripotent stem cell-derived cardiovascular cells. *Cell Stem Cell* 2014, 15, 750-61.

25. Templin, C.; Zweigerdt, R.; Schwanke, K.; Olmer, R.; Ghadri, J. R.; Emmert, M. Y.; Muller, E.; Kuest, S. M.; Cohrs, S.; Schibli, R., et al. Transplantation and tracking of human-induced pluripotent stem cells in a pig model of myocardial infarction: assessment of cell survival,

engraftment, and distribution by hybrid single photon emission computed tomography/computed tomography of sodium iodide symporter transgene expression. *Circulation* 2012, 126, 430-9.

26. Xiong, Q.; Ye, L.; Zhang, P.; Lepley, M.; Tian, J.; Li, J.; Zhang, L.; Swingen, C.; Vaughan, J. T.; Kaufman, D. S., et al. Functional consequences of human induced pluripotent stem cell therapy: myocardial ATP turnover rate in the in vivo swine heart with postinfarction remodeling. *Circulation* 2013, 127, 997-1008.

27. Shaoxin, Z.; Tong, W.; Jingying, H.; Peifen, L.; Yanling, F.; Tianzhu, G.; Jingfeng, W. GW25-e0865 Cardiac stem cell transplantation improve electrophysiological stability in rats with myocardial infarction via inhibition of TGF-β1 pathway. *J. Am. Coll. Caridol.* 2014, 64.

28. Hong, K. U.; Guo, Y.; Li, Q. H.; Cao, P.; Al-Maqtari, T.; Vajravelu, B. N.; Du, J.; Book, M. J.; Zhu, X.; Nong, Y., et al. c-kit+ Cardiac stem cells alleviate post-myocardial infarction left ventricular dysfunction despite poor engraftment and negligible retention in the recipient heart. *PLoS One* 2014, 9, e96725.

29. Fernandes, S.; van Rijen, H. V.; Forest, V.; Evain, S.; Leblond, A. L.; Merot, J.; Charpentier, F.; de Bakker, J. M.; Lemarchand, P. Cardiac cell therapy: overexpression of connexin43 in skeletal myoblasts and prevention of ventricular arrhythmias. *J. Cell. Mol. Med.* 2009, 13, 3703-12.

30. Harada, S.; Nakamura, Y.; Shiraya, S.; Fujiwara, Y.; Kishimoto, Y.; Onohara, T.; Otsuki, Y.; Kishimoto, S.; Yamamoto, Y.; Hisatome, I., et al. Smooth muscle cell sheet transplantation preserve cardiac function and minimize cardiac remodeling in a rat myocardial infarction model. *J. Cardiothorac. Surg.* 2016, 11, 131.

31. Li, R. K.; Jia, Z. Q.; Weisel, R. D.; Merante, F.; Mickle, D. A. Smooth muscle cell transplantation into myocardial scar tissue improves heart

function. *J. Mol. Cell. Cardiol.* 1999, 31, 513-22.

32. Donndorf, P.; Strauer, B. E.; Haverich, A.; Steinhoff, G. Stem cell therapy for the treatment of acute myocardial infarction and chronic ischemic heart disease. *Curr. Pharm. Biotechnol.* 2013, 14, 12-9.

33. Anthony, D. F.; Shiels, P. G. Exploiting paracrine mechanisms of tissue regeneration to repair damaged organs. *Transplant Res* 2013, 2, 10.

34. Gnecchi, M.; He, H.; Liang, O. D.; Melo, L. G.; Morello, F.; Mu, H.; Noiseux, N.; Zhang, L.; Pratt, R. E.; Ingwall, J. S., et al. Paracrine action accounts for marked protection of ischemic heart by Akt-modified mesenchymal stem cells. *Nat. Med.* 2005, 11, 367-8.

35. Gnecchi, M.; Zhang, Z.; Ni, A.; Dzau, V. J. Paracrine mechanisms in adult stem cell signaling and therapy. *Circ. Res.* 2008, 103, 1204-19.

36. Li, Z.; Guo, J.; Chang, Q.; Zhang, A. Paracrine role for mesenchymal stem cells in acute myocardial infarction. *Biol. Pharm. Bull.* 2009, 32, 1343-6.

37. Schaefer, A.; Zwadlo, C.; Fuchs, M.; Meyer, G. P.; Lippolt, P.; Wollert, K. C.; Drexler, H. Long-term effects of intracoronary bone marrow cell transfer on diastolic function in patients after acute myocardial infarction: 5-year results from the randomized-controlled BOOST trial--an echocardiographic study. *Eur. J. Echocardiogr.* 2010, 11, 165-71.

38. Kudo, M.; Wang, Y.; Wani, M. A.; Xu, M.; Ayub, A.; Ashraf, M. Implantation of bone marrow stem cells reduces the infarction and fibrosis in ischemic mouse heart. *J. Mol. Cell. Cardiol.* 2003, 35, 1113-9.

39. Orlic, D.; Kajstura, J.; Chimenti, S.; Bodine, D. M.; Leri, A.; Anversa, P. Bone marrow stem cells regenerate infarcted myocardium. *Pediatr. Transplant.* 2003, 7 Suppl 3, 86-8.

40. Pittenger, M. F.; Martin, B. J. Mesenchymal stem cells and their potential as cardiac therapeutics. *Circ. Res.* 2004, 95, 9-20.

41. Roell, W.; Lewalter, T.; Sasse, P.; Tallini, Y. N.; Choi, B. R.; Breitbach, M.; Doran, R.; Becher, U. M.; Hwang, S. M.; Bostani, T., et al.

Engraftment of connexin 43-expressing cells prevents post-infarct arrhythmia. *Nature* 2007, 450, 819-24.

42. Beeres, S. L.; Zeppenfeld, K.; Bax, J. J.; Dibbets-Schneider, P.; Stokkel, M. P.; Fibbe, W. E.; van der Wall, E. E.; Atsma, D. E.; Schalij, M. J. Electrophysiological and arrhythmogenic effects of intramyocardial bone marrow cell injection in patients with chronic ischemic heart disease. *Heart Rhythm* 2007, 4, 257-65.

43. Chen, H. S.; Kim, C.; Mercola, M. Electrophysiological challenges of cell-based myocardial repair. *Circulation* 2009, 120, 2496-508.

44. Chang, M. G.; Tung, L.; Sekar, R. B.; Chang, C. Y.; Cysyk, J.; Dong, P.; Marban, E.; Abraham, M. R. Proarrhythmic potential of mesenchymal stem cell transplantation revealed in an in vitro coculture model. *Circulation* 2006, 113, 1832-41.

45. Han, J.; Kim, B.; Shin, J. Y.; Ryu, S.; Noh, M.; Woo, J.; Park, J. S.; Lee, Y.; Lee, N.; Hyeon, T., et al. Iron oxide nanoparticle-mediated development of cellular gap junction crosstalk to improve mesenchymal stem cells' therapeutic efficacy for myocardial infarction. *ACS Nano* 2015, 9, 2805-19.

46. Hu, X.; Yu, S. P.; Fraser, J. L.; Lu, Z.; Ogle, M. E.; Wang, J. A.; Wei, L. Transplantation of hypoxia-preconditioned mesenchymal stem cells improves infarcted heart function via enhanced survival of implanted cells and angiogenesis. *J. Thorac. Cardiovasc. Surg.* 2008, 135, 799-808.

47. Gnecchi, M.; He, H.; Noiseux, N.; Liang, O. D.; Zhang, L.; Morello, F.; Mu, H.; Melo, L. G.; Pratt, R. E.; Ingwall, J. S., et al. Evidence supporting paracrine hypothesis for Akt-modified mesenchymal stem cell-mediated cardiac protection and functional improvement. *FASEB J.* 2006, 20, 661-9.

48. Uemura, R.; Xu, M.; Ahmad, N.; Ashraf, M. Bone marrow stem cells prevent left ventricular remodeling of ischemic heart through paracrine signaling. *Circ. Res.* 2006, 98, 1414-21.

49. Ungerleider, J. L.; Christman, K. L. Concise review: injectable biomaterials for the treatment of myocardial infarction and peripheral artery disease: translational challenges and progress. *Stem Cells Transl. Med.* 2014, 3, 1090-9.

50. Binsalamah, Z. M.; Paul, A.; Khan, A. A.; Prakash, S.; Shum-Tim, D. Intramyocardial sustained delivery of placental growth factor using nanoparticles as a vehicle for delivery in the rat infarct model. *Int. J. Nanomedicine* 2011, 6, 2667-78.

51. Che, H. L.; Muthiah, M.; Ahn, Y.; Son, S.; Kim, W. J.; Seonwoo, H.; Chung, J. H.; Cho, C. S.; Park, I. K. Biodegradable particulate delivery of vascular endothelial growth factor plasmid from polycaprolactone/polyethylenimine electrospun nanofibers for the treatment of myocardial infarction. *J. Nanosci. Nanotechnol.* 2011, 11, 7073-7.

52. Davis, M. E.; Hsieh, P. C.; Takahashi, T.; Song, Q.; Zhang, S.; Kamm, R. D.; Grodzinsky, A. J.; Anversa, P.; Lee, R. T. Local myocardial insulin-like growth factor 1 (IGF-1) delivery with biotinylated peptide nanofibers improves cell therapy for myocardial infarction. *Proc. Natl. Acad. Sci. U. S. A.* 2006, 103, 8155-60.

53. Hao, X.; Silva, E. A.; Mansson-Broberg, A.; Grinnemo, K. H.; Siddiqui, A. J.; Dellgren, G.; Wardell, E.; Brodin, L. A.; Mooney, D. J.; Sylven, C. Angiogenic effects of sequential release of VEGF-A165 and PDGF-BB with alginate hydrogels after myocardial infarction. *Cardiovasc. Res.* 2007, 75, 178-85.

54. Hsieh, P. C.; Davis, M. E.; Gannon, J.; MacGillivray, C.; Lee, R. T. Controlled delivery of PDGF-BB for myocardial protection using injectable self-assembling peptide nanofibers. *J. Clin. Invest.* 2006, 116, 237-48.

55. Park, J.; Kim, Y. S.; Ryu, S.; Kang, W. S.; Park, S.; Han, J.; Jeong, H. C.;

Hong, B. H.; Ahn, Y.; Kim, B. S. Graphene potentiates the myocardial repair efficacy of mesenchymal stem cells by stimulating the expression of angiogenic growth factors and gap junction protein. *Adv. Funct. Mater.* 2015, 25, 2590-2600.

56. Kraehenbuehl, T. P.; Zammaretti, P.; Van der Vlies, A. J.; Schoenmakers, R. G.; Lutolf, M. P.; Jaconi, M. E.; Hubbell, J. A. Three-dimensional extracellular matrix-directed cardioprogenitor differentiation: systematic modulation of a synthetic cell-responsive PEG-hydrogel. *Biomaterials* 2008, 29, 2757-66.

57. Tokunaga, M.; Liu, M. L.; Nagai, T.; Iwanaga, K.; Matsuura, K.; Takahashi, T.; Kanda, M.; Kondo, N.; Wang, P.; Naito, A. T., et al. Implantation of cardiac progenitor cells using self-assembling peptide improves cardiac function after myocardial infarction. *J. Mol. Cell. Cardiol.* 2010, 49, 972-83.

58. Au, H. T.; Cheng, I.; Chowdhury, M. F.; Radisic, M. Interactive effects of surface topography and pulsatile electrical field stimulation on orientation and elongation of fibroblasts and cardiomyocytes. *Biomaterials* 2007, 28, 4277-93.

59. Zong, X.; Bien, H.; Chung, C. Y.; Yin, L.; Fang, D.; Hsiao, B. S.; Chu, B.; Entcheva, E. Electrospun fine-textured scaffolds for heart tissue constructs. *Biomaterials* 2005, 26, 5330-8.

60. Hsiao, C. W.; Bai, M. Y.; Chang, Y.; Chung, M. F.; Lee, T. Y.; Wu, C. T.; Maiti, B.; Liao, Z. X.; Li, R. K.; Sung, H. W. Electrical coupling of isolated cardiomyocyte clusters grown on aligned conductive nanofibrous meshes for their synchronized beating. *Biomaterials* 2013, 34, 1063-72.

61. Kim, D. H.; Kshitiz; Smith, R. R.; Kim, P.; Ahn, E. H.; Kim, H. N.; Marban, E.; Suh, K. Y.; Levchenko, A. Nanopatterned cardiac cell patches promote stem cell niche formation and myocardial regeneration. *Integr. Biol. (Camb.)* 2012, 4, 1019-33.

62. Lin, Y. D.; Ko, M. C.; Wu, S. T.; Li, S. F.; Hu, J. F.; Lai, Y. J.; Harn, H. I.; Laio, I. C.; Yeh, M. L.; Yeh, H. I., et al. A nanopatterned cell-seeded cardiac patch prevents electro-uncoupling and improves the therapeutic efficacy of cardiac repair. *Biomater. Sci.* 2014, 2, 567-80.

63. Stout, D. A.; Basu, B.; Webster, T. J. Poly(lactic-co-glycolic acid): carbon nanofiber composites for myocardial tissue engineering applications. *Acta Biomater.* 2011, 7, 3101-12.

64. Wickham, A. M.; Islam, M. M.; Mondal, D.; Phopase, J.; Sadhu, V.; Tamas, E.; Polisetti, N.; Richter-Dahlfors, A.; Liedberg, B.; Griffith, M. Polycaprolactone-thiophene-conjugated carbon nanotube meshes as scaffolds for cardiac progenitor cells. *J. Biomed. Mater. Res. B Appl. Biomater.* 2014, 102, 1553-61.

65. You, J. O.; Rafat, M.; Ye, G. J.; Auguste, D. T. Nanoengineering the heart: conductive scaffolds enhance connexin 43 expression. *Nano Lett.* 2011, 11, 3643-8.

66. Dvir, T.; Timko, B. P.; Brigham, M. D.; Naik, S. R.; Karajanagi, S. S.; Levy, O.; Jin, H.; Parker, K. K.; Langer, R.; Kohane, D. S. Nanowired three-dimensional cardiac patches. *Nat. Nanotechnol.* 2011, 6, 720-5.

67. Mooney, E.; Mackle, J. N.; Blond, D. J.; O'Cearbhaill, E.; Shaw, G.; Blau, W. J.; Barry, F. P.; Barron, V.; Murphy, J. M. The electrical stimulation of carbon nanotubes to provide a cardiomimetic cue to MSCs. *Biomaterials* 2012, 33, 6132-9.

68. Martins, A. M.; Eng, G.; Caridade, S. G.; Mano, J. F.; Reis, R. L.; Vunjak-Novakovic, G. Electrically conductive chitosan/carbon scaffolds for cardiac tissue engineering. *Biomacromolecules* 2014, 15, 635-43.

69. Crowder, S. W.; Liang, Y.; Rath, R.; Park, A. M.; Maltais, S.; Pintauro, P. N.; Hofmeister, W.; Lim, C. C.; Wang, X.; Sung, H. J. Poly(epsilon-caprolactone)-carbon nanotube composite scaffolds for enhanced cardiac differentiation of human mesenchymal stem cells. *Nanomedicine (Lond)*

2013, 8, 1763-76.

70. Kharaziha, M.; Shin, S. R.; Nikkhah, M.; Topkaya, S. N.; Masoumi, N.; Annabi, N.; Dokmeci, M. R.; Khademhosseini, A. Tough and flexible CNT-polymeric hybrid scaffolds for engineering cardiac constructs. *Biomaterials* 2014, 35, 7346-54.

71. Frantz, S.; Nahrendorf, M. Cardiac macrophages and their role in ischemic heart disease. *Cardiovasc. Res.* 2014, cvu025.

72. Gombozhapova, A.; Rogovskaya, Y.; Shurupov, V.; Rebenkova, M.; Kzhyshkowska, J.; Popov, S. V.; Karpov, R. S.; Ryabov, V. Macrophage activation and polarization in post-infarction cardiac remodeling. *J. Biomed. Sci.* 2017, 24, 13.

73. Hulsmans, M.; Sam, F.; Nahrendorf, M. Monocyte and macrophage contributions to cardiac remodeling. *J. Mol. Cell. Cardiol.* 2016, 93, 149-55.

74. Weinberger, T.; Schulz, C. Myocardial infarction: a critical role of macrophages in cardiac remodeling. *Front. Physiol.* 2015, 6, 107.

75. Wynn, T. A.; Vannella, K. M. Macrophages in Tissue Repair, Regeneration, and Fibrosis. *Immunity* 2016, 44, 450-62.

76. Ben-Mordechai, T.; Holbova, R.; Landa-Rouben, N.; Harel-Adar, T.; Feinberg, M. S.; Abd Elrahman, I.; Blum, G.; Epstein, F. H.; Silman, Z.; Cohen, S., et al. Macrophage subpopulations are essential for infarct repair with and without stem cell therapy. *J. Am. Coll. Cardiol.* 2013, 62, 1890-901.

77. Harel-Adar, T.; Ben Mordechai, T.; Amsalem, Y.; Feinberg, M. S.; Leor, J.; Cohen, S. Modulation of cardiac macrophages by phosphatidylserine-presenting liposomes improves infarct repair. *Proc. Natl. Acad. Sci. U. S. A.* 2011, 108, 1827-32.

78. Jeong, H. Y.; Kang, W. S.; Hong, M. H.; Jeong, H. C.; Shin, M. G.; Jeong, M. H.; Kim, Y. S.; Ahn, Y. 5-Azacytidine modulates interferon regulatory

factor 1 in macrophages to exert a cardioprotective effect. *Sci. Rep.* 2015, 5, 15768.

79. Kim, Y. S.; Jeong, H. Y.; Kim, A. R.; Kim, W. H.; Cho, H.; Um, J.; Seo, Y.; Kang, W. S.; Jin, S. W.; Kim, M. C., et al. Natural product derivative BIO promotes recovery after myocardial infarction via unique modulation of the cardiac microenvironment. *Sci. Rep.* 2016, 6, 30726.

80. Kim, Y. S.; Kang, W. S.; Kwon, J. S.; Hong, M. H.; Jeong, H. y.; Jeong, H. C.; Jeong, M. H.; Ahn, Y. Protective role of 5-azacytidine on myocardial infarction is associated with modulation of macrophage phenotype and inhibition of fibrosis. *J. Cell. Mol. Med.* 2014, 18, 1018-1027.

81. Leblond, A. L.; Klinkert, K.; Martin, K.; Turner, E. C.; Kumar, A. H.; Browne, T.; Caplice, N. M. Systemic and cardiac depletion of M2 macrophage through CSF-1R signaling inhibition alters cardiac function post myocardial infarction. *PLoS One* 2015, 10, e0137515.

82. Zeng, L.; Hu, Q.; Wang, X.; Mansoor, A.; Lee, J.; Feygin, J.; Zhang, G.; Suntharalingam, P.; Boozer, S.; Mhashilkar, A., et al. Bioenergetic and functional consequences of bone marrow-derived multipotent progenitor cell transplantation in hearts with postinfarction left ventricular remodeling. *Circulation* 2007, 115, 1866-75.

83. Baraniak, P. R.; McDevitt, T. C. Stem cell paracrine actions and tissue regeneration. *Regen. Med.* 2010, 5, 121-43.

84. Ratajczak, M. Z.; Kucia, M.; Jadczyk, T.; Greco, N. J.; Wojakowski, W.; Tendera, M.; Ratajczak, J. Pivotal role of paracrine effects in stem cell therapies in regenerative medicine: can we translate stem cell-secreted paracrine factors and microvesicles into better therapeutic strategies? *Leukemia* 2012, 26, 1166-73.

85. Amado, L. C.; Saliaris, A. P.; Schuleri, K. H.; St John, M.; Xie, J. S.; Cattaneo, S.; Durand, D. J.; Fitton, T.; Kuang, J. Q.; Stewart, G., et al. Cardiac repair with intramyocardial injection of allogeneic mesenchymal

stem cells after myocardial infarction. *Proc. Natl. Acad. Sci. U. S. A.* 2005, 102, 11474-9.

86. Hare, J. M.; Fishman, J. E.; Gerstenblith, G.; DiFede Velazquez, D. L.; Zambrano, J. P.; Suncion, V. Y.; Tracy, M.; Ghersin, E.; Johnston, P. V.; Brinker, J. A., et al. Comparison of allogeneic vs autologous bone marrow-derived mesenchymal stem cells delivered by transendocardial injection in patients with ischemic cardiomyopathy: the POSEIDON randomized trial. *JAMA* 2012, 308, 2369-79.

87. Houtgraaf, J. H.; den Dekker, W. K.; van Dalen, B. M.; Springeling, T.; de Jong, R.; van Geuns, R. J.; Geleijnse, M. L.; Fernandez-Aviles, F.; Zijlsta, F.; Serruys, P. W., et al. First experience in humans using adipose tissue-derived regenerative cells in the treatment of patients with ST-segment elevation myocardial infarction. *J. Am. Coll. Cardiol.* 2012, 59, 539-40.

88. Hastings, C. L.; Roche, E. T.; Ruiz-Hernandez, E.; Schenke-Layland, K.; Walsh, C. J.; Duffy, G. P. Drug and cell delivery for cardiac regeneration. *Adv. Drug Deliv. Rev.* 2015, 84, 85-106.

89. Antonitsis, P.; Ioannidou-Papagiannaki, E.; Kaidoglou, A.; Papakonstantinou, C. In vitro cardiomyogenic differentiation of adult human bone marrow mesenchymal stem cells. The role of 5-azacytidine. *Interact. Cardiovasc. Thorac. Surg.* 2007, 6, 593-7.

90. Xu, W. R.; Zhang, X. R.; Qian, H.; Zhu, W.; Sun, X. C.; Hu, J.; Zhou, H.; Chen, Y. C. Mesenchymal stem cells from adult human bone marrow differentiate into a cardiomyocyte phenotype in vitro. *Exp. Biol. Med.* 2004, 229, 623-631.

91. Song, H.; Hwang, H. J.; Chang, W.; Song, B. W.; Cha, M. J.; Kim, I. K.; Lim, S.; Choi, E. J.; Ham, O.; Lee, C. Y., et al. Cardiomyocytes from phorbol myristate acetate-activated mesenchymal stem cells restore electromechanical function in infarcted rat hearts. *Proc. Natl. Acad. Sci. U. S. A.* 2011, 108, 296-301.

92. Bartunek, J.; Croissant, J. D.; Wijns, W.; Gofflot, S.; de Lavareille, A.; Vanderheyden, M.; Kaluzhny, Y.; Mazouz, N.; Willemsen, P.; Penicka, M., et al. Pretreatment of adult bone marrow mesenchymal stem cells with cardiomyogenic growth factors and repair of the chronically infarcted myocardium. *Am. J. Physiol. Heart Circ. Physiol.* 2007, 292, H1095-104.

93. Connell, J. P.; Augustini, E.; Moise, K. J., Jr.; Johnson, A.; Jacot, J. G. Formation of functional gap junctions in amniotic fluid-derived stem cells induced by transmembrane co-culture with neonatal rat cardiomyocytes. *J. Cell. Mol. Med.* 2013, 17, 774-81.

94. Fukuhara, S.; Tomita, S.; Yamashiro, S.; Morisaki, T.; Yutani, C.; Kitamura, S.; Nakatani, T. Direct cell-cell interaction of cardiomyocytes is key for bone marrow stromal cells to go into cardiac lineage in vitro. *J. Thorac. Cardiovasc. Surg.* 2003, 125, 1470-1480.

95. Nishiyama, N.; Miyoshi, S.; Hida, N.; Uyama, T.; Okamoto, K.; Ikegami, Y.; Miyado, K.; Segawa, K.; Terai, M.; Sakamoto, M., et al. The significant cardiomyogenic potential of human umbilical cord blood-derived mesenchymal stem cells in vitro. *Stem Cells* 2007, 25, 2017-24.

96. Ryu, S.; Yoo, J.; Jang, Y.; Han, J.; Yu, S. J.; Park, J.; Jung, S. Y.; Ahn, K. H.; Im, S. G.; Char, K., et al. Nanothin coculture membranes with tunable pore architecture and thermoresponsive functionality for transfer-printable stem cell-derived cardiac sheets. *ACS Nano* 2015, 9, 10186-202.

97. Pijnappels, D. A.; Schalij, M. J.; Ramkisoensing, A. A.; van Tuyn, J.; de Vries, A. A.; van der Laarse, A.; Ypey, D. L.; Atsma, D. E. Forced alignment of mesenchymal stem cells undergoing cardiomyogenic differentiation affects functional integration with cardiomyocyte cultures. *Circ. Res.* 2008, 103, 167-76.

98. Zamilpa, R.; Navarro, M. M.; Flores, I.; Griffey, S. Stem cell mechanisms during left ventricular remodeling post-myocardial infarction: Repair and regeneration. *World J. Cardiol.* 2014, 6, 610-20.

99. Bhang, S. H.; Cho, S. W.; La, W. G.; Lee, T. J.; Yang, H. S.; Sun, A. Y.; Baek, S. H.; Rhie, J. W.; Kim, B. S. Angiogenesis in ischemic tissue produced by spheroid grafting of human adipose-derived stromal cells. *Biomaterials* 2011, 32, 2734-47.

100. Hwang, H. J.; Chang, W.; Song, B. W.; Song, H.; Cha, M. J.; Kim, I. K.; Lim, S.; Choi, E. J.; Ham, O.; Lee, S. Y., et al. Antiarrhythmic potential of mesenchymal stem cell is modulated by hypoxic environment. *J. Am. Coll. Cardiol.* 2012, 60, 1698-706.

101. Kinnaird, T.; Stabile, E.; Burnett, M. S.; Lee, C. W.; Barr, S.; Fuchs, S.; Epstein, S. E. Marrow-derived stromal cells express genes encoding a broad spectrum of arteriogenic cytokines and promote in vitro and in vivo arteriogenesis through paracrine mechanisms. *Circ. Res.* 2004, 94, 678-85.

102. Zhao, S. L.; Zhang, Y. J.; Li, M. H.; Zhang, X. L.; Chen, S. L. Mesenchymal stem cells with overexpression of midkine enhance cell survival and attenuate cardiac dysfunction in a rat model of myocardial infarction. *Stem Cell. Res. Ther.* 2014, 5, 37.

103. Nahrendorf, M.; Swirski, F. K. Monocyte and macrophage heterogeneity in the heart. *Circ. Res.* 2013, 112, 1624-33.

104. Nahrendorf, M.; Pittet, M. J.; Swirski, F. K. Monocytes: protagonists of infarct inflammation and repair after myocardial infarction. *Circulation* 2010, 121, 2437-45.

105. Swirski, F. K.; Nahrendorf, M. Macrophage-stem cell crosstalk after myocardial infarction. *J. Am. Coll. Cardiol.* 2013, 62, 1902-4.

106. Nahrendorf, M.; Swirski, F. K.; Aikawa, E.; Stangenberg, L.; Wurdinger, T.; Figueiredo, J. L.; Libby, P.; Weissleder, R.; Pittet, M. J. The healing myocardium sequentially mobilizes two monocyte subsets with divergent and complementary functions. *J. Exp. Med.* 2007, 204, 3037-47.

107. Martinez, F. O.; Gordon, S. The M1 and M2 paradigm of macrophage activation: time for reassessment. *F1000Prime Rep* 2014, 6, 13.

108. Martinez, F. O.; Sica, A.; Mantovani, A.; Locati, M. Macrophage activation and polarization. *Front. Biosci.* 2007, 13, 453-461.

109. Mia, S.; Warnecke, A.; Zhang, X. M.; Malmström, V.; Harris, R. A. An optimized protocol for human M2 macrophages using M-CSF and IL-4/IL-10/TGF-β yields a dominant immunosuppressive phenotype. *Scand. J. Immunol.* 2014, 79, 305-314.

110. Roszer, T. Understanding the mysterious M2 macrophage through activation markers and effector mechanisms. *Mediators Inflamm.* 2015, 2015, 816460.

111. Makita, N.; Hizukuri, Y.; Yamashiro, K.; Murakawa, M.; Hayashi, Y. IL-10 enhances the phenotype of M2 macrophages induced by IL-4 and confers the ability to increase eosinophil migration. *Int. Immunol.* 2015, 27, 131-41.

112. Seo, D. W.; Yi, Y. J.; Lee, M. S.; Yun, B. S.; Lee, S. M. Differential modulation of lipopolysaccharide-induced inflammatory cytokine production by and antioxidant activity of fomentariol in RAW264.7 cells. *Mycobiology* 2015, 43, 450-7.

113. Hirst, S. M.; Karakoti, A. S.; Tyler, R. D.; Sriranganathan, N.; Seal, S.; Reilly, C. M. Anti-inflammatory properties of cerium oxide nanoparticles. *Small* 2009, 5, 2848-56.

114. Ma, J. S.; Kim, W. J.; Kim, J. J.; Kim, T. J.; Ye, S. K.; Song, M. D.; Kang, H.; Kim, D. W.; Moon, W. K.; Lee, K. H. Gold nanoparticles attenuate LPS-induced NO production through the inhibition of NF-kappaB and IFN-beta/STAT1 pathways in RAW264.7 cells. *Nitric Oxide* 2010, 23, 214-9.

115. Sumbayev, V. V.; Yasinska, I. M.; Garcia, C. P.; Gilliland, D.; Lall, G. S.; Gibbs, B. F.; Bonsall, D. R.; Varani, L.; Rossi, F.; Calzolai, L. Gold nanoparticles downregulate interleukin-1β-induced pro-inflammatory responses. *Small* 2013, 9, 472-477.

116. Jain, S.; Tran, T. H.; Amiji, M. Macrophage repolarization with targeted

alginate nanoparticles containing IL-10 plasmid DNA for the treatment of experimental arthritis. *Biomaterials* 2015, 61, 162-77.

117. Yang, C. X.; Gao, S.; Kjems, J. Folic acid conjugated chitosan for targeted delivery of siRNA to activated macrophages in vitro and in vivo. *J. Mater. Chem. B* 2014, 2, 8608-8615.

118. Alvarez-Erviti, L.; Seow, Y.; Yin, H.; Betts, C.; Lakhal, S.; Wood, M. J. Delivery of siRNA to the mouse brain by systemic injection of targeted exosomes. *Nat. Biotechnol.* 2011, 29, 341-5.

119. Tran, T. H.; Rastogi, R.; Shelke, J.; Amiji, M. M. Modulation of macrophage functional polarity towards anti-inflammatory phenotype with plasmid DNA delivery in CD44 targeting hyaluronic acid nanoparticles. *Sci. Rep.* 2015, 5, 16632.

120. Simpson, D.; Liu, H.; Fan, T. H.; Nerem, R.; Dudley, S. C., Jr. A tissue engineering approach to progenitor cell delivery results in significant cell engraftment and improved myocardial remodeling. *Stem Cells* 2007, 25, 2350-7.

121. Jin, J.; Jeong, S. I.; Shin, Y. M.; Lim, K. S.; Lee, Y. M.; Koh, H. C.; Kim, K. S. Transplantation of mesenchymal stem cells within a poly (lactide-co-ε-caprolactone) scaffold improves cardiac function in a rat myocardial infarction model. *Eur. J. Heart Fail.* 2009, 11, 147-153.

122. Lin, Y. D.; Yeh, M. L.; Yang, Y. J.; Tsai, D. C.; Chu, T. Y.; Shih, Y. Y.; Chang, M. Y.; Liu, Y. W.; Tang, A. C.; Chen, T. Y., et al. Intramyocardial peptide nanofiber injection improves postinfarction ventricular remodeling and efficacy of bone marrow cell therapy in pigs. *Circulation* 2010, 122, S132-41.

123. Cui, X. J.; Xie, H.; Wang, H. J.; Guo, H. D.; Zhang, J. K.; Wang, C.; Tan, Y. Z. Transplantation of mesenchymal stem cells with self-assembling polypeptide scaffolds is conducive to treating myocardial infarction in rats. *Tohoku J. Exp. Med.* 2010, 222, 281-289.

124. Guo, H. D.; Cui, G. H.; Wang, H. J.; Tan, Y. Z. Transplantation of marrow-derived cardiac stem cells carried in designer self-assembling peptide nanofibers improves cardiac function after myocardial infarction. *Biochem. Biophys. Res. Commun.* 2010, 399, 42-8.

125. Kang, B. J.; Kim, H.; Lee, S. K.; Kim, J.; Shen, Y.; Jung, S.; Kang, K. S.; Im, S. G.; Lee, S. Y.; Choi, M., et al. Umbilical-cord-blood-derived mesenchymal stem cells seeded onto fibronectin-immobilized polycaprolactone nanofiber improve cardiac function. *Acta Biomater* 2014, 10, 3007-17.

126. Ravichandran, R.; Venugopal, J. R.; Mueller, M.; Sundarrajan, S.; Mukherjee, S.; Pliska, D.; Wintermantel, E.; Ramakrishna, S. Buckled structures and 5-azacytidine enhance cardiogenic differentiation of adipose-derived stem cells. *Nanomedicine (Lond)* 2013, 8, 1985-97.

127. Ravichandran, R.; Sridhar, R.; Venugopal, J. R.; Sundarrajan, S.; Mukherjee, S.; Ramakrishna, S. Gold nanoparticle loaded hybrid nanofibers for cardiogenic differentiation of stem cells for infarcted myocardium regeneration. *Macromol. Biosci.* 2014, 14, 515-25.

128. Webber, M. J.; Han, X.; Murthy, S. N.; Rajangam, K.; Stupp, S. I.; Lomasney, J. W. Capturing the stem cell paracrine effect using heparin-presenting nanofibres to treat cardiovascular diseases. *J. Tissue Eng. Regen. Med.* 2010, 4, 600-10.

129. Park, J.; Park, S.; Ryu, S.; Bhang, S. H.; Kim, J.; Yoon, J. K.; Park, Y. H.; Cho, S. P.; Lee, S.; Hong, B. H., et al. Graphene-regulated cardiomyogenic differentiation process of mesenchymal stem cells by enhancing the expression of extracellular matrix proteins and cell signaling molecules. *Adv. Healthc. Mater.* 2014, 3, 176-81.

130. Terrovitis, J.; Lautamaki, R.; Bonios, M.; Fox, J.; Engles, J. M.; Yu, J.; Leppo, M. K.; Pomper, M. G.; Wahl, R. L.; Seidel, J., et al. Noninvasive quantification and optimization of acute cell retention by in vivo positron

emission tomography after intramyocardial cardiac-derived stem cell delivery. *J. Am. Coll. Cardiol.* 2009, 54, 1619-26.

131. Lee, W. Y.; Wei, H. J.; Lin, W. W.; Yeh, Y. C.; Hwang, S. M.; Wang, J. J.; Tsai, M. S.; Chang, Y.; Sung, H. W. Enhancement of cell retention and functional benefits in myocardial infarction using human amniotic-fluid stem-cell bodies enriched with endogenous ECM. *Biomaterials* 2011, 32, 5558-67.

132. Karam, J. P.; Muscari, C.; Montero-Menei, C. N. Combining adult stem cells and polymeric devices for tissue engineering in infarcted myocardium. *Biomaterials* 2012, 33, 5683-95.

133. Ruvinov, E.; Harel-Adar, T.; Cohen, S. Bioengineering the infarcted heart by applying bio-inspired materials. *J. Cardiovasc. Transl. Res.* 2011, 4, 559-74.

134. Chiu, L. L.; Iyer, R. K.; Reis, L. A.; Nunes, S. S.; Radisic, M. Cardiac tissue engineering: current state and perspectives. *Front. Biosci. (Landmark Ed)* 2012, 17, 1533-50.

135. Dubois, G.; Segers, V. F.; Bellamy, V.; Sabbah, L.; Peyrard, S.; Bruneval, P.; Hagege, A. A.; Lee, R. T.; Menasche, P. Self-assembling peptide nanofibers and skeletal myoblast transplantation in infarcted myocardium. *J. Biomed. Mater. Res. B Appl. Biomater.* 2008, 87, 222-8.

136. McWhorter, F. Y.; Wang, T.; Nguyen, P.; Chung, T.; Liu, W. F. Modulation of macrophage phenotype by cell shape. *Proc. Natl. Acad. Sci. U. S. A.* 2013, 110, 17253-8.

137. Chen, S.; Jones, J. A.; Xu, Y.; Low, H. Y.; Anderson, J. M.; Leong, K. W. Characterization of topographical effects on macrophage behavior in a foreign body response model. *Biomaterials* 2010, 31, 3479-91.

138. Refai, A. K.; Textor, M.; Brunette, D. M.; Waterfield, J. D. Effect of titanium surface topography on macrophage activation and secretion of proinflammatory cytokines and chemokines. *J. Biomed. Mater. Res. A*

2004, 70, 194-205.

139. Shin, K. H.; Jang, Y.; Kim, B. S.; Jang, J.; Kim, S. H. Highly conductive reduced graphene oxide produced via pressure-assisted reduction at mild temperature for flexible and transparent electrodes. *Chem. Commun. (Camb.)* 2013, 49, 4887-9.

140. Bandaru, P. R. Electrical properties and applications of carbon nanotube structures. *J. Nanosci. Nanotechnol.* 2007, 7, 1239-67.

141. Shevach, M.; Fleischer, S.; Shapira, A.; Dvir, T. Gold nanoparticle-decellularized matrix hybrids for cardiac tissue engineering. *Nano Lett.* 2014, 14, 5792-6.

142. Severs, N. J.; Bruce, A. F.; Dupont, E.; Rothery, S. Remodelling of gap junctions and connexin expression in diseased myocardium. *Cardiovasc. Res.* 2008, 80, 9-19.

143. Ilinskaya, A. N.; Dobrovolskaia, M. A. Immunosuppressive and anti-inflammatory properties of engineered nanomaterials. *Br. J. Pharmacol.* 2014, 171, 3988-4000.

144. Mitchell, L. A.; Lauer, F. T.; Burchiel, S. W.; McDonald, J. D. Mechanisms for how inhaled multiwalled carbon nanotubes suppress systemic immune function in mice. *Nat. Nanotechnol.* 2009, 4, 451-6.

145. Hachani, R.; Lowdell, M.; Birchall, M.; Thanh, N. T. Tracking stem cells in tissue-engineered organs using magnetic nanoparticles. *Nanoscale* 2013, 5, 11362-73.

146. Chertok, B.; Moffat, B. A.; David, A. E.; Yu, F.; Bergemann, C.; Ross, B. D.; Yang, V. C. Iron oxide nanoparticles as a drug delivery vehicle for MRI monitored magnetic targeting of brain tumors. *Biomaterials* 2008, 29, 487-96.

147. Bhang, S. H.; Han, J.; Jang, H. K.; Noh, M. K.; La, W. G.; Yi, M.; Kim, W. S.; Kwon, Y. K.; Yu, T.; Kim, B. S. pH-triggered release of manganese from MnAu nanoparticles that enables cellular neuronal differentiation

without cellular toxicity. *Biomaterials* 2015, 55, 33-43.

148. Kim, J. A.; Lee, N.; Kim, B. H.; Rhee, W. J.; Yoon, S.; Hyeon, T.; Park, T. H. Enhancement of neurite outgrowth in PC12 cells by iron oxide nanoparticles. *Biomaterials* 2011, 32, 2871-7.

149. Chen, Y. C.; Hsiao, J. K.; Liu, H. M.; Lai, I. Y.; Yao, M.; Hsu, S. C.; Ko, B. S.; Chen, Y. C.; Yang, C. S.; Huang, D. M. The inhibitory effect of superparamagnetic iron oxide nanoparticle (Ferucarbotran) on osteogenic differentiation and its signaling mechanism in human mesenchymal stem cells. *Toxicol. Appl. Pharmacol.* 2010, 245, 272-9.

150. Huang, X.; Zhang, F.; Wang, Y.; Sun, X.; Choi, K. Y.; Liu, D.; Choi, J. S.; Shin, T. H.; Cheon, J.; Niu, G., et al. Design considerations of iron-based nanoclusters for noninvasive tracking of mesenchymal stem cell homing. *ACS Nano* 2014, 8, 4403-14.

151. Baek, S.; Oh, J.; Song, J.; Choi, H.; Yoo, J.; Park, G. Y.; Han, J.; Chang, Y.; Park, H.; Kim, H. Generation of integration-free induced neurons using graphene oxide-polyethylenimine. *Small* 2016.

152. Bao, H.; Pan, Y.; Ping, Y.; Sahoo, N. G.; Wu, T.; Li, L.; Li, J.; Gan, L. H. Chitosan-functionalized graphene oxide as a nanocarrier for drug and gene delivery. *Small* 2011, 7, 1569-1578.

153. Choi, H. Y.; Lee, T. J.; Yang, G. M.; Oh, J.; Won, J.; Han, J.; Jeong, G. J.; Kim, J.; Kim, J. H.; Kim, B. S., et al. Efficient mRNA delivery with graphene oxide-polyethylenimine for generation of footprint-free human induced pluripotent stem cells. *J. Control. Release* 2016, 235, 222-35.

154. Kim, H.; Namgung, R.; Singha, K.; Oh, I.-K.; Kim, W. J. Graphene oxide–polyethylenimine nanoconstruct as a gene delivery vector and bioimaging tool. *Bioconjugate Chem.* 2011, 22, 2558-2567.

155. Liu, J.; Cui, L.; Losic, D. Graphene and graphene oxide as new nanocarriers for drug delivery applications. *Acta Biomater* 2013, 9, 9243-57.

156. Kim, S. H.; Moon, H. H.; Kim, H. A.; Hwang, K. C.; Lee, M.; Choi, D. Hypoxia-inducible vascular endothelial growth factor-engineered mesenchymal stem cells prevent myocardial ischemic injury. *Mol. Ther.* 2011, 19, 741-50.

157. Hummers Jr, W. S.; Offeman, R. E. Preparation of graphitic oxide. *J. Am. Chem. Soc.* 1958, 80, 1339-1339.

158. Zhang, X.; Goncalves, R.; Mosser, D. M. The isolation and characterization of murine macrophages. *Curr. Protoc. Immunol.* 2008, Chapter 14, Unit 14 1.

159. Liang, C. P.; Chang, C. H.; Liang, C. C.; Hung, K. Y.; Hsieh, C. W. In vitro antioxidant activities, free radical scavenging capacity, and tyrosinase inhibitory of flavonoid compounds and ferulic acid from Spiranthes sinensis (Pers.) Ames. *Molecules* 2014, 19, 4681-94.

160. Gandhiappan, J.; Rengasamy, R. Comparative study on antioxidant activity of different species of Solanaceae family. *Adv. Appl. Sci. Res* 2012, 3, 1538-1544.

161. Hatzistergos, K. E.; Quevedo, H.; Oskouei, B. N.; Hu, Q.; Feigenbaum, G. S.; Margitich, I. S.; Mazhari, R.; Boyle, A. J.; Zambrano, J. P.; Rodriguez, J. E., et al. Bone marrow mesenchymal stem cells stimulate cardiac stem cell proliferation and differentiation. *Circ. Res.* 2010, 107, 913-22.

162. Nagaya, N.; Kangawa, K.; Itoh, T.; Iwase, T.; Murakami, S.; Miyahara, Y.; Fujii, T.; Uematsu, M.; Ohgushi, H.; Yamagishi, M., et al. Transplantation of mesenchymal stem cells improves cardiac function in a rat model of dilated cardiomyopathy. *Circulation* 2005, 112, 1128-35.

163. Williams, A. R.; Hare, J. M. Mesenchymal stem cells: biology, pathophysiology, translational findings, and therapeutic implications for cardiac disease. *Circ. Res.* 2011, 109, 923-40.

164. Quevedo, H. C.; Hatzistergos, K. E.; Oskouei, B. N.; Feigenbaum, G. S.; Rodriguez, J. E.; Valdes, D.; Pattany, P. M.; Zambrano, J. P.; Hu, Q.;

McNiece, I., et al. Allogeneic mesenchymal stem cells restore cardiac function in chronic ischemic cardiomyopathy via trilineage differentiating capacity. *Proc. Natl. Acad. Sci. U. S. A.* 2009, 106, 14022-7.

165. Piao, H.; Youn, T. J.; Kwon, J. S.; Kim, Y. H.; Bae, J. W.; Bora, S.; Kim, D. W.; Cho, M. C.; Lee, M. M.; Park, Y. B. Effects of bone marrow derived mesenchymal stem cells transplantation in acutely infarcting myocardium. *Eur. J. Heart Fail.* 2005, 7, 730-8.

166. Orlic, D.; Kajstura, J.; Chimenti, S.; Jakoniuk, I.; Anderson, S. M.; Li, B.; Pickel, J.; McKay, R.; Nadal-Ginard, B.; Bodine, D. M., et al. Bone marrow cells regenerate infarcted myocardium. *Nature* 2001, 410, 701-5.

167. Duran, J. M.; Makarewich, C. A.; Sharp, T. E.; Starosta, T.; Zhu, F.; Hoffman, N. E.; Chiba, Y.; Madesh, M.; Berretta, R. M.; Kubo, H., et al. Bone-derived stem cells repair the heart after myocardial infarction through transdifferentiation and paracrine signaling mechanisms. *Circ. Res.* 2013, 113, 539-52.

168. Mureli, S.; Gans, C. P.; Bare, D. J.; Geenen, D. L.; Kumar, N. M.; Banach, K. Mesenchymal stem cells improve cardiac conduction by upregulation of connexin 43 through paracrine signaling. *Am. J. Physiol. Heart Circ. Physiol.* 2013, 304, H600-9.

169. Mazhari, R.; Hare, J. M. Mechanisms of action of mesenchymal stem cells in cardiac repair: potential influences on the cardiac stem cell niche. *Nat. Clin. Pract. Cardiovasc. Med.* 2007, 4 Suppl 1, S21-6.

170. Hahn, J. Y.; Cho, H. J.; Kang, H. J.; Kim, T. S.; Kim, M. H.; Chung, J. H.; Bae, J. W.; Oh, B. H.; Park, Y. B.; Kim, H. S. Pre-treatment of mesenchymal stem cells with a combination of growth factors enhances gap junction formation, cytoprotective effect on cardiomyocytes, and therapeutic efficacy for myocardial infarction. *J. Am. Coll. Cardiol.* 2008, 51, 933-43.

171. Carvalho, J. L.; Braga, V. B.; Melo, M. B.; Campos, A. C.; Oliveira, M. S.;

Gomes, D. A.; Ferreira, A. J.; Santos, R. A.; Goes, A. M. Priming mesenchymal stem cells boosts stem cell therapy to treat myocardial infarction. *J. Cell. Mol. Med.* 2013, 17, 617-25.

172. Ranganath, S. H.; Levy, O.; Inamdar, M. S.; Karp, J. M. Harnessing the mesenchymal stem cell secretome for the treatment of cardiovascular disease. *Cell Stem Cell* 2012, 10, 244-58.

173. Wen, Z.; Zheng, S.; Zhou, C.; Wang, J.; Wang, T. Repair mechanisms of bone marrow mesenchymal stem cells in myocardial infarction. *J. Cell. Mol. Med.* 2011, 15, 1032-43.

174. Mohanty, S.; Bose, S.; Jain, K. G.; Bhargava, B.; Airan, B. TGFβ1 contributes to cardiomyogenic-like differentiation of human bone marrow mesenchymal stem cells. *Int. J. Cardiol.* 2011.

175. Makino, S.; Fukuda, K.; Miyoshi, S.; Konishi, F.; Kodama, H.; Pan, J.; Sano, M.; Takahashi, T.; Hori, S.; Abe, H., et al. Cardiomyocytes can be generated from marrow stromal cells in vitro. *J. Clin. Invest.* 1999, 103, 697-705.

176. Murasawa, S.; Kawamoto, A.; Horii, M.; Nakamori, S.; Asahara, T. Niche-dependent translineage commitment of endothelial progenitor cells, not cell fusion in general, into myocardial lineage cells. *Arterioscler. Thromb. Vasc. Biol.* 2005, 25, 1388-94.

177. Cselenyak, A.; Pankotai, E.; Horvath, E. M.; Kiss, L.; Lacza, Z. Mesenchymal stem cells rescue cardiomyoblasts from cell death in an in vitro ischemia model via direct cell-to-cell connections. *BMC Cell Biol.* 2010, 11, 29.

178. Song, D.; Liu, X.; Liu, R.; Yang, L.; Zuo, J.; Liu, W. Connexin 43 hemichannel regulates H9c2 cell proliferation by modulating intracellular ATP and [Ca2+]. *Acta Biochim. Biophys. Sin. (Shanghai)* 2010, 42, 472-82.

179. Lee, N.; Choi, Y.; Lee, Y.; Park, M.; Moon, W. K.; Choi, S. H.; Hyeon, T. Water-dispersible ferrimagnetic iron oxide nanocubes with extremely high

r(2) relaxivity for highly sensitive in vivo MRI of tumors. *Nano Lett.* 2012, 12, 3127-31.

180. Singh, N.; Jenkins, G. J.; Asadi, R.; Doak, S. H. Potential toxicity of superparamagnetic iron oxide nanoparticles (SPION). *Nano Rev.* 2010, 1.

181. Turk, M. J.; Reddy, J. A.; Chmielewski, J. A.; Low, P. S. Characterization of a novel pH-sensitive peptide that enhances drug release from folate-targeted liposomes at endosomal pHs. *Biochim. Biophys. Acta* 2002, 1559, 56-68.

182. Li, K.; Chi, Y.; Gao, K.; Yan, Q.; Matsue, H.; Takeda, M.; Kitamura, M.; Yao, J. Connexin43 hemichannel-mediated regulation of connexin43. *PLoS One* 2013, 8, e58057.

183. Sato, D.; Xie, L. H.; Sovari, A. A.; Tran, D. X.; Morita, N.; Xie, F.; Karagueuzian, H.; Garfinkel, A.; Weiss, J. N.; Qu, Z. Synchronization of chaotic early afterdepolarizations in the genesis of cardiac arrhythmias. *Proc. Natl. Acad. Sci. U. S. A.* 2009, 106, 2983-8.

184. De Bakker, J.; Van Capelle, F.; Janse, M. J.; Tasseron, S.; Vermeulen, J. T.; De Jonge, N.; Lahpor, J. R. Slow conduction in the infarcted human heart.'Zigzag'course of activation. *Circulation* 1993, 88, 915-926.

185. Zhang, H.; Yuan, X.; Jin, P. F.; Hou, J. F.; Wang, W.; Wei, Y. J.; Hu, S. Alteration of parasympathetic/sympathetic ratio in the infarcted myocardium after Schwann cell transplantation modified electrophysiological function of heart: a novel antiarrhythmic therapy. *Circulation* 2010, 122, S193-200.

186. Nattel, S.; Maguy, A.; Le Bouter, S.; Yeh, Y. H. Arrhythmogenic ion-channel remodeling in the heart: heart failure, myocardial infarction, and atrial fibrillation. *Physiol. Rev.* 2007, 87, 425-56.

187. Reinecke, H.; Minami, E.; Virag, J. I.; Murry, C. E. Gene transfer of connexin43 into skeletal muscle. *Hum. Gene Ther.* 2004, 15, 627-36.

188. He, X. Q.; Chen, M. S.; Li, S. H.; Liu, S. M.; Zhong, Y.; McDonald

Kinkaid, H. Y.; Lu, W. Y.; Weisel, R. D.; Li, R. K. Co-culture with cardiomyocytes enhanced the myogenic conversion of mesenchymal stromal cells in a dose-dependent manner. *Mol. Cell. Biochem.* 2010, 339, 89-98.

189. Plotnikov, E.; Khryapenkova, T.; Vasileva, A.; Marey, M.; Galkina, S.; Isaev, N.; Sheval, E.; Polyakov, V.; Sukhikh, G.; Zorov, D. Cell-to-cell cross-talk between mesenchymal stem cells and cardiomyocytes in co-culture. *J. Cell. Mol. Med.* 2008, 12, 1622-1631.

190. Takahashi, K.; Ito, Y.; Morikawa, M.; Kobune, M.; Huang, J.; Tsukamoto, M.; Sasaki, K.; Nakamura, K.; Dehari, H.; Ikeda, K., et al. Adenoviral-delivered angiopoietin-1 reduces the infarction and attenuates the progression of cardiac dysfunction in the rat model of acute myocardial infarction. *Mol. Ther.* 2003, 8, 584-92.

191. Zhou, L.; Ma, W.; Yang, Z.; Zhang, F.; Lu, L.; Ding, Z.; Ding, B.; Ha, T.; Gao, X.; Li, C. VEGF165 and angiopoietin-1 decreased myocardium infarct size through phosphatidylinositol-3 kinase and Bcl-2 pathways. *Gene Ther.* 2005, 12, 196-202.

192. Stavropoulou, A.; Philippou, A.; Halapas, A.; Sourla, A.; Pissimissis, N.; Koutsilieris, M. uPA, uPAR and TGFbeta(1) expression during early and late post myocardial infarction period in rat myocardium. *In Vivo* 2010, 24, 647-52.

193. Kinnaird, T.; Stabile, E.; Burnett, M. S.; Shou, M.; Lee, C. W.; Barr, S.; Fuchs, S.; Epstein, S. E. Local delivery of marrow-derived stromal cells augments collateral perfusion through paracrine mechanisms. *Circulation* 2004, 109, 1543-9.

194. Isogai, C.; Laug, W. E.; Shimada, H.; Declerck, P. J.; Stins, M. F.; Durden, D. L.; Erdreich-Epstein, A.; DeClerck, Y. A. Plasminogen activator inhibitor-1 promotes angiogenesis by stimulating endothelial cell migration toward fibronectin. *Cancer Res.* 2001, 61, 5587-94.

195. Zaman, A. K.; Fujii, S.; Schneider, D. J.; Taatjes, D. J.; Lijnen, H. R.; Sobel, B. E. Deleterious effects of lack of cardiac PAI-1 after coronary occlusion in mice and their pathophysiologic determinants. *Histochem. Cell Biol.* 2007, 128, 135-45.

196. Rychli, K.; Huber, K.; Wojta, J. Pigment epithelium-derived factor (PEDF) as a therapeutic target in cardiovascular disease. *Expert Opin. Ther. Targets* 2009, 13, 1295-302.

197. Rosano, J. M.; Cheheltani, R.; Wang, B.; Vora, H.; Kiani, M. F.; Crabbe, D. L. Targeted delivery of VEGF after a myocardial infarction reduces collagen deposition and improves cardiac function. *Cardiovasc. Eng. Technol.* 2012, 3, 237-247.

198. Ellison, G. M.; Nadal-Ginard, B.; Torella, D. Optimizing cardiac repair and regeneration through activation of the endogenous cardiac stem cell compartment. *J. Cardiovasc. Transl. Res.* 2012, 5, 667-77.

199. Trivedi, P.; Tray, N.; Nguyen, T.; Nigam, N.; Gallicano, G. I. Mesenchymal stem cell therapy for treatment of cardiovascular disease: helping people sooner or later. *Stem Cells Dev.* 2010, 19, 1109-20.

200. Dai, W.; Hale, S. L.; Martin, B. J.; Kuang, J. Q.; Dow, J. S.; Wold, L. E.; Kloner, R. A. Allogeneic mesenchymal stem cell transplantation in postinfarcted rat myocardium: short- and long-term effects. *Circulation* 2005, 112, 214-23.

201. Henkel, D. M.; Witt, B. J.; Gersh, B. J.; Jacobsen, S. J.; Weston, S. A.; Meverden, R. A.; Roger, V. L. Ventricular arrhythmias after acute myocardial infarction: a 20-year community study. *Am. Heart J.* 2006, 151, 806-12.

202. Deuse, T.; Peter, C.; Fedak, P. W.; Doyle, T.; Reichenspurner, H.; Zimmermann, W. H.; Eschenhagen, T.; Stein, W.; Wu, J. C.; Robbins, R. C., et al. Hepatocyte growth factor or vascular endothelial growth factor gene transfer maximizes mesenchymal stem cell-based myocardial salvage after

acute myocardial infarction. *Circulation* 2009, 120, S247-54.

203. Noiseux, N.; Gnecchi, M.; Lopez-Ilasaca, M.; Zhang, L.; Solomon, S. D.; Deb, A.; Dzau, V. J.; Pratt, R. E. Mesenchymal stem cells overexpressing Akt dramatically repair infarcted myocardium and improve cardiac function despite infrequent cellular fusion or differentiation. *Mol. Ther.* 2004, 14, 840-850.

204. Iso, Y.; Spees, J. L.; Serrano, C.; Bakondi, B.; Pochampally, R.; Song, Y. H.; Sobel, B. E.; Delafontaine, P.; Prockop, D. J. Multipotent human stromal cells improve cardiac function after myocardial infarction in mice without long-term engraftment. *Biochem. Biophys. Res. Commun.* 2007, 354, 700-6.

205. Mazo, M.; Gavira, J. J.; Abizanda, G.; Moreno, C.; Ecay, M.; Soriano, M.; Aranda, P.; Collantes, M.; Alegria, E.; Merino, J., et al. Transplantation of mesenchymal stem cells exerts a greater long-term effect than bone marrow mononuclear cells in a chronic myocardial infarction model in rat. *Cell Transplant.* 2010, 19, 313-28.

206. Mazo, M.; Planat-Benard, V.; Abizanda, G.; Pelacho, B.; Leobon, B.; Gavira, J. J.; Penuelas, I.; Cemborain, A.; Penicaud, L.; Laharrague, P., et al. Transplantation of adipose derived stromal cells is associated with functional improvement in a rat model of chronic myocardial infarction. *Eur. J. Heart Fail.* 2008, 10, 454-62.

207. Tang, Y. L.; Tang, Y.; Zhang, Y. C.; Qian, K.; Shen, L.; Phillips, M. I. Improved graft mesenchymal stem cell survival in ischemic heart with a hypoxia-regulated heme oxygenase-1 vector. *J. Am. Coll. Cardiol.* 2005, 46, 1339-50.

208. Segers, V. F.; Lee, R. T. Stem-cell therapy for cardiac disease. *Nature* 2008, 451, 937-42.

209. Weissberg, P. L.; Qasim, A. Stem cell therapy for myocardial repair. *Heart* 2005, 91, 696-702.

210. Satessa, G.; Lenjisa, J.; Gebremariam, E.; Woldu, M. Stem cell therapy for myocardial infarction: challenges and prospects. *J. Stem Cell Res. Ther* 2015, 5, 1-5.

211. Choo, E. H.; Lee, J. H.; Park, E. H.; Park, H. E.; Jung, N. C.; Kim, T. H.; Koh, Y. S.; Kim, E.; Seung, K. B.; Park, C., et al. Infarcted myocardium-primed dendritic cells improve remodeling and cardiac function after myocardial infarction by modulating the regulatory T cell and macrophage polarization. *Circulation* 2017, 135, 1444-1457.

212. Mittal, M.; Siddiqui, M. R.; Tran, K.; Reddy, S. P.; Malik, A. B. Reactive oxygen species in inflammation and tissue injury. *Antioxid. Redox Signal.* 2014, 20, 1126-67.

213. Hori, M.; Nishida, K. Oxidative stress and left ventricular remodelling after myocardial infarction. *Cardiovasc. Res.* 2009, 81, 457-64.

214. Bruno, B. J.; Miller, G. D.; Lim, C. S. Basics and recent advances in peptide and protein drug delivery. *Ther. Deliv.* 2013, 4, 1443-67.

215. Pisal, D. S.; Kosloski, M. P.; Balu-Iyer, S. V. Delivery of therapeutic proteins. *J. Pharm. Sci.* 2010, 99, 2557-75.

216. Vaishya, R.; Khurana, V.; Patel, S.; Mitra, A. K. Long-term delivery of protein therapeutics. *Expert Opin. Drug Deliv.* 2015, 12, 415-40.

217. Oro, D.; Yudina, T.; Fernandez-Varo, G.; Casals, E.; Reichenbach, V.; Casals, G.; Gonzalez de la Presa, B.; Sandalinas, S.; Carvajal, S.; Puntes, V., et al. Cerium oxide nanoparticles reduce steatosis, portal hypertension and display anti-inflammatory properties in rats with liver fibrosis. *J. Hepatol.* 2016, 64, 691-8.

218. Kim, C. K.; Kim, T.; Choi, I. Y.; Soh, M.; Kim, D.; Kim, Y. J.; Jang, H.; Yang, H. S.; Kim, J. Y.; Park, H. K., et al. Ceria nanoparticles that can protect against ischemic stroke. *Angew. Chem. Int. Ed. Engl.* 2012, 51, 11039-43.

219. Wang, C. Y.; Wang, X. Q.; Lu, T.; Liu, F. S.; Guo, B. F.; Wen, N. Y.; Du, Y.

W.; Lin, H.; Tang, J.; Zhang, L. Multi-functionalized graphene oxide complex as a plasmid delivery system for targeting hepatocellular carcinoma therapy. *RSC Adv.* 2016, 6, 22461-22468.

220. Kanakia, S.; Toussaint, J. D.; Mullick Chowdhury, S.; Tembulkar, T.; Lee, S.; Jiang, Y. P.; Lin, R. Z.; Shroyer, K. R.; Moore, W.; Sitharaman, B. Dose ranging, expanded acute toxicity and safety pharmacology studies for intravenously administered functionalized graphene nanoparticle formulations. *Biomaterials* 2014, 35, 7022-31.

221. Yang, K.; Gong, H.; Shi, X.; Wan, J.; Zhang, Y.; Liu, Z. In vivo biodistribution and toxicology of functionalized nano-graphene oxide in mice after oral and intraperitoneal administration. *Biomaterials* 2013, 34, 2787-95.

222. Qiu, Y.; Wang, Z.; Owens, A. C.; Kulaots, I.; Chen, Y.; Kane, A. B.; Hurt, R. H. Antioxidant chemistry of graphene-based materials and its role in oxidation protection technology. *Nanoscale* 2014, 6, 11744-55.

223. Liu, H.; Liu, T.; Li, L.; Hao, N.; Tan, L.; Meng, X.; Ren, J.; Chen, D.; Tang, F. Size dependent cellular uptake, in vivo fate and light-heat conversion efficiency of gold nanoshells on silica nanorattles. *Nanoscale* 2012, 4, 3523-9.

224. Nicolete, R.; dos Santos, D. F.; Faccioli, L. H. The uptake of PLGA micro or nanoparticles by macrophages provokes distinct in vitro inflammatory response. *Int. Immunopharmacol.* 2011, 11, 1557-63.

225. Hsiao, I.-L.; Gramatke, A. M.; Joksimovic, R.; Sokolowski, M.; Gradzielski, M.; Haase, A. Size and cell type dependent uptake of silica nanoparticles. *J. Nanomed. Nanotechnol.* 2014, 5, 1.

226. Champion, J. A.; Walker, A.; Mitragotri, S. Role of particle size in phagocytosis of polymeric microspheres. *Pharm. Res.* 2008, 25, 1815-21.

227. Ma, J.; Liu, R.; Wang, X.; Liu, Q.; Chen, Y.; Valle, R. P.; Zuo, Y. Y.; Xia, T.; Liu, S. Crucial role of lateral size for graphene oxide in activating

macrophages and stimulating pro-inflammatory responses in cells and animals. *ACS Nano* 2015, 9, 10498-515.

228. Thomas, T. P.; Goonewardena, S. N.; Majoros, I. J.; Kotlyar, A.; Cao, Z.; Leroueil, P. R.; Baker, J. R. Folate-targeted nanoparticles show efficacy in the treatment of inflammatory arthritis. *Arthritis Rheum.* 2011, 63, 2671-2680.

229. Paulos, C. M.; Turk, M. J.; Breur, G. J.; Low, P. S. Folate receptor-mediated targeting of therapeutic and imaging agents to activated macrophages in rheumatoid arthritis. *Adv. Drug Deliv. Rev.* 2004, 56, 1205-17.

230. Rollett, A.; Reiter, T.; Nogueira, P.; Cardinale, M.; Loureiro, A.; Gomes, A.; Cavaco-Paulo, A.; Moreira, A.; Carmo, A. M.; Guebitz, G. M. Folic acid-functionalized human serum albumin nanocapsules for targeted drug delivery to chronically activated macrophages. *Int. J. Pharm.* 2012, 427, 460-6.

231. Ferrari, A. C. Raman spectroscopy of graphene and graphite: disorder, electron–phonon coupling, doping and nonadiabatic effects. *Solid State Commun.* 2007, 143, 47-57.

232. Stankovich, S.; Dikin, D. A.; Piner, R. D.; Kohlhaas, K. A.; Kleinhammes, A.; Jia, Y.; Wu, Y.; Nguyen, S. T.; Ruoff, R. S. Synthesis of graphene-based nanosheets via chemical reduction of exfoliated graphite oxide. *Carbon* 2007, 45, 1558-1565.

233. Day, S. M.; Duquaine, D.; Mundada, L. V.; Menon, R. G.; Khan, B. V.; Rajagopalan, S.; Fay, W. P. Chronic iron administration increases vascular oxidative stress and accelerates arterial thrombosis. *Circulation* 2003, 107, 2601-6.

234. Kell, D. B. Iron behaving badly: inappropriate iron chelation as a major contributor to the aetiology of vascular and other progressive inflammatory and degenerative diseases. *BMC Med. Genomics* 2009, 2, 2.

235. Liu, Y.; Liu, X.; Zhong, F.; Tian, R.; Zhang, K.; Zhang, X.; Li, T. Comparative study of phenolic compounds and antioxidant activity in different species of cherries. *J. Food Sci.* 2011, 76, C633-8.

236. Frangogiannis, N. G. The inflammatory response in myocardial injury, repair, and remodelling. *Nat. Rev. Cardiol.* 2014, 11, 255-65.

237. Tan, H. Y.; Wang, N.; Li, S.; Hong, M.; Wang, X.; Feng, Y. The Reactive oxygen species in macrophage polarization: reflecting its dual role in progression and treatment of human diseases. *Oxid. Med. Cell. Longev.* 2016, 2016, 2795090.

238. Sovari, A. A. Cellular and Molecular Mechanisms of Arrhythmia by Oxidative Stress. *Cardiol. Res. Pract.* 2016, 2016, 9656078.

239. Hsu, H. Y.; Wen, M. H. Lipopolysaccharide-mediated reactive oxygen species and signal transduction in the regulation of interleukin-1 gene expression. *J. Biol. Chem.* 2002, 277, 22131-9.

240. Yamada, H.; Arai, T.; Endo, N.; Yamashita, K.; Fukuda, K.; Sasada, M.; Uchiyama, T. LPS-induced ROS generation and changes in glutathione level and their relation to the maturation of human monocyte-derived dendritic cells. *Life Sci.* 2006, 78, 926-33.

241. Matsue, H.; Edelbaum, D.; Shalhevet, D.; Mizumoto, N.; Yang, C.; Mummert, M. E.; Oeda, J.; Masayasu, H.; Takashima, A. Generation and function of reactive oxygen species in dendritic cells during antigen presentation. *J. Immunol.* 2003, 171, 3010-8.

242. Cuevas-Rodríguez, E. O.; Dia, V. P.; Yousef, G. G.; García-Saucedo, P. A.; López-Medina, J.; Paredes-López, O.; Gonzalez de Mejia, E.; Lila, M. A. Inhibition of pro-inflammatory responses and antioxidant capacity of Mexican blackberry (Rubus spp.) extracts. *J. Agric. Food Chem.* 2010, 58, 9542-9548.

243. Shiraishi, M.; Shintani, Y.; Shintani, Y.; Ishida, H.; Saba, R.; Yamaguchi, A.; Adachi, H.; Yashiro, K.; Suzuki, K. Alternatively activated

macrophages determine repair of the infarcted adult murine heart. *J. Clin. Invest.* 2016, 126, 2151-66.

244. Sridharan, R.; Cameron, A. R.; Kelly, D. J.; Kearney, C. J.; O'Brien, F. J. Biomaterial based modulation of macrophage polarization: a review and suggested design principles. *Mater. Today* 2015, 18, 313-325.

245. de Bakker, J. M.; van Capelle, F. J.; Janse, M. J.; Tasseron, S.; Vermeulen, J. T.; de Jonge, N.; Lahpor, J. R. Slow conduction in the infarcted human heart. 'Zigzag' course of activation. *Circulation* 1993, 88, 915-26.

246. Yan, J.; Kong, W.; Zhang, Q.; Beyer, E. C.; Walcott, G.; Fast, V. G.; Ai, X. c-Jun N-terminal kinase activation contributes to reduced connexin43 and development of atrial arrhythmias. *Cardiovasc. Res.* 2013, 97, 589-97.

247. Roma-Lavisse, C.; Tagzirt, M.; Zawadzki, C.; Lorenzi, R.; Vincentelli, A.; Haulon, S.; Juthier, F.; Rauch, A.; Corseaux, D.; Staels, B., et al. M1 and M2 macrophage proteolytic and angiogenic profile analysis in atherosclerotic patients reveals a distinctive profile in type 2 diabetes. *Diab. Vasc. Dis. Res.* 2015, 12, 279-89.

248. Gupta, K. K.; Xu, Z.; Castellino, F. J.; Ploplis, V. A. Plasminogen activator inhibitor-1 stimulates macrophage activation through Toll-like Receptor-4. *Biochem. Biophys. Res. Commun.* 2016, 477, 503-8.

249. Kubala, M.; Placencio, V.; DeClerck, Y. Plasminogen activator inhibitor-1 increases migration of monocytes to the tumor and skews their differentiation towards M2 macrophage phenotype (TUM6P. 1002). *J. Immunol.* 2015, 194, 141.26-141.26.

250. Zajac, E.; Schweighofer, B.; Kupriyanova, T. A.; Juncker-Jensen, A.; Minder, P.; Quigley, J. P.; Deryugina, E. I. Angiogenic capacity of M1- and M2-polarized macrophages is determined by the levels of TIMP-1 complexed with their secreted proMMP-9. *Blood* 2013, 122, 4054-67.

251. Porta, C.; Rimoldi, M.; Raes, G.; Brys, L.; Ghezzi, P.; Di Liberto, D.; Dieli, F.; Ghisletti, S.; Natoli, G.; De Baetselier, P., et al. Tolerance and M2

(alternative) macrophage polarization are related processes orchestrated by p50 nuclear factor kappaB. *Proc. Natl. Acad. Sci. U. S. A.* 2009, 106, 14978-83.

252. Petrovic-Djergovic, D.; Popovic, M.; Chittiprol, S.; Cortado, H.; Ransom, R. F.; Partida-Sánchez, S. CXCL10 induces the recruitment of monocyte-derived macrophages into kidney, which aggravate puromycin aminonucleoside nephrosis. *Clin. Exp. Immunol.* 2015, 180, 305-315.

253. Tomita, K.; Freeman, B. L.; Bronk, S. F.; LeBrasseur, N. K.; White, T. A.; Hirsova, P.; Ibrahim, S. H. CXCL10-mediates macrophage, but not other innate immune cells-associated inflammation in murine nonalcoholic steatohepatitis. *Sci. Rep.* 2016, 6.

254. Xu, Y.; Meng, C.; Liu, G.; Yang, D.; Fu, L.; Zhang, M.; Zhang, Z.; Xia, H.; Yao, S.; Zhang, S. Classically activated macrophages protect against lipopolysaccharide-induced acute lung injury by expressing amphiregulin in mice. *Anesthesiology* 2016, 124, 1086-99.

255. He, Z.; Zhang, H.; Yang, C.; Zhou, Y.; Zhou, Y.; Han, G.; Xia, L.; Ouyang, W.; Zhou, F.; Zhou, Y., et al. The interaction between different types of activated RAW 264.7 cells and macrophage inflammatory protein-1 alpha. *Radiat. Oncol.* 2011, 6, 86.

256. Yamane, S.; Ishida, S.; Hanamoto, Y.; Kumagai, K.; Masuda, R.; Tanaka, K.; Shiobara, N.; Yamane, N.; Mori, T.; Juji, T., et al. Proinflammatory role of amphiregulin, an epidermal growth factor family member whose expression is augmented in rheumatoid arthritis patients. *J. Inflamm. (Lond)* 2008, 5, 5.

257. Szabó, C.; Scott, G. S.; Virág, L.; Egnaczyk, G.; Salzman, A. L.; Shanley, T. P.; Haskó, G. Suppression of macrophage inflammatory protein (MIP)-1α production and collagen-induced arthritis by adenosine receptor agonists. *Br. J. Pharmacol.* 1998, 125, 379-387.

258. Wen, G.; Zhang, C.; Chen, Q.; Luong le, A.; Mustafa, A.; Ye, S.; Xiao, Q.

A Novel Role of Matrix Metalloproteinase-8 in Macrophage Differentiation and Polarization. *J. Biol. Chem.* 2015, 290, 19158-72.

259. Wen, G.; Chen, Q.; Luong, L. A.; Mustafa, A.; Shu, Y.; Xiao, Q. Matrix metalloproteinase-8 (MMP8) modulates M2 macrophage polarization and molecular mechanisms involved. *Atherosclerosis* 2014, 237, e15.

260. Yan, X.; Anzai, A.; Katsumata, Y.; Matsuhashi, T.; Ito, K.; Endo, J.; Yamamoto, T.; Takeshima, A.; Shinmura, K.; Shen, W., et al. Temporal dynamics of cardiac immune cell accumulation following acute myocardial infarction. *J. Mol. Cell. Cardiol.* 2013, 62, 24-35.

261. Cheng, B.; Chen, H. C.; Chou, I. W.; Tang, T. W.; Hsieh, P. C. Harnessing the early post-injury inflammatory responses for cardiac regeneration. *J. Biomed. Sci.* 2017, 24, 7.

262. Jablonski, K. A.; Amici, S. A.; Webb, L. M.; Ruiz-Rosado Jde, D.; Popovich, P. G.; Partida-Sanchez, S.; Guerau-de-Arellano, M. Novel Markers to Delineate Murine M1 and M2 Macrophages. *PLoS One* 2015, 10, e0145342.

요약 (국문초록)

심근 경색은 전세계의 주요 사망 원인 중 하나로 심장 관련 질환의 대부분을 차지한다. 심근 경색은 심장으로의 혈액 공급이 감소하고 심장 괴사가 발생하는 것에서 유래하기 때문에 성공적인 심장 기능 회복을 위해서는 조직 공학적 접근이 필요하다. 최근 다양한 종류의 세포 및 나노입자가 경색증 이후 심장 기능 회복을 위한 효율적인 치료제로써 주목받고 있으며, 세포와 나노 입자 사이의 융합 치료법이 각광 받고 있다. 최근 연구에도 불구하고 대다수의 나노 물질은 전달 매개체로써 주로 이용되어 왔으며, 어떠한 기전 및 역할을 통해 나노 입자가 세포 거동을 능동적으로 조절하고 세포의 치료 효능을 극대화 시킬 수 있는지에 관한 연구가 진행되지 않았다.

본 논문에서는 심근경색 치료를 위해 산화철 나노 입자 또는 산화 그래핀과 같이 생체재료로써 널리 사용되는 나노 입자를 통한 줄기세포 또는 면역 세포의 융합치료제 개발을 제시하고자 한다. 보다 구체적으로, 이들 나노 입자의 생물학적 역할과 나노 입자 본질의 화학적 성질이 세포 거동을 조절하는 방법을 밝히고자 하며, 이를 위한 본 논문의 주요 목표는 다음과 같다. 1) 산화철 나노 입자의 금속 이온 전달 능력 규명과 세포 신호 전달 조절 및 세포 간극 접합 증진 현상 연구하고 2) 탄소 기반 산화 그래핀이 세포 내 항산화 화학 작용 및 면역 조절 기능에 참여, 심근 경색 치료에 필요한 대식세포의 거동을 제어함에 관한 연구를 진행하고자 한다.

첫째, 본 연구를 통해 산화철 나노 입자가 심장 세포에서 세포 내 신호 전달을 조절할 수 있으며 이후 줄기세포와의 공동 배양에서 세포 간극 결합 형성을 향상시킬 수 있음을 규명하였다. 줄기세포와 심장 세포의 공동 배양은 생체 이식에 앞서 줄기세포를 심근 세포와 유사하도

록 분화시키는 플랫폼으로써, 줄기세포와 심장 세포 사이의 활동적인 간극 접합이 줄기세포 분화에 결정적이다. 본 연구에서는 산화철 나노 입자가 심장 세포 내에서 간극 결합 단백질인 코넥신 43의 발현을 증가시킬 수 있음을 보고하였다. 이후 줄기세포는 나노 입자가 내포된 심장 세포와 공배양되어 활발한 생체 분자 이동을 보였고, 전기 생리학적 심장 마커와 심장 치료에 유리한 단백질 분비가 증가하였다. 레트 심근경색 모델에 이렇게 분화된 줄기세포를 이식한 결과, 심장 섬유증이 현저히 감소시키고, 심장 조직 재생 및 기능이 촉진되었다.

둘째, 탄소 기반의 sp2 화학구조를 지닌 그래핀 산화물이 세포 내 활성산소를 효과적으로 억제 할 수 있고, 대식세포의 염증 활성화를 예방할 수 있음을 확인하였다. 또한, 우리는 그래핀 산화물 나노 입자를 DNA 전달체로 이용, 심장 경색 부위의 염증 세포를 조직 재생성 대식세포로 분화시켰다. 심근경색 이후 과도한 수의 염증성 대식세포가 환부에 증식하면서 조직 괴사가 악화되고 조절되지 않은 활성산소 농도가 적절한 조직 재생을 크게 저해하는 것으로 알려져 있다. 본 연구를 통해 우리는 산화 그래핀이 활성산소 억제제로 작용, 대식세포의 염증 활성화를 방지 할 수 있음을 입증하였고, 이후 DNA 전달을 통해 대식세포의 치료성 분화를 크게 향상시켰다. 또한, 마우스 심근경색 모델에 이 그래핀 산화물 이식을 통해 면역 세포 반응을 현저히 감소시키고, 심장 기능 회복을 위해 심장 섬유증을 완화시켰다.

주요어: 산화철 나노입자, 그래핀 옥사이드, 세포 거동조절, 심근경색, 조직공학

학번 : 2011-30990